ADA086765

UNSTEADY SWIRLING FLOWS IN GAS TURBINES

Annual Technical Report

April 1, 1979 through March 31, 1980

Contract F 49620-78-C-0045

LEVEL ⅠⅠ

Prepared for:

Directorate of Aerospace Sciences

Air Force Office of Scientific Research

Bolling Air Force Base

Washington, D.C. 20332

DTIC

ELECTE

S JUL 1 5 1980

C

By:

M. Kurosaka

University of Tennessee Space Institute

Tullahoma, Tennessee 37388

May 1980

DDC FILE COPY

80 7 14 113

SECURITY CLASSIFICATION OF THIS PAGE (When Data Entered)

REPORT DOCUMENTATION PAGE	READ INSTRUCTIONS BEFORE COMPLETING FORM

1. REPORT NUMBER	2. GOVT ACCESSION NO.	3. RECIPIENT'S CATALOG NUMBER
AFOSR-TR-80-0509	AD-A086765	Annual

4. TITLE (and Subtitle)	5. TYPE OF REPORT & PERIOD COVERED
UNSTEADY SWIRLING FLOWS IN GAS TURBINES	INTERIM technical rept. 1 Apr 1979 — 31 Mar 1980
	6. PERFORMING ORG. REPORT NUMBER

7. AUTHOR(s)	8. CONTRACT OR GRANT NUMBER(s)
M. KUROSAKA	F49620-78-C-0045 new

9. PERFORMING ORGANIZATION NAME AND ADDRESS	10. PROGRAM ELEMENT, PROJECT, TASK AREA & WORK UNIT NUMBERS
UNIVERSITY OF TENNESSEE SPACE INSTITUTE AEROSPACE AND MECHANICAL ENGINEERING TULLAHOMA, TENNESSEE 37388	2307A4 61102F

11. CONTROLLING OFFICE NAME AND ADDRESS	12. REPORT DATE
AIR FORCE OFFICE OF SCIENTIFIC RESEARCH/NA BLDG 410 BOLLING AIR FORCE BASE, DC 20332	May 1980
	13. NUMBER OF PAGES 147

14. MONITORING AGENCY NAME & ADDRESS(if different from Controlling Office)	15. SECURITY CLASS. (of this report)
	UNCLASSIFIED
	15a. DECLASSIFICATION/DOWNGRADING SCHEDULE

16. DISTRIBUTION STATEMENT (of this Report)

Approved for public release; distribution unlimited

17. DISTRIBUTION STATEMENT (of the abstract entered in Block 20, if different from Report)

18. SUPPLEMENTARY NOTES

19. KEY WORDS (Continue on reverse side if necessary and identify by block number)

AIRCRAFT ENGINE
FLOW-INDUCED OSCILLATION
UNSTEADY FLOW

20. ABSTRACT (Continue on reverse side if necessary and identify by block number)

This report covers the second year's activity on the unsteady swirling flows in gas turbines. The objective of the investigation is to acquire fundamental understanding of a phenomenon characterized by violent fluctuations occurring in swirling air flows in aircraft engines; this flow instability, dubbed here as 'vortex whistle', is known to be capable of causing severe fatigue failure in gas turbine components. In the period reported here, effort has been concentrated upon confirming the analytical results obtained in the first year.

DD FORM 1473
1 JAN 73

and, also, upon designing and constructing a test rig to be used in Phase II.
First, instead of using the boundary layer approximation as a starting point
on the analysis, as done in the last year, in the present report period, we the analysis
started from the compressible unsteady Navier-Stokes equations; this was
necessary in order to assess the importance of the so-called higher order
effects in the boundary layer upon the streaming. Resorting to the apparatus of
a matched asymptotic expansion, the analytical representation of the
acoustic streaming was derived anew. The results are in essential agreement
with our previous conclusions and we were able to confirm, on firmer ground,
the existence of the threshold swirl beyond which the free vortex distribution
changes into a forced vortex type; these are written up in a paper form
appended to this report. Second, based upon the analytical results, a test
rig with two different tangential injection manifolds was designed, con-
structed and installed; the acquisition of the data from them will form the
central effort of the next, Phase II activity.

TABLE OF CONTENTS

1. Objective

a) <u>Overall objective</u> is to acquire fundamental understanding of a phenomenon characterized by violent fluctuation of swirling flow, which is often found to occur in various aircraft engine components. This flow instability, dubbed here as "Vortex Whistle", is one of the most subtle and treacherous flow-induced vibration problems in gas turbines. In contrast to the other well-known unsteady flow problems in turbomachinery such as rotating stall, surge, aeroacoustic noise and flutter, at present, little is known about this phenomenon -- despite its importance to the aircraft engine overall structural integrity. The resultant vibration induced by the "Vortex Whistle" can sometimes become so violent that the bladings and the structural members of gas turbines suffer serious damage. Perhaps for the reason that the phenomena have appeared in seemingly unrelated incidents concealed under various disguises, so far no investigations appear to have been carried upon.

In the present effort, we will conduct a comprehensive and systematic investigation into the "Vortex Whistle" with its objective to offer a unifying explanation for this least understood problem and to contribute to assuring adequate design margins in order to alleviate this severe flow-induced vibration problem encountered in gas turbines. The entire program is comprised of

theoretical and experimental investigations. In Phase I, covering the two-year period between April 1, 1978, and March, 1980, a theoretical investigation has been conducted and completed. Based upon this framework, we shall carry out the experimental program in the second phase starting April 1, 1980. In order to accelerate the pace of the entire investigation, a part of the experimental investigation corresponding to the second phase has been conducted concurrently with Phase I.

b) The objectives of the first year; Phase I - 1, (April 1, 1978 to March 31, 1979), the activity of which was reported in the first annual report, were to lay out the basic analytical formulation and from it to obtain the preliminary theoretical explanation of the problem.

c) The objectives of the second year; Phase I - 2, (April 1, 1979 to March 31, 1980), whose outcome is summarized herein, are to refine the foregoing analysis and resolve the several important issues raised in the first year. Throughout the first and the second year, the theoretical effort has been focused on devising a flow model which is simple enough to be amenable to analysis, but still captures the essential physics and exhibits the key feature of the "Vortex Whistle" phenomenon.

In addition, based upon the results of the analysis, the test apparatus has been designed, constructed and installed, the data acquisition therefrom comprising the central part of the second phase activity.

2. Features of "Vortex Whistle" Phenomenon

"Vortex Whistle" has been known to occur in various gas turbine components such as (a) a downstream section of variable vanes followed by accelerating flow (b) an inducer section of centrifugal compressors installed with variable pre-swirl vanes and (c) turbine cooling air cavity where the air enters through ports located on rotating parts. The common features of this unsteady flow oscillation may be summarized as follows:

(a) The most unmistakable characteristics of "Vortex Whistle" is that the frequency of fluctuation is <u>discrete</u> and it becomes higher as the flow rate increases.

(b) It is induced by high swirl flow: if the vane angle is set in such a way as to produce less swirl, whistle disappears.

(c) However, the role of vanes in connection with the "Vortex Whistle" seems only to impart the swirling motion to the fluid; in the place of vanes, a single or several tangential injection of flow produces the similar oscillation.

(d) The <u>steady</u> velocity distribution appears to affect intimately the occurrence of the whistle. For example, small change in duct configuration or design change from free vortex to forced vortex has sometimes succeeded in eliminating the pulsation of flow.

(e) The amplitude of oscillation often becomes exceedingly large. Interestingly and curiously enough, in such situations the steady flow distribution in the radial direction -- both velocity and temperature -- becomes markedly altered. For instance, for swirl within a coannular passage between outer and inner surfaces, the free vortex distribution of swirl flow observed at points below certain threshold swirl Mach number is found to be converted into a shape somewhat similar to a forced vortex above the threshold Mach number -- with reduced swirl velocity near the inner surface. At the same time, the steady total temperature distribution in the radial direction exhibits the temperature drop as much as $30^{\circ}F$ at the core of the vortex; this immediately presents its important and intriguing implications related to Ranque-Hilsch vortex cooling effect (e.g. Ref. 1).

3. Significant Achievements to Date.

The following are the significant results accrued in the second year's activity from April 1, 1979, to March 31, 1980.

(a) Analytical investigation

The problem posed is to study the characteristics of disturbance-induced flow field within an annular passage between concentric circular cylinders.

As reported in our first annual report, in the first year, linearized acoustic wave problem was analyzed and the frequency-swirl relationship was obtained; the comparison with the available experimental data showed favorable quantitative agreement with the experimental data and reproduced the trend stated in (a) of Section 2. In addition, the expression of the steady streaming was derived using the boundary layer approximation as a starting point; the result predicted the existence of the reversal in the direction of tangential streaming and based on this, we were able to explain the observed deformation of steady profile, referred to Section 2(e).

Although these results of the first year were highly encouraging, the use of the boundary layer approximation as a starting point raised some questions on the expression of the steady streaming thus derived. The reason is that the streaming is obtained as a second order quantity while the boundary layer approximation is the so-called,

first order approximation to the full Navier-Stokes equations. Thus, for example, the effect of curvature is neglected in the boundary layer approximation and we have to confirm whether it influences the steady streaming or not; the variation of viscosity due to temperature fluctuation has been neflected in the first year's analysis and this effect needs to be assessed.

To face these problems once and for all, in the second year, we decided to use the Navier-Stokes equation as the starting point of the refined analysis. By using the apparatus of a matched asymptotic expansion, we derived the expression of streaming anew.

In the main, this improved expression agrees essentially with the first year's result based upon the boundary layer approximations, the only major difference being in the presence of the viscosity fluctuation in response to temperature unsteadiness. Even this does not, however, affect the values of the threshold swirl Mach number. Thus, we are able to confirm the conclusions reached in our initial efforts, which we summarize next.

The streaming in the tangential direction suffers a sudden reversal of its direction above the threshold swirl, the physical reason being due to the Doppler shift caused by swirl; and at the same time, the absolute magnitude of acoustic streaming becomes considerably increased.

The specific value of swirl at the threshold depends on the explicit relationship between the frequency and the

prescribed radial distribution of tangential velocity.
For the steady free vortex distribution between co-annular
cylinders, which corresponds to the one referred to (e)
of Section 2, the threshold steady swirl is shown to
range from subsonic to supersonic tangential Mach number,
its specific values being dependent upon the ratio of the
outer to inner radius of the cylinder and the wave modes.
Below the threshold, the tangential streaming on the surface
of the inner cylinder is in the same direction as the steady
swirl; however, beyond this, the streaming abruptly reverses
its direction and starts to retrogress in the direction
opposite to steady swirl. Surely, then, this tends to
decrease the total d.c. component of circumferential velocity,
which is the sum of steady swirl with tangential streaming,
its reduction being sizeable near the threshold; close to
the inner cylinder, the radial profile is converted into one
not unlike a forced vortex. This behavior appears to be
consistent with the observation made in (e) of Section 2.

We also extended the analysis to include the steady
Rankine vortex distribution within a single pipe, which
corresponds to the so-called Ranque-Hilsch tube. There,
for the fundamental mode of disturbance, any amount of swirl
always makes the tangential streaming near the tube periphery
rotate in the same direction as the steady swirl itself; for
such a wave, no threshold swirl exists. Its magnitude be-
coming of considerable strength, the total d.c. component
of circumferental velocity in a free vortex region is in-

creased and the entire Rankine vortex is now converted into a forced vortex.

These conversions toward forced vortex type by streaming tend to separate the flow, with the initially uniform total temperature, into hotter air near the outer radius and colder air near the inner radius or the center-line -- this is the Ranque-Hilsch effect.

The details of the foregoing analysis carried out as Phase I are written up in a paper entitled " Steady Streaming in Swirling Flow and Separation of Energy" to be submitted for publication.

(b) Experimental investigations

Based upon the effect of governing parameters predicted in (a), a test rig has been designed in order to correlate the analysis with experiments. The primary consideration in the design was the establishment of a well-defined swirling flow in a straight co-annular tube of sufficient diameter to allow the insertion of probes without causing a major disturbance of the flow; the ratio of the radii of inner and outer tubes is to be varied over a range of parameters in order to make comparisons with the trend predicted by analysis.

It was decided that the tube should be transparent to allow flow visualization studies and a three-inch outer diameter plexiglass tube of 30 inches in length was selected (Fig. 1). The manifold section, into which the compressed air flows, is fabricated of transparent

plastic. Eight nozzles of 3/8 inches diameter equally
spaced around the circumference of the tube and rounded
at their entrance, direct this compressed air tangentially
into the main co-annular rube. At the other end of the
30-inch long tube, a 60° cone-shaped valve is located to
regulate the amount of through flow.
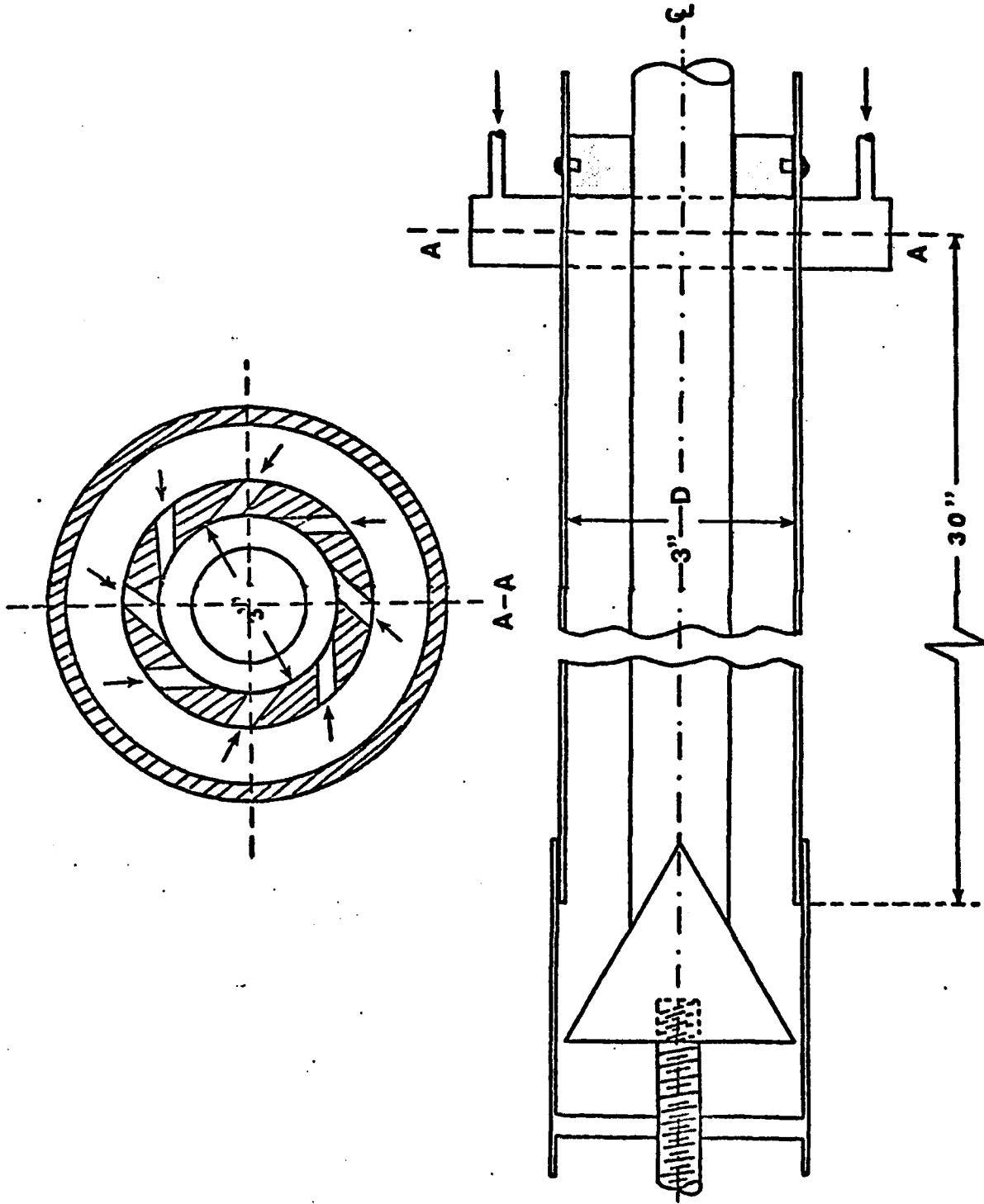
Figure 1. Vortex Whistle Test Rig (A) With Tangential Inlet

Figure 2. View of Vortex Whistle Test Rig with
Fixed Tangential Inlet.

Six different inner tubes of varying radii are to be used in order to investigate the effect of the outer/inner radius ratio. The air entering the manifold is fed through a specially constructed acoustic muffler. The photo of the entire test arrangement is shown in Fig. 2.

In addition to the manifold of fixed inlet geometry described above, another manifold containing variable guide vanes has been designed (Fig. 3); the latter is interchangeable with the former, provides the variation in swirl/axial velocity ratio, and the bulk of data is planned to be taken with this manifold. The variable guide vanes consist of 24 streamlined airfoils, placed symmetrically in a circular array around the side plate of the manifold. The vane angles can be set at any desired value between zero (purely radial flow) and 65 degrees, by rotating a circular ring which contains 24 small pivots fitted into slots provided in airfoils. The photo of this variable vane manifold is shown in Figure 4.

Currently check-out tests of ths test rig are being carried out.

24 VANES

A-A

₵

A

A

D

3"

30"
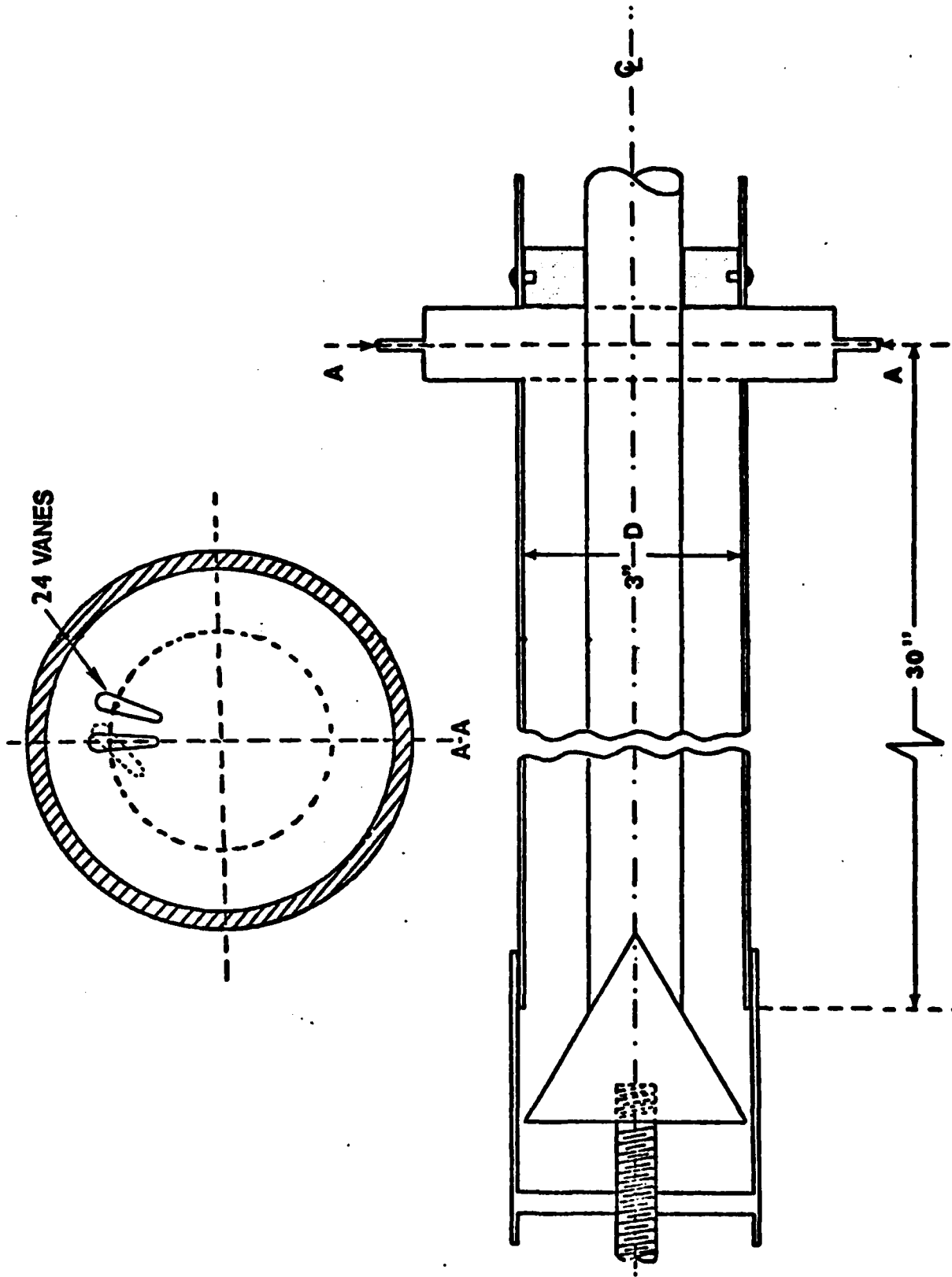
Figure 3. Vortex Whistle Test Rig (B) With Controlled Inlet Guide Vanes

Figure 4.   View of Variable Guide Vane Manifold.

4. Implications of Conclusions Obtained During

   Phase I Effort as Related to Aircraft Gas Turbines

Once confirmed by further investigations to be carried out in Phase II, the implications of these conclusions obtained from Phase I program, as related to the aircraft engine technology are twofold:

(a) By explicit recognition of the dependence of vortex whistle upon the governing parameters as found in the present investigation, it appears possible to avoid the catastrophic structural failure by de-tuning the natural frequency of various engine components from this discrete frequency.

(b) The existence of transition from free vortex to non-free vortex type above certain critical swirl Mach number implies that in the steady aerodynamic design of rotors/stators, a due consideration may have to be given to this acoustic streaming.

5. Written Publications

"Steady Streaming in Swirling Flow and Separation of Energy" (attached as Appendix and to be submitted for publication).

6. Future Plans

    (a) <u>For remainder of present contrant (Phase II,</u>
        <u>April 1, 1980 to September 30, 1981)</u>.

The phase II program will be comprised of (1) detailed data acquisition of 'Vortex Whistle' by utilizing the testing designed and constructed during Phase I, as described in Section 3(b) and, (2) concurrent continuation and refinement of analysis, if necessary.

The experimental program will be initiated first by installing the manifold of fixed geometry type and the measurement of steady temperature and pressure distribution will be carried out in the test configuration where the inner tube will be removed. The compressed air with the inlet pressure of 10, 15 and 20 psig will be directed into the manifold and flow field traverse will be made. The objective of this test run is to check out the rig and instrumentation by making comparison with the well-documented data taken in a similar set-up. Upon completion of this, the manifold will be replaced by the alternative one with variable guide vanes; this will allow one to vary the ratio of swirl velocity to axial velocity. After checking the uniformity of the incoming flow by means of flow visualization, we measure the variation of steady velocity and temperature profile as the swirl Mach number is increased; particular attention will be focused upon the data acquisition near the critical swirl Mach number. In conjunction

with this, unsteady flow measurement will be carrued out
to define the acoustic characteristics of the vortex
whistle; both the microphones placed externally and the
miniature kulites mounted flush with the internal surface
of the outer tube will be used for this. Among the
acoustic signatures to be measured and analyzed are fre-
quency of vortex whistle, its intensity and rotating pat-
terns of sound. In the event where the level of its inten-
sity in the test rig were not sufficiently high, it would
be amplified by a speaker, which will provide an additional
source of excitement. Based upon the measured frequency,
an acoustic suppressor will be designed and installed on
the test rig and the effect of sound suppression upon the
steady flow profile near the critical Mach number will be
investigated. As an added related effort, the similar
effect upon the Ranque-Hilsch tube will be examined by
installment of an acoustic suppressor on the commercially
available vortex tube, which has been already procured in
the Phase I period. With regard to the analysis, we make
comparisons of the data with the preliminary analysis
carried out in Phase I and, if necessary, modify it.

(b) Next increment

In the foregoing phases; the outer and inner
cylinders simulating the outer and inner casing of the
gas turbine are held stationary. For the actual aircraft
engine turbomachinery, the inner casing is rotating, of
course. This rotational effect is considered to be im-

portant in the present study of streaming, affecting
the frequency parameter. Thus in the next increment
of the contract, the investigation of this effect will
be proposed.

REFERENCES

1. Hilsch, R., "The Use of the Expansion of Gases in a Centrifugal Field as a Cooling Process," The Review of Scientific Instruments, Vol. 18, No. 2, pp. 108-113, 1947.

2. Rokowski, W. J. and Ellis, D. H., "Experimental Analysis of Blade Instability - Interim Technical Report - Vol. 1," R78AEG 275, Aircraft Engine Business Group, General Electric Company, Evandale, Ohio. March 1978.

APPENDIX

Steady Streaming in Swirling

Flow and Separation of Energy

M. Kurosaka

The University of Tennessee Space Institute
Tullahoma, Tennessee 37388

ABSTRACT

This paper concerns the steady streaming induced by
unsteady disturbances in a swirling flow contained
within concentric circular cylinders or a single tube.
The investigation is motivated, in the first place, by
a newly observed phenomenon, which reveals that the
acoustic streaming is accountable for the deformation
of base, steady swirl profile, leading to the radial
separation of total temperature (the Ranque-Hilsch
effect). This, in turn, offers a clue into the hithet-
to unheeded mechanism of the Ranque-Hilsch effect itself.
Starting from the full, compressible, unsteady Navier-
Stokes equations, the acoustic streaming is studied by
the method of matched asymptotic expansions; based on
the results, experimental observations are explained.

1. Introduction

1.1 Background

The subject of acoustic streaming owes its origin
to Lord Rayleigh's landmark memoir (1884); led by Faraday's
observation (1831) and the patterns in the Kundt tube, he showed
that sound waves can and do generate steady current through
the very action of Reynolds stresses, which are induced near
the solid boundary by the periodic disturbances themselves.
For the modern review of the subject in general, we refer
to the recent expository lecture by Lighthill (1978-a).

Not only can we demonstrate the acoustic streaming
in assorted laboratory experiments using a vibrating dia-
phragm, cylinder and the like, but it has been suggested as
a possible explanation ranging from the roll torque effects
of rocket motors in flight (Swithenbank and Sotter 1964;
Flandro 1964, 1967) to the blood flow phenomena in the
coronary arteries (Secomb 1978).

Of late, a striking acoustic streaming phenomenon,
with its features alien to others, revealed itself unexpect-
edly in a swirling flow experiment (Danforth 1977; Rakowski,
Ellis and Bankhead 1978; Rakowski and Ellis 1978), display-
ing a grossly deformed pattern of steady flow and temperature.
And, at the same time, it afforded a glimpse into the dimly
foreseen mechanism of energy separation -- the Ranque-Hilsch
effects. Although the phenomenon was detected in a test

rig called an annular cascade simulating flow in aircraft
engines and, as a matter of fact, cropped up in the check-
out tests as an undesirable side-effect to be eliminated
later, its undeniable significance -- in divulging the clues
to connect the acoustic streaming with thermal effects --
appears to transcend beyond the special interest of turbo-
machinery technology and merit wider scientific attention.

Here we outline its layout briefly. The annular cas-
cade was conceived with the objective to investigate some
aero-elastic aspects of compressor bladings in a non-rotat-
ing environment. As a whole, it is in the shape of a
stationary, annular conduit formed between inner and outer
casings: first, air enters the vehicle, axially and uniformly,
and is immediately imparted a tangential motion by passing
through variable swirl vanes, the adjustment of whose angle
induces the change in swirl; then,it flows spiralling aft,
through the transition piece, to the test section where an
array of removable test airfoils are normally mounted on outer
casings in the circumferential direction and in a cascade
arrangement; and finally, upon being realigned in the axial
direction by deswirl vanes, the air exhausts to the exit.

During the check-out test of the vehicle, the pres-
ence of loudly audible, unsteady flow was immediately un-
covered. The disturbance became manifest beyond certain
conditions called an acoustic boundary. It was organized,

periodic, and spinning circumferentially with the first tangential mode; the amplitude of total pressure exceeded 20% of steady state levels, an intense fluctuation indeed. Its fundamental frequency was in the range of 300 to 400 Hz, aerodynamically ordered and, in fact, was found to increase almost proportionally to the swirl, a point to be made here and recalled later. As the swirl was increased, several higher harmonics were found to accompany this fundamental frequency. The measurements were taken <u>without test airfoils installed in the test section.</u> Hence, nothing lay in the way of the flow path between the upstream swirl vanes and the downstream deswirl vanes. Before we go further, we can not too strongly emphasize the fact that, despite its aim, all the components of the annular cascade are not rotating, but stationary.

Among the other effects of this vigorous pulsation in swirling flow, the phenomenon that arouses our attention is the unexpected change of steady-state or time-average components of the flow field, or its "d.c." parts. When the swirl was small and outside of the acoustic boundary, the <u>steady-state</u> tangential velocity distribution in the radial direction was in the form of a free vortex, with the obvious exception of thin boundary layers found near the inner and outer surfaces; the <u>steady-state</u> total temperature was uniform. The former was what had precisely been intended in the design, the latter as expected. However, when the swirl was increased beyond

the acoustic boundary, then above a certain swirl, the tangential velocity near the inner wall became abruptly reduced to a considerable extent, the radial profile transfigured from a free vortex into one somewhat akin to a forced vortex; what is equally surprising is that the total temperature, initially uniform at the inlet and equal to 97^OF, spontaneously separated into hotter stream of about 118^OF near the outer wall and colder one of 83^OF near the inner wall, with the difference as distinct as 35^OF! This latter reminds us of none other than the Ranque-Hilsch effect.

Faced with the severity of dynamic flow field, which posed a serious threat to the subsequent use of the rig for flutter testing of airfoils, the annular cascade was modified and both inner and outer walls were provided with tuned acoustic absorber. And this did remove the unacceptable dynamic flow disturbances. Ever since, the vehicle has successfully been in use for aeroelastic purposes, the details of which are, however, outside of our present interest.

Instead, we focus our capital concern to what happens to the profiles of steady flow, now that the unsteady fluctuation has been eliminated. The answer: the change in the velocity and temperature distribution has vanished. The free vortex remains so throughout even above

the swirl, where, before the suppression of organized
disturbance, it has been converted into a forced vortex
type; the total temperature remains uniform in the radial
direction throughout -- the Ranque-Hilsch effect is gone.

Beyond doubt the acoustic streaming[*] did somehow
deform the steady flow field, both in velocity and tem-
perature, and this affords an unmistakably obvious clue
into the mechanism of little understood Ranque- Hilsch
effects, which we shall discuss in some detail below.

We recall that in the Ranque-Hilsch tube (Ranque
1933; Hilsch 1947), the compressed air enters near one
end of a single straight tube through one or several
tangential injection nozzles. Then, once within the tube,
the swirling air segregates by itself into two streams of
different total temperature: the hotter air near the
periphery of the tube and the colder one at the centerline,
a separation effect already mentioned with regard to the
annular cascade. Between the Ranque-Hilsch tube and the
annular cascade, the visible difference in the internal
flow passage is that the former is made of a single tube,

---

* We eliminate the possibility of vortex breakdown (e.g.
Hall 1972) on the following grounds. First, the breakdown
is essentially a steady phenomenon; the one described here
was unsteady. Second, the measurement in the annular cascade
did not exhibit any reversal of flow in the axial direction.

the latter of an annulus (this will turn out to be a not so trifling dissimilarity as it might seem now). As a matter of further detail, in the conventional Ranque-Hilsch tube the cold air is immediately extracted from an orifice located on one end,near the inlet nozzle,and the hot air spiralling downstream escapes from the other end where a throttling exhaust valve is located; this is the so-called counter-flow type. Even by closing the cold orifice, the air flowing only in one direction toward the exhaust valve can still produce the radial separation; this is called uni-flow type.

Detailed measurements of the internal flow distribution in the Ranque-Hilsch tube, taken at the condition of *optimam cooling,show that,* in every instance a forced vortex type is formed immediately near the entrance to the tube , even at a location as practically close as possible to the inlet nozzle (for uni-flow type, Eckert and Hartnett, 1955, Hartnett and Eckert 1957, Lay 1959; for uni-flow type with vortex chamber, Savino and Ragsdale 1961; for counter-flow type Scheller and Brown 1957, Sibulkin 1962, Takahama 1965, Bruun 1969). The forced vortex occupies the almost entire cross section (except in the reighborhood of the boundary layer on the tube periphery, of course) and remains so from the entrance to the exit. Mark with attention that at this condition any vestige of what may be characterized as a free vortex type has nowhere been detected. Also ,

right at the entry, the radial separation of total temperature occurs. Contrary to some earlier belief, the maximum tangential velocity near the periphery of tubes needs not to be supersonic to create the effect, even the speed of 500 ft/sec or so suffices.

Although the actual total temperature separation in Ranque-Hilsch tubes is beyond all question, none of the theoretical explanations devised so far appear to have found unreserved acceptance. Take, for example, the turbulent migration theory (Van Deemter 1952; Deissler and Perlmutter 1960; Linderstrøm-˥ ˥ 1971). This rests upon the assumption that when a lump of fluid migrates radially by turbulent motion, it tends to separate the total temperature by the combination of the following two separate mechanisms of stochastic origin: (1) formation of a forced vortex and (2) creation of a static temperature distribution approaching an adiabatic one, the latter through the heat transfer process in a centrifugal field originally postulated by Knoernschild (1948). However, confrontation with the experimental evidence already available in the literature reveals, that the contention of turbulence as a dominant catalytic agent for the Ranque-Hilsch effect appears to suffer from a serious flaw.

Let us turn our attention temporarily away from the Ranque-Hilsch tube proper, and inspect the measurements

in apparatus with the tangential injection identical
to the one for the Ranque-Hilsch tube, but constructed
instead to create a vortex for purposes other than
energy separation (Ter Linden, 1949, for cyclone separa-
tor; Keyes 1961, for containment of fission material;
Tsai 1964, for plasma jet generator; Gyarmathy 1969,
for von Ohain swirl chamber; Batson & Sforzini 1970, for
swirl in solid propellant rocket motors.) There, unmis-
takable free vortex type prevails at the entrance and
elsewhere, with the obvious exception of the innermost
core near the tube's centerline; the total temperature
at the entrance remains virtually uniform[*] in the radial
direction and equal to the inlet total temperature (Batson &

---

[*]To be more precise, Batson & Sforzini's data shows that the
total temperature is uniform from the periphery of the
tube to the boundary of the inner core, which occupies
about 10% of tube radius from the centerline. (In the core,
the tangential velocity distribution is of a forced vortex
type and the total temperature dips slightly.) Under
conditions fulfilled in their experiments, this is theoreti-
cally consistent with Mack's results (1960) where he has
shown that even for viscous, heat-conducting flow, the total
temperature of a free vortex remains virtually uniform (and
exactly so for the Prandtl number of 0.5) provided the
swirl Mach number is less than one.

Sforzini, ibid.) Even in these test rigs, the turbulence level would be more or less the same as for the Ranque-Hilsch tube. Contrast this with the sudden formation of a forced vortex and the separation of total temperature right at the entrance of the Ranque-Hilsch tube. If turbulence is the primary agent at work, then under circumstances not unlike each other, why, in the particular case of the Ranque-Hilsch tube, can it eradicate any traces of a free vortex and suddenly separate total temperature, while in the others it can still preserve a predominantly free vortex and virtually uniform total temperature?

This dichotonomous branching has been left unexplained by the turbulent migration theory. Although the space does not permit us to dwell on the details of other theories (Schepper 1951; Sibulkin ibid.), they do not appear to be free of similar serious objections.

The experimental evidence mentioned in the opening of this section on the annular cascade compells us to turn toward acoustic streaming as the more dominant cause of the Ranque-Hilsch effect -- the acoustic streaming induced through the Reynolds stresses which are caused by organized periodic disturbances rather than by stochastic motion.

Close scrutiny of the available past literature on the Ranque-Hilsch tube reveals, surely, the allusion to the

presence of an intense periodic disturbance observed by many
experimenters. Hilsch(ibid.) himself mentions that a
boiling sound was audible if the exhaust valve was set at
optimum position for cooling. McGee (1950), Savino and
Ragsdale (ibid.), Ragsdale (1961),Kendall (1962, for a
vortex chamber), and Syred and Beer (1972) recount in
one way or the other, the disturbance of pure tone type,
whistle or scream. In fact, Savino and Ragsdale record
an incident where a loud screaming noise was accompanied by
10° - 20°F change in total temperature, a phenomenon
where the experience of the annular cascade leaps immediately
to mind. None of them, however, proceeded beyond the stage
of giving passing observations to it.

To a certain extent, the work of Sprenger (1951)
foreshadows our premises in its spirit. In the Ranque-Hilsch tube
with its hot end closed and only its cold end open, he measured
periodic disturbance by spreading Lycopodium to form a
Kundt pattern! However, the pattern was apparently used to
measure only the wave length of discrete disturbances, since
he did not pin the Ranque-Hilsch effect down to the acoustic
streaming. Rather, by appealing to the analogy[*] of

_____

[*]Reynolds (1961), while advocating the turbulence migration
theory, refers Sprenger's idea as due originally to Ackeret
without citing the reference: to date, we have been unable
to locate the original source.

the resonance tube (e.g. Hartmann 1931), he later simply
suggested (1954) that the organized unsteadiness might
produce the energy separation.

Highly suggestive also were the circumstances
which led to the discovery of vortex whistle by Vonnegut
(1954). While engaged in experiments exploring the
application of the Ranque-Hilsch cooling effect (as a
possible means of measuring the true static temperature
of air from aircraft in flight), Vonnegut (1950) observed
the presence of a pure tone noise. Although he did not
connect it with a mechanism of the Ranque-Hilsch effect,
from this hint he constructed a musical instrument, the so-
called vortex whistle, where air, injected tangentially into
a cylinder of larger diameter, swirls into a smaller tube;
the sound thus emitted is found to have a discrete frequency,
which is proportional to flow rate. Recall, now, that the
frequency[*] of the pure tone noise in the similar, swirling
flow within the annular cascade was also proportional to the
Mach number.

---

[*]Strickly speaking, finer distinction has to be drawn between
the two frequency-swirl relationships, as will be made clear
in Section 7.

1.2 Outline of Present Investigations

Against the precedent setting, we shall, in the
present paper, pose the following model problem: periodic
disturbances in swirling flows within straight co-annular
cylinders or a single tube. We shall solve it by deriving
an explicit expression for its acoustic streaming; then, we
shall seek to display such key features as the transfigura-
tion of steady swirl from one type to another at certain
threshold steady swirl; and we shall attempt to explain
the Ranque-Hilsch effect on the basis of streaming caused
by Reynolds stresses due to organized periodic disturbances.

Acoustic streaming is, of course, an induced
steady or d.c. component, and as such we have to distinguish
it sharply from the base, steady flow initially imposed before
the disturbances are set up. For brevity, we shall, here
and henceforth, refer to the latter simply as steady flow
and its sum with the former as the total d.c. component.

Now, without a single exception, the only known
analytical method to obtain streaming, the present one not
excepted, is to resort to the use of a perturbation scheme
and take a temporal average of the second-order equation,
which contains products of the first order quantities. Thus,
if we started from the conventional boundary layer equations,
which corresponds of course to the first order approximation
to the full Navier-Stokes equations, we would be asked as to
the effects of what are collectively called the higher-order
approximation to boundary layer theory (e.g. Van Dyke

1969) on the streaming. In this very connection, upon treating the problem of streaming around an oscillating cylinder, Stuart (1966) justly voiced a note of caution on the possible effect of curvature, which could be of the same second order as the streaming itself. (For this particular effect, in his definitive work on streaming for incompressible flow otherwise in a state of rest, Riley (1967) shows conclusively from a matched asymptotic expansion that, as far as the leading term of the streaming is concerned, the curvature has no influence within the unsteady boundary layer.) In the present case we are besieged with more than a single effect of possible second-order correction. For example, both steady and unsteady boundary layers formed over the cylindrical surfaces present the problem of a steady as well as an unsteady displacement thickness; the fluctuation of temperature gives rise to changes in the viscosity, which, coupled with temporal variation in strain, might beget additional Reynolds stresses, as will be found to be indeed the case; the flow being compressible, even the effect of the second coefficient of viscosity must be assessed, as has, in fact, been done by Van Dyke (1962-a) for steady compressible boundary layers .

To face these problems once and for all, we shall abandon the standard boundary layer equations and start

afresh with the full, compressible and unsteady Navier-Stokes equations, retaining even the second coefficient of viscosity. Under the conditions of several parameters to be small, we shall use the matched asymptotic expansions to ferret out the leading term of the acoustic streaming in swirling flow within co-annular cylinders; by following this avenue of plunging into the equation in its full generality, we can not avoid somewhat elaborate alegbra, which constitutes Section 3 through 6.

One of our centerpiece results is equation (42), which expresses the acoustic streaming in the circumferential direction near the cylindrical surfaces. This will explicitly show the following: it suffers a sudden reversal of its direction above a threshold steady swirl, the physical reason being due to the Doppler shift caused by swirl; and this holds regardless of the values of the streaming Reynolds number. At the same time, the absolute magnitude of acoustic streaming itself becomes considerably increased.

The specific value of swirl at the threshold depends on the explicit relationship between the frequency and the prescribed radial distribution of tangential velocity.

The derivation of the latter relation will be found in
its entirety in the Appendix. With the aid of this,
we shall be in a position to discuss the behavior around
the threshold in Section 7.

For the steady free vortex distribution between co-
annular cylinders, which corresponds to the one for the
annular cascade, the threshold steady swirl will be
shown to range from subsonic to supersonic tangen-
tial Mach number, its specific values being strongly dependent
upon the ratio of outer to inner radius of the cylinder
and the wave modes. Below the threshold, the tangential
streaming on the surface of the inner cylinder is in
the same direction as the steady swirl; however, beyond
this, the streaming abruptly reverses its direction and
starts to retrogress in the direction opposite to steady
swirl. Surely, then, this tends to decrease the total d.c.
component of circumferential velocity; its reduction being
sizeable near the threshold, close to the inner cylinder
the radial profile is converted into one not unlike a
forced vortex. This behavior appears to be consistent
with the observation made about the annular cascade in
1.1.

We turn now to the steady Rankine vortex dis-
tribution within a single pipe, which corresponds to the

Ranque-Hilsch tube. There, for the fundamental mode
of disturbance, any amount of swirl always makes the
tangential streaming near the tube periphery rotate
in the same direction as the steady swirl itself; for
such a wave, no threshold swirl exists. Its magnitude
becoming of considerable strength, the total d.c. component of
circumferential velocity in a free vortex region is increased and the
entire Rankine vortex is now converted into a forced
vortex;if such a fundamental mode of disturbance is not
sufficiently excited,the Rankine vortex remains vir-
tually unaffected. (In all these, if the calculated
streaming becomes of considerable magnitude, obviously
the small disturbance approximations break down. We
assert, however, that as usual this does, at the very
least, indicate what is to be expected in real situa-
tions). In the light of our discussion in 1.1, this seems
to explain the appearance of swirl either in the form of
a forced vortex preferred for the Ranque-Hilsch tube or
of a Rankine vortex for others. In agreement with this
also is the following observation of Takahama and Soga
(1966) made in a Ranque-Hilsch tube: while, at the
optimum position of the exhaust valve, the forced vortex
is found, in the same tube with the exhaust valve now at off-
optimum position, one indeed finds a well-defined Rankine
vortex.

Whatever the initial study swirl distribution
may be, this feature they both have in common: the con-
version toward forced vortex type by streaming -- and
this tends to separate the flow, with the initially uniform
total temperature, into hotter air near the outer radius and
colder air near either the inner radius or the centerline;
this is indeed the Ranque-Hilsch effect.

Details of the physical discussion we summarize
in Section 8.

2. Statement of Problem

We pose the problem of obtaining the acoustic streaming in an annular duct between two circular cylinders, straight and stationery, as sketched in Figure 1: r_o denotes the radius of the outer cylinder, r_i of the inner cylinder. The fluid is compressible and taken as a perfect gas. We assume that, throughout the entire duct length, L, of our interest, the steady boundary layers formed over the cylindrical surfaces are thin; in the inviscid annular region bounded by and outside of them, both the circumferential and axial velocity are the predominant components of steady flow, as shown in Figure 1. Superimposed upon this steady flow are the fully three-dimensional unsteady excitations, whose forms are to be specified in the inviscid annular region and whose streaming effects we are interested in.

Before decomposing into steady and unsteady parts, we begin by writing out unsteady, compressible Navier-Stokes equations in cylindrical coordinates (r, ϕ, z) with corresponding velocity $\vec{q} = (u, v, w)$:

$$\frac{\partial \rho}{\partial t} + \frac{1}{r}\frac{\partial (r\rho u)}{\partial r} + \frac{1}{r}\frac{\partial (\rho v)}{\partial \phi} + \frac{\partial (\rho w)}{\partial z} = 0 , \qquad (1\text{-}a)$$

$$\frac{\partial (\rho u)}{\partial t} + \frac{1}{r}\frac{\partial}{\partial r}(r\rho u^2) + \frac{1}{r}\frac{\partial}{\partial \phi}(\rho u v) + \frac{\partial}{\partial z}(\rho u w) - \frac{\rho v^2}{r}$$

$$= -\frac{\partial p}{\partial r} + 2\frac{\partial}{\partial r}\left(\mu\frac{\partial u}{\partial r}\right) + \frac{1}{r}\frac{\partial}{\partial\phi}\left[\mu\left(\frac{1}{r}\frac{\partial u}{\partial\phi} + \frac{\partial v}{\partial r} - \frac{v}{r}\right)\right]$$

$$+ \frac{\partial}{\partial z}\left[\mu\left(\frac{\partial u}{\partial z} + \frac{\partial w}{\partial r}\right)\right] + \frac{2\mu}{r}\left(\frac{\partial u}{\partial r} - \frac{1}{r}\frac{\partial v}{\partial\phi} - \frac{u}{r}\right)$$

$$+ \frac{\partial}{\partial r}(\mu^{(2)}\vec{\nabla}\cdot\vec{q}), \tag{1-b}$$

$$\frac{\partial(\rho v)}{\partial t} + \frac{1}{r}\frac{\partial}{\partial r}(r\rho uv) + \frac{1}{r}\frac{\partial}{\partial\phi}(\rho v^2) + \frac{\partial}{\partial z}(\rho vw) + \frac{\rho uv}{r}$$

$$= -\frac{1}{r}\frac{\partial p}{\partial\phi} + \frac{\partial}{\partial r}\left[\mu\left(\frac{1}{r}\frac{\partial u}{\partial\phi} + \frac{\partial v}{\partial r} - \frac{v}{r}\right)\right] + \frac{2}{r}\frac{\partial}{\partial\phi}\left[\mu\left(\frac{1}{r}\frac{\partial v}{\partial\phi} + \frac{u}{r}\right)\right]$$

$$+ \frac{\partial}{\partial z}\left[\mu\left(\frac{1}{r}\frac{\partial w}{\partial\phi} + \frac{\partial v}{\partial z}\right)\right] + \frac{2\mu}{r}\left(\frac{1}{r}\frac{\partial u}{\partial\phi} + \frac{\partial v}{\partial r} - \frac{v}{r}\right) + \frac{1}{r}\frac{\partial}{\partial\phi}(\mu^{(2)}\vec{\nabla}\cdot\vec{q}), \tag{1-c}$$

$$\frac{\partial(\rho w)}{\partial t} + \frac{1}{r}\frac{\partial}{\partial r}(r\rho uw) + \frac{1}{r}\frac{\partial(\rho vw)}{\partial\phi} + \frac{\partial(\rho w^2)}{\partial z}$$

$$= -\frac{\partial p}{\partial z} + \frac{1}{r}\frac{\partial}{\partial r}\left[\mu r\left(\frac{\partial u}{\partial z} + \frac{\partial w}{\partial r}\right)\right] + \frac{1}{r}\frac{\partial}{\partial\phi}\left[\mu\left(\frac{1}{r}\frac{\partial w}{\partial\phi} + \frac{\partial v}{\partial z}\right)\right]$$

$$+ 2\frac{\partial}{\partial z}\left(\mu\frac{\partial w}{\partial z}\right) + \frac{\partial}{\partial z}(\mu^{(2)}\vec{\nabla}\cdot\vec{q}), \tag{1-d}$$

$$\rho c_p\frac{D\theta}{Dt} - \frac{Dp}{Dt}$$

$$= \frac{c_p}{P_r}\left[\frac{1}{r}\frac{\partial}{\partial r}\left(\mu r\frac{\partial\theta}{\partial r}\right) + \frac{1}{r^2}\frac{\partial}{\partial\phi}\left(\mu\frac{\partial\theta}{\partial\phi}\right) + \frac{\partial}{\partial z}\left(\mu\frac{\partial\theta}{\partial z}\right)\right]$$

$$+ \mu \left\{ 2 \left[\left(\frac{\partial u}{\partial r} \right)^2 + \left(\frac{1}{r} \frac{\partial v}{\partial \phi} + \frac{u}{r} \right)^2 + \left(\frac{\partial w}{\partial z} \right)^2 \right] + \left(\frac{1}{r} \frac{\partial w}{\partial \phi} + \frac{\partial v}{\partial z} \right)^2 \right.$$

$$\left. + \left(\frac{\partial u}{\partial z} + \frac{\partial w}{\partial r} \right)^2 + \left(\frac{1}{r} \frac{\partial u}{\partial \phi} + \frac{\partial v}{\partial r} - \frac{v}{r} \right)^2 \right\} + \mu^{(2)} (\vec{\nabla} \cdot \vec{q})^2 ,$$

$$(1\text{-e})$$

$$p = c_p \frac{\gamma - 1}{\gamma} \rho \theta \tag{1-f}$$

$$\mu = \mu(\theta) , \quad \mu^{(2)} = \mu^{(2)}(\theta) , \tag{1-g}$$

where
$$\vec{\nabla} \cdot \vec{q} = \frac{1}{r} \frac{\partial}{\partial r} (ru) + \frac{1}{r} \frac{\partial v}{\partial \phi} + \frac{\partial w}{\partial z} ,$$

$$\frac{D}{Dt} = \frac{\partial}{\partial t} + u \frac{\partial}{\partial r} + \frac{v}{r} \frac{\partial}{\partial \phi} + w \frac{\partial}{\partial z} .$$

$\mu^{(2)}$ denotes the second coefficient of viscosity, the one that vanishes for a monatomic gas, μ the coefficient of viscosity, P_r the Prandtl number, θ temperature, the rest of the notation being standard. The inertia terms of the momentum equations are rendered in the above form in order to ease the subsequent streaming calculations. In the energy equation, both the specific heat, c_p, and P_r are taken, as usual, to be constant; equation (1-g) simply states the viscosity law.

The boundary condition on the cylindrical surfaces is $\vec{q} = 0$. The thermal condition depends, in general, on the details of the unsteady heat transfer through the walls. For

simplicity, we assume that either the wall temperature
is maintained to be constant, its unsteady part being
kept to be equal to zero, or the walls are insulated.
(Dunn and Lin (1955) have shown that the former corres-
ponds to the situation where the thermal inertia of the
wall prevents the surface temperature from responding
to high frequency fluctuation, as to be expected.)

3. Preliminary Considerations

We now decompose the flow field into the steady part and the one related to unsteady disturbance such as

$$\vec{q} = \vec{Q} + \vec{q}', \tag{2-a}$$

where $\vec{Q} = (U, V, W)$ and $\vec{q}' = (u', v', w')$; likewise

$$p = P + p', \tag{2-b}$$

$$\rho = R + \rho', \tag{2-c}$$

$$\theta = \Theta + \theta'. \tag{2-d}$$

$$\mu = M + \mu', \tag{2-e}$$

$$\mu^{(2)} = M^{(2)} + \mu'^{(2)}, \tag{2-f}$$

Henceforth, primes denotes unsteady disturbances, which contain both a.c. and d.c. components, the latter being streaming induced by the former. In an effort to seek a tractable ingress to the problem, we assume disturbances to be organized, regular and endowed with the fundamental frequency ω, the stochastic part of it being neglected in comparison, in accordance with the discussions of Section 1.1. Of our central interest is the effect of $\vec{Q}$ upon the streaming.

Henceforth, it is convenient to render r, z, and t dimensionless, by referring length to r_i and time to ω, they being denoted as starred quantities; i.e. $r^* = r/r_i$, $z^* = z/r_i$, and $t^* = \omega t$. We also define the ratio of the outer

cylinder radius to that of the inner cylinder

$$\frac{r_o}{r_1} = \lambda \ .$$

(3)

The next subsection concerns some preliminary consideration on the steady flow, followed by the one on the unsteady disturbance.

3.1 Base, Steady Flow

We assume that the steady flow is axisymmetric and apply the standard outer and inner expansion (Van Dyke, 1962 a and b) in powers of $R_e^{-1/2}$ where R_e is the Reynolds number, whose choice of characteristic values is left unspecified at this point. We first examine the leading terms, denoted by subscript 0, in the following outer expansions:

$$\vec{Q} = \vec{Q}_0 + R_e^{-1/2}\vec{Q}_1 + \text{---}, \qquad (4\text{-}a)$$

$$P = P_0 + R_e^{-1/2}P_1 + \text{---}, \qquad (4\text{-}b)$$

$$R = R_0 + R_e^{-1/2}R_1 + \text{---}, \qquad (4\text{-}c)$$

$$\theta = \theta_0 + R_e^{-1/2}\theta_1 + \text{---}, \qquad (4\text{-}d)$$

$$M = M_0 + R_e^{-1/2}M_1 + \text{--}, \qquad (4\text{-}e)$$

$$M^{(2)} = M_0^{(2)} + R_e^{-1/2}M_1^{(2)} + \text{---}, \qquad (4\text{-}f)$$

where $\vec{Q}_0 = (U_0, V_0, W_0)$, $\vec{Q}_1 = (U_1, V_1, W_1)$, etc. As usual, matching yields $U_0 = 0$ on the walls and henceforth we are interested in the case where

$$U_0 = 0, \qquad (5)$$

at any values of r^* standing for the outer variable. All the leading terms or "inviscid" flow are taken to be independent of z^* (as well as ϕ), in view of the assumption of thin boundary layers stated in Section 2; they are all functions of r^* only, and may be written out explicitly as

$$V_0 = V_0(r*),\tag{5-b}$$

$$W_0 = W_0(r*),\tag{5-c}$$

$$P_0 = P_0(r*),\tag{5-d}$$

$$R_0 = R_0(r*),\tag{5-e}$$

$$\Theta_0 = \Theta_0(r*),\tag{5-f}$$

etc. Then, the only nontrivial equation among equation (1) is the following,

$$\frac{1}{r*} R_0 V_0^2 = \frac{dP_0}{dr*},\tag{6}$$

which expresses the radial equilibrium of r-component of momentum. As is well known in the theory of turbomachines (e.g. Marble 1964, p. 144), if the corresponding stagnation enthalpy be uniform in the radial direction, and further-more if and only if $V_0(r*)$ be of free vortex type, W_0 remains uniform in the radial direction; for other steady tangential velocity distribution, W_0 varies in the radial distribution even for uniform stagnation enthalpy.

If we assume that the corresponding entropy remains constant everywhere, then

$$\frac{P_0}{R_0^\gamma} = \text{constant},\tag{7-a}$$

or equivalently

$$c_p R_0 \frac{\partial \Theta_0}{\partial r*} - \frac{\partial P_0}{\partial r*} = 0.\tag{7-b}$$

Finally the radial dependence of the inviscid acoustic speed, defined as $c_p(\gamma - 1)\ \theta_0 = A_0^2$, is given by

$$[A_0(r^*)]^2 = [A_0\ (r^* = \lambda)]^2 - (\gamma - 1)\int_{r^*}^{\lambda} \frac{1}{r^*}[\nabla_0]^2\ dr^*, \qquad (8)$$

where $A_0(r^* = \lambda)$ denotes acoustic speed at the periphery of the outer wall in the co-annular duct.

The leading terms of the inner expansion, constitutes, of course, the conventional, compressible steady boundary layer equations (the second coefficient of viscosity does not show itself until the third order (Van Dyke 1962 a)). On both cylindrical surfaces, the boundary layers are rotationally symmetric and develop in the z direction. Their structures being complicated by the presence of two components of inviscid stream, swirl and axial flow, one would certainly have to rest content to derive them by such methods as adopted, for example, by Taylor (1950) for a swirl atomizer problem or the like. However, as will be shown later, in so far as we limit out attention to the leading term of acoustic streaming under the conditions where R_e is large and the steady swirl not far from its threshold value, the case of our deepest interest, the details of the steady boundary layer need not be worked out.

3.2 Linearized, Inviscid Waves

We now turn to $\vec{q}'$ of equation (2-a) and the other similar unsteady disturbances, upon which our emphasis lies.

Before ushering in the more precise formalism of the asymptotic expansion, we pave the way for it by considering, in less stringent manner, the linearized inviscid disturbances. By the usual small perturbation of equation (1) around the inviscid steady flows of Section 3.1 and <u>tentatively</u> setting

$$u' = \bar{u}(r*) e^{i(m\phi + kr_i z* - t*)}, \tag{9-a}$$

$$v' = \bar{v}(r*) e^{i(m\phi + kr_i z* - t*)}, \tag{9-b}$$

$$w' = \bar{w}(r*) e^{i(m\phi + kr_i z* - t*)}, \tag{9-c}$$

and the like, we obtain immediately

$$if\bar{\rho} + \frac{1}{r*} \frac{d}{dr*}(r*R_0\bar{u}) + \frac{im}{r*}R_0\bar{v} + ikr_i R_0\bar{w} = 0, \tag{10-a}$$

$$if\bar{u} - \frac{2}{r*}V_0\bar{v} = -\frac{1}{R_0} \frac{d\bar{p}}{dr*} + \frac{\bar{\rho}}{[R_o]^2} \frac{dP_0}{dr*}, \tag{10-b}$$

$$if\bar{v} + \frac{1}{r*} \frac{d}{dr*}(r*V_0)\bar{u} = -\frac{im}{R_0 r*}\bar{p}, \tag{10-c}$$

$$if\bar{w} + \frac{dW_0}{dr*}\bar{u} = -\frac{ikr_i}{R_0}\bar{p}, \tag{10-d}$$

$$\frac{\bar{\theta}}{\theta_0} - \frac{(\gamma - 1)}{\gamma} \frac{\bar{p}}{P_0} = 0 \, , \tag{10-e}$$

$$\bar{p} = c_p \frac{\gamma - 1}{\gamma} (\theta_0 \bar{\rho} + R_o \bar{\theta}), \tag{10-f}$$

with the boundary condition

$$\bar{u} = 0 \quad \text{at } r* = 1 \quad \text{and } r* = \lambda, \tag{10-g}$$

where

$$f(r*) = \left(-\omega + V_0 \frac{1}{r_i} \frac{m}{r*} + kW_o \right) r_i . \tag{10-h}$$

In the above, the quantities with the subscript 0 again stand for the ones of steady inviscid flow, all being functions of $r*$ only; in deriving (10-b), the radial equilibrium relation of equation (6) has been taken into account. These set of equations are idential to the ones studies by Kerrebrock (1977).

By inspection of the above, we realize at once that the real parts of u' and of all the rest oscillate with a phase difference equal to $\frac{\pi}{2}$ -- a fact first exploited by Lord Kelvin (1880) for his analysis of incompressible flow; we will use this later for the present compressible flow alike.

Of crucial importance among the foregoing equations is the fact that frequency ω does not appear by itself, but arises in the exclusive form of (10-h). That

is,

$$f(r^*) \equiv \left[-\omega + \frac{m}{r_i r^*} V_0 (r^*) + k W_0(r^*) \right] r_i$$

where m and k are wave numbers in the circumferential
and axial direction, respectively; obviously this
embodies the Doppler shift caused by the steady inviscid
swirl V_0, and the axial velocity W_0. Notice that the
shift is dependent upon the radial position r^*.

In order to obtain the acoustic streaming,
these linear disturbances are, of course, to be enforced,
as the external excitation, upon the viscous flow near
the walls; therefore, in forming parameters containing
the frequency, the relevant frequency to be used there-
in is not bare ω, but the above f, in which form it has
recommended itself.

With regard to the above set of equations
themselves, together with the boundary condition equation
(10-g), they determine the relationship between the
frequency parameter f and the steady flow field, wave
numbers and outer and inner tube radii; upon obtaining
the acoustic streaming, we shall later need such explicit
formulae. For now, instead, we proceed directly to obtain
the viscous response near the solid walls, relegating
derivation of frequency relationship to the Appendix.

4. Construction of Expansion Series and Matching

For both inner and outer cylindrical surfaces, an analysis can be carried out in the same way. To render it concrete, we choose here, as henceforth, the one near the inner cylinder located at $r^* = 1$, the other one corresponding to the outer surface being simply obtained by the obvious replacement.

Then, for the reason just stated in the preceeding section, the appropriate frequency parameter pertaining to such a study is (10-h) evaluated at $r^* = 1$, denoted as f_i:

$$f_i = f(r^* = 1) = \left(-\omega + \frac{m}{r_i} V_{ex} + k W_{ex}\right) r_i, \tag{11}$$

where subscript "ex" henceforth stands for the external flow or the leading term of the outer expansion of steady flow evaluated at $r^* = 1$: namely,

$$V_{ex} = V_0 (r^* = 1), \tag{12-a}$$

$$W_{ex} = W_0 (r^* = 1), \tag{12-b}$$

and the like; we note that they are all independent of z^* as well as ϕ (and of r^*, of course).

In characterizing the unsteady response near such
a solid surface, three dimensionless parameters dis-
tinguish themselves. The first is defined by

$$\alpha \equiv \frac{\tilde{u}}{f_i} \quad , \tag{13}$$

where $\tilde{u}$ is an amplitude parameter, a measure of
the intensity of disturbances. The second, β, is the
ratio of the unsteady boundary layer thickness $\delta^{\prime}$ to
r_i, where $\delta^{\prime}$ is defined as

$$\delta^{\prime} \equiv \left[\frac{M_{ex} r_i}{R_{ex} \mid f_i \mid} \right]^{\frac{1}{2}} \quad . \tag{14}$$

Hence,

$$\beta = \frac{\delta^{\prime}}{r_i} = \left[\frac{M_{ex}}{R_{ex} \mid f_i \mid r_i} \right]^{\frac{1}{2}} \quad . \tag{15}$$

The absolute form of f_i is needed in the above, for it can and
does switch its sign depending on the relative magnitudes
of ω and the external velocities. If $V_{ex} = W_{ex} = 0$, these
two parameters are reduced to the ones employed by Riley
(ibid.) for his investigation of streaming in the absence
of base, steady flow; there, as long as the frequency is
prescribed and held fixed, both remain obviously unchanged.
This is to be contrasted with the following present situation:
as steady flow varies, the unsteady boundary thickness $\delta^{\prime}$
changes; consequently, β does not remain the same even for

a given frequency. For example, δ' or β increases when f_i is decreased by the change in V_{ex} only. Likewise α does not remain the same.

The third and last parameter ε is a measure of relative magnitude between steady boundary layer thickness, δ to the unsteady one, δ'; the former is defined as

$$\delta = L \, R_e^{-1/2} \, , \tag{16-a}$$

in terms of the duct length, L, and where R_e, the Reynolds number, so far purposely left undefined, now denotes precisely

$$R_e \equiv \frac{W_{ex}\rho_{ex}}{M_{ex}} L \, . \tag{16-b}$$

Hence,

$$\varepsilon = \frac{\delta}{\delta'} = \frac{L}{\beta R_e^{1/2} r_i} \tag{16-c}$$

on account of equations (16-a) and (14). Recognize here that if the Reynolds number is sufficiently high, ε can indeed by a small number, in so far as we are interested in the region not too remote from the turning point to be defined later as $f_i = 0$.

Our interest is directed to the situation where α ,
β and ϵ are all small in their magnitudes. Physically
this may be considered, as follows: the amplitude of
unsteady excitation is small; and compared to the
cylinder radius, the unsteady boundary layer thickness
is thin, within which thinner steady boundary layers at
the high Reynolds number is embedded.

We name the annular region confined between the
outer edge of the unsteady boundary layer and that
of the steady boundary layer * as the "middle deck";
then, the "lower deck" naturally suggests itself as the
annular cross section between the outer edge of the steady
boundary layer and the cylindrical solid surface. The

---

*The main stream consisting of both swirl and axial
velocity, to be precise we have to take the possible pre-
sence of more than a single thickness of the steady boundary
layer into consideration (Cooke 1952). If definiteness
requires it, we may choose the thickest among them as
corresponding to the outer edge of the steady boundary
layer.

double deck structures are present near both the outer
and inner cylindrical surfaces; Figure 2 shows this
schematically and in disproportionately magnified manner.
The annulus bounded by two middle decks we call "core".

We turn now to the construction of series expansions
appropriate for each region, starting from the middle
deck.

4.1 Middle-Deck Series Expansion

Let n be a middle deck variable or inner variable, scaled to the unsteady boundary layer thickness and defined by

$$n = \frac{r^* - 1}{\beta} \quad . \tag{17}$$

We first turn to the steady flow field within the middle deck, corresponding to the first terms on the right hand side of equation (2), and express them in the following form:

$$U = W_{ex} \eta(r^*, z^*; R_e) \quad , \tag{18-a}$$

$$V = V_{ex} \left[1 + \xi(r^*, z^*; R_e)\right] \tag{18-b}$$

$$W = W_{ex} \left[1 + \zeta(r^*, z^*; R_e)\right], \tag{18-c}$$

$$R = R_{ex} \chi(r^*, z^*; R_e) \quad , \tag{18-d}$$

$$\theta = \theta_{ex} \tau(r^*, z^*; R_e), \tag{18-e}$$

$$P = R_{ex} V_{ex}^2 \psi(r^*, z^*; R_e) \quad , \tag{18-f}$$

$$M = M_{ex} \sigma(r^*, z^*; R_e), \tag{18-g}$$

$$\text{and } M^{(2)} = M_{ex} \sigma^{(2)}(r^*, z^*; R_e). \tag{18-h}$$

By definition, the middle deck lies exterior to the steady boundary layer; hence, such outer expansions of steady flow as equation (4) and (5) are applicable here. We expand ξ, η , etc., in powers of $R_e^{-1/2}$, which is proportional to $\epsilon\beta$ from equation (16-c) and obtain

$$U = W_{ex}\epsilon\beta\eta_1(r^*, z^*) + \cdots \quad , \tag{19-a}$$

$$V = W_{ex}\left[1 + \xi_0(r^*) + \epsilon\beta\xi_1(r^*, z^*) + \cdots\right] , \tag{19-b}$$

$$W = W_{ex}\left[1 + \zeta_0(r^*) + \epsilon\beta\zeta_1(r^*, z^*) + \cdots\right] \quad , \tag{19-c}$$

$$R = R_{ex}\left[\chi_0(r^*) + \epsilon\beta\chi_1(r^*, z^*) + \cdots\right] \quad , \tag{19-d}$$

$$\theta = \theta_{ex}\left[\tau_0(r^*) + \epsilon\beta\tau_1(r^*, z^*) + \cdots\right] \quad , \tag{19-e}$$

etc.,where

$$\xi_0(r^* = 1) = \zeta_0(r^* = 1) = 0; \quad \chi_0(r^* = 1) = \tau_0(r^* = 1) -- \doteq 1. \tag{19-f}$$

The last one, (19-f), follows owing to the very definition of quantities with subscript "ex". We,then,expand the leading term with subscript "0" around $r^* = 1$, make use of equation (19-f) and finally express these in terms of the

middle-deck variable n. Thus we have

$$U = W_{ex}\epsilon\beta \ \eta_1(n,z^*)+--- \quad , \tag{20-a}$$

$$V = V_{ex}\left[1 + a_1 n\beta + a_2(n\beta)^2 + --- + \epsilon\beta\xi_1(n,z^*)+---\right], \tag{20-b}$$

$$W = W_{ex}\left[1 + b_1 n\beta + b_2(n\beta)^2 + --- + \epsilon\beta\zeta_1(n,z^*)+---\right], \tag{20-c}$$

$$R = R_{ex}\left[1 + c_1 n\beta + c_2(n\beta)^2 + --- + \epsilon\beta\chi_1(n,z^*)+---\right], \tag{20-d}$$

$$\theta = \theta_{ex}\left[1 + d_1 n\beta + d_2(n\beta)^2 + --- + \epsilon\beta\sigma_1(n,z^*)+---\right], \tag{20-e}$$

and the like, where a_1, a_2, ...; b_1, b_2, ...,etc. are all constants.

For the unsteady parts, denoted with primes in equation (2), we expand them in terms of α, β and ϵ with the triple indices affixed to each term: for instance,

$$u'_{ijk}$$

where i stands for the order of α, j for β, and ϵ for k. Accordingly we write

$$u' = \tilde{u}\beta \ (u'_{000} + \alpha u'_{100} + \beta u'_{010} + \epsilon u'_{001} +---) \ , \tag{21-a}$$

$$v' = \tilde{u} \ (v'_{000} + \alpha v'_{100} + \beta v'_{010} + \epsilon v'_{001} +---) \ , \tag{21-b}$$

$$w' = \tilde{u} \ (w'_{000} + \alpha w'_{100} + \beta w'_{010} + \epsilon w'_{001} + ---) \ , \tag{21-c}$$

$$p' = \tilde{u} \ R_{ex} f_i \ (p'_{000}+ \alpha p'_{100} + \beta p'_{010} + \epsilon p'_{001} +---), \tag{21-d}$$

$$\rho' = \tilde{u} \ \frac{R_{ex}}{A_{ex}} \ (\rho'_{000} + \alpha\rho'_{100} + \beta\rho'_{010} + \epsilon\rho'_{001} +---), \tag{21-e}$$

$$\theta' = \tilde{u} \ \frac{\theta_{ex}}{A_{ex}} \ (\theta'_{000} + \alpha\theta'_{100} + \beta\theta'_{010} + \epsilon\theta'_{001} +---), \tag{21-f}$$

$$\mu' = \tilde{u} \, \frac{M_{ex}}{A_{ex}} (\mu'_{000} + \alpha\mu'_{100} + \beta\mu'_{010} + \epsilon\mu'_{001} + \text{---}) \, , \quad (21\text{-g})$$

$$\mu^{(2)'} = \tilde{u} \, \frac{M_{ex}}{A_{ex}} (\mu'_{000}{}^{(2)} + \alpha\mu'_{100}{}^{(2)} + \beta\mu'_{010}{}^{(2)} + \epsilon\mu'_{001}{}^{(2)} + \text{--}) \, ,$$

$$(21\text{-h})$$

where in the last two equations, the leading terms are related to the one of θ' on account of (1-g) as

$$\mu'_{000} = \theta'_{000} \left[\frac{d\sigma}{d\tau} \right]_{\tau=1} \, , \quad (22\text{-a})$$

$$\mu'_{000}{}^{(2)} = \theta'_{000} \left[\frac{d\sigma^{(2)}}{d\tau} \right]_{\tau=1} \, . \quad (22\text{-b})$$

The derivatives of σ and $\sigma^{(2)}$ defined in equations (18-g) and (18-h), respectively, are to be evaluated at the steady temperature corresponding to the inviscid value on the wall. Note that the leading term of u' is $O(\beta)$; the others are taken to be $O(1)$. All the first terms in the brackets with indices (0,0,0) representing linearized viscous disturbances, we express them explicitly as

$$u'_{000} = \bar{u}_{000} (n) \, e^{i(m\phi + kr_i z* - t*)} \, , \quad (23\text{-a})$$

$$v'_{000} = \bar{v}_{000} (n) \, e^{i(m\phi + kr_i z* - t*)} \, , \quad (23\text{-b})$$

$$w'_{000} = \bar{w}_{000} (n) \, e^{i(m\phi + kr_i z* - t*)} \, , \quad (23\text{-c})$$

and the like.

4.2 Core Series Expansion

In the core, r^*, is the appropriate radial coordinate or the outer variable. The expression for the steady flow, equation (20), is immediately applicable to the core as well.

For the unsteady part, we expand them in series structually similar to (21) except for u' where the leading term is now elevated from $O(\beta)$ to $O(1)$, and equal to the others. Thus we have

$$u' = \tilde{u} \, (U'_{000} + \alpha U'_{100} + \beta U'_{010} + \epsilon U'_{001} + \text{---}) \,, \qquad (24\text{-}a)$$

$$v' = \tilde{u} \, (V'_{000} + \alpha V'_{100} + \beta V'_{010} + \epsilon V'_{001} + \text{---}) \,, \qquad (24\text{-}b)$$

$$w' = \tilde{u} \, (W'_{000} + \alpha W'_{100} + \beta W'_{010} + \epsilon W'_{001} + \text{---}) \,, \qquad (24\text{-}c)$$

$$p' = \tilde{u} \, R_{ex} f_i (P'_{000} + \alpha P'_{100} + \beta P'_{010} + \epsilon P'_{001} + \text{--}). \qquad (24\text{-}d)$$

$$\rho' = \tilde{u} \, \frac{R_{ex}}{A_{ex}} \, (R'_{000} + \alpha R'_{100} + \beta R'_{010} + \epsilon R'_{001} + \text{---}), \qquad (24\text{-}e)$$

$$t' = \tilde{u} \, \frac{\Theta_{ex}}{A_{ex}} \, (\Theta'_{000} + \alpha \Theta'_{100} + \beta \Theta'_{010} + \epsilon \Theta'_{001} + \text{--}), \qquad (24\text{-}f)$$

$$\mu' = \tilde{u} \, \frac{M_{ex}}{A_{ex}} \, (M'_{000} + \alpha M'_{100} + \beta M'_{010} + \epsilon M'_{001} + \text{--}), \qquad (24\text{-}g)$$

$$\mu^{(2)'} = \tilde{u} \, \frac{M_{ex}}{A_{ex}} \, (M'_{000}{}^{(2)} + \alpha M'_{100}{}^{(2)} + \beta M'_{010}{}^{(2)} + \epsilon M'_{001}{}^{(2)} + \text{--}),$$
$$\qquad (24\text{-}h)$$

where again the leading terms of the last two equations are related to Θ'_{000}, the first term of θ', by

$$M'_{000} = \theta'_{000}\left[\frac{d\sigma}{d\tau}\right]_{\tau = \tau_0(r*)}, \tag{25-a}$$

$$M'_{000}{}^{(2)} = \theta'_{000}\left[\frac{d\sigma^{(2)}}{d\tau}\right]_{\tau = \tau_0(r*)}. \tag{25-b}$$

The derivatives are to be evaluated at the steady temperature corresponding to the inviscid value.

The leading terms represent the linearized inviscid disturbances and take the following forms:

$$U'_{000} = \bar{U}_{000}(r*)\, e^{i(m\phi + kr_i z* - t*)}, \tag{26-a}$$

$$V'_{000} = \bar{V}_{000}(r*)\, e^{i(m\phi + kr_i z* - t*)}, \tag{26-b}$$

$$W'_{000} = \bar{W}_{000}(r*)\, e^{i(m\phi + kr_i z* - t*)}, \tag{26-c}$$

etc; these correspond to equation (9) but, here and henceforth, we are denoting them by the formalized triple indices instead.

4.3 Matching between and Middle Deck and the Core

Standard matching procedures (Van Dyke, 1962 a and b) applied between the middle deck and the core expansion series yields at once the required matching condition. For u´, we have

$$U_{000}´(1,\phi,z^*,t^*)= 0 \ , \tag{27-a}$$

$$U_{001}´(1,\phi,z^*,t^*)= 0 \tag{27-b}$$

$$U_{100}´(1,\phi,z^*,t^*)= 0, \tag{27-c}$$

$$U_{010}´(1,\phi,z^*,t^*)= \lim_{n \to \infty}\left[u_{000}´(n,\phi,z^*,t^*)-\frac{\partial u_{000}´}{\partial n}\,n\right] \ . \tag{27-d}$$

The last equation represents the influence of an unsteady displacement thickness, exactly analogous to its steady counterpart (Van Dyke, ibid.). For v´, we have

$$V_{000}´\ (1,\phi,z^*,t^*)= \lim_{n \to \infty} v_{000}´(n,\phi,z^*,t^*), \tag{28-a}$$

$$V_{001}´\ (1,\phi,z^*,t^*)= \lim_{n \to \infty} v_{001}´(n,\phi,z^*,t^*), \tag{28-b}$$

$$V_{100}´\ (1,\phi,z^*,t^*)= \lim_{n \to \infty} v_{100}´(n,\phi,z^*,t^*), \tag{28-c}$$

$$V_{010}´\ (1,\phi,z^*,t^*)= \lim_{n}\left\{ v_{010}´(n,\phi,z^*,t^*)-\left[\frac{\partial V_{000}´}{\partial r^*}\right]_{r^*=1}n \right\} . \tag{28-d}$$

The identically same relationships hold for w´, p´, ρ´, and θ´. The matching for μ´ yields

$$M_{000}'(1,\phi,z^*,t^*) = \lim_{n\to\infty} \mu_{000}'(n,\phi,z^*,t^*) \ , \tag{29-a}$$

$$M_{001}'(1,\phi,z^*,t^*) = \lim_{n\to\infty} \mu_{001}'(n,\phi,z^*,t^*) \ , \tag{29-b}$$

$$M_{010}'(1,\phi,z^*,t^*) = \lim_{n\to\infty} \left\{ \mu_{010}'(n,\phi,z^*,t^*) \right.$$

$$-\left[\frac{d^2\sigma}{d\tau^2}\right]_{\tau=1} \left[\frac{d\tau_0}{dr^*}\right]_{r^*=1} n \ \theta_{000}(1,\phi,z^*,t^*)$$

$$\left. -\left[\frac{d\sigma}{d\tau}\right]_{\tau=1} \left[\frac{\partial\theta_{000}'}{\partial r^*}\right]_{r^*=1} n \right\} \quad . \tag{29-c}$$

The same matching conditions hold for $\mu^{(2)}$.

4.4 Lower Deck and the Transfer of Boundary Conditions

Even in the lower deck, the appropriate radial variable is "n" introduced in equation (17). Complications arise, however, in the lower deck due to the steady flow field immersed in its entirety within the steady boundary layer, whose structural complexity has already been mentioned in Section 3.1. Though rotationally symmetric, not only does the steady profile change radially from the solid wall to the outer edge of the steady boundary layer but also, owing to its axial development, it is dependent on the z coordinate as well; due to the presence of both swirl and axial flow in the main stream, the steady flow field is fully three-dimensional; it is through this that the unsteady disturbances propagate.

One can circumvent this difficulty associated with the lower deck by transferring the boundary condition on the solid wall to the inner edge of the middle deck; such bypassing is valid for terms like (0,0,0), (0,1,0) and (1,0,0) but not for (0,0,1). Take, for example, v' . We compare its exact solution denoted as $v'^{(e)}$, assumed to be somehow known in both middle and lower decks, with the present one for the middle deck, denoted here temporarily as $v'^{(md)}$. Then at the inner edge of the middle deck located at $n = \varepsilon(z^*)$, we have

$$v'^{(e)}(n = \varepsilon(z^*), z^*, \phi, t^*) = v'^{(md)}(n = \varepsilon(z^*), z^*, \phi, t^*).$$

Substitute equation (21-b) into the right hand side and expand both sides around $n = 0$. Then from the no slip condition on the wall, the left hand side becomes $O(\varepsilon)$ and the right hand side yields

$$v'_{000} = v'_{010} = v'_{100} = 0 \qquad \text{at } n = 0. \tag{30}$$

Although not so with v'_{001}, this will not present difficulty as far as the leading term of the streaming is concerned. Exactly identical relationships can be derived for u' and w' (For the former, match $\beta u'^{(e)}$ with its middle deck counterpart, equation (21-a).) Likewise, for the thermal condition where the unsteady temperature on the wall is maintained to be zero, we have

$$\theta'_{000} = \theta'_{010} = \theta'_{100} = 0 \qquad \text{at } n = 0, \tag{31}$$

but $\quad \theta'_{001} \neq 0;$

for the thermally insulated wall

$$\frac{\partial \theta'_{000}}{\partial n} = \frac{\partial \theta'_{010}}{\partial n} = \frac{\partial \theta'_{100}}{\partial n} = 0 \qquad \text{at } n = 0, \tag{32}$$

but $\quad \dfrac{\partial \theta'_{001}}{\partial n} \neq 0.$

5. Hierarchic Structure of Expansion Series: "Family Tree"

Substitution of the expansion series in the preceeding Section 4 into equation (1) yields sets of equations appropriate for each order. In this section, we assemble them in hierarchic order, and describe their salient features before presenting the details of the solution.

5.1 (0,0,0) Core

The set of equations is given by:

$$\left\{ 1 + m\frac{V_{ex}}{f_i}\left[\xi_0 - \frac{r^*_{-1}}{r^*}(1+\xi_0)\right] + \frac{kr_iW_{ex}}{f_i}\zeta_0 \right\} i\bar{R}_{000}$$

$$+ \frac{A_{ex}}{f_i}\left\{ \frac{1}{r^*}\frac{d}{dr^*}\left[r^*\chi_0\bar{U}_{000}\right] + \frac{im}{r^*}\chi_0\bar{V}_{000} + ikr_i\chi_0\bar{W}_{000} \right\} = 0,$$

$$(33\text{-}a)$$

$$\chi_0\left\{ i\bar{U}_{000} + im\frac{V_{ex}}{f_i}\left[\xi_0 - \frac{r^*_{-1}}{r^*}(1+\xi_0)\right]\bar{U}_{000} + \frac{ikr_iW_{ex}}{f_i}\zeta_0\bar{U}_{000} \right.$$

$$\left. - \frac{2V_{ex}}{f_i}\frac{1}{r^*}(1+\xi_0)\bar{V}_{000} \right\} - \frac{V_{ex}^2}{f_iA_{ex}}\frac{1}{r^*}\bar{R}_{000}(1+\xi_0)^2$$

$$= -\frac{d\bar{P}_{000}}{dr^*} , \qquad (33\text{-}b)$$

$$\chi_0\left\{ i\bar{V}_{000} + im\frac{V_{ex}}{f_i}\left[\xi_0 - \frac{r^*_{-1}}{r^*}(1+\xi_0)\right]\bar{V}_{000} + \frac{ikr_iW_{ex}}{f_i}\zeta_0\bar{V}_{000} \right.$$

$$\left. + \frac{V_{ex}}{f_i}\bar{U}_{000}\frac{\partial\xi_0}{\partial r^*} + \frac{V_{ex}}{f_i}\frac{1+\xi_0}{r^*}\bar{U}_{000} \right\} = -\frac{im}{r^*}\bar{P}_{000},$$

$$(33\text{-}c)$$

$$\chi_0\left\{ i\bar{W}_{000} + im\frac{V_{ex}}{f_i}\left[\xi_0 - \frac{r^*_{-1}}{r^*}(1+\xi_0)\right]\bar{W}_{000} + \frac{ikr_iW_{ex}}{f_i}\zeta_0\bar{W}_{000} \right.$$

$$\left. + \frac{W_{ex}}{f_i}\frac{\partial\zeta_0}{\partial r^*}\bar{U}_{000} \right\} = -ikr_i\bar{P}_{000} , \qquad (33\text{-}d)$$

$$\chi_0\bar{\Theta}_{000} - \frac{f_i}{A_{ex}}(\gamma-1)\bar{P}_{000} = 0 , \qquad (33\text{-}e)$$

$$\frac{f_i}{A_{ex}}\gamma\bar{P}_{000} = \tau_0\bar{R}_{000} + \chi_0\bar{\Theta}_{000}. \qquad (33\text{-}f)$$

with the boundary condition

$$\overline{U}_{000}(r^* \overset{*}{=} 1) = 0, \tag{33-g}$$

and the similar condition to be satisfied on the outer cylinder.

This set of equations, once restored in the original variables, is identical to equation (10) corresponding to the linearized, inviscid disturbance. They are complete, independent of (0,0,0) of the middle deck or any other higher order equations. They being treated in detail in the Appendix, we do not deal with them any more here.

5.2 (0,0,0) Middle Deck

The set of equations is given by:

$$i\bar{\rho}_{000} + \frac{A_{ex}}{f_i}\left[\frac{d\bar{u}_{000}}{dn} + im\bar{v}_{000} + ikr_i\bar{w}_{000}\right] = 0, \qquad (34\text{-}a)$$

$$i\bar{v}_{000} = i\bar{V}_{000}(\overset{*}{r}=1) \pm \frac{d^2\bar{v}_{000}}{dn^2}, \qquad (34\text{-}b)$$

$$i\bar{w}_{000} = \frac{ikr_i}{m}\bar{V}_{000}(\overset{*}{r}=1) \pm \frac{d^2\bar{w}_{000}}{dn^2}, \qquad (34\text{-}c)$$

$$i\bar{\theta}_{000} + i\frac{f_i}{mA_{ex}}(\gamma-1)\bar{V}_{000}(\overset{*}{r}=1) = \pm\frac{1}{P_r}\frac{d^2\theta_{000}}{dn^2}, \qquad (34\text{-}d)$$

$$-\frac{f_i}{mA_{ex}}\gamma\bar{V}_{000}(\overset{*}{r}=1) = \bar{\rho}_{000} + \bar{\theta}_{000}, \qquad (34\text{-}e)$$

where $\pm$ corresponds to $f_i > 0$ or $f_i < 0$, respectively.
The boundary conditions are:

$$\bar{u}_{000} = \bar{v}_{000} = \bar{w}_{000} = 0, \qquad \text{at } n = 0 \qquad (34\text{-}f)$$

$$\bar{\theta}_{000} = 0, \quad \text{or} \quad \frac{d\bar{\theta}_{000}}{dn} = 0, \quad \text{at } n = 0 \qquad (34\text{-}g)$$

$$\bar{v}_{000}(n=\infty) = \bar{V}_{000}(\overset{*}{r}=1), \qquad (34\text{-}h)$$

$$\bar{w}_{000}(n=\infty) = \frac{kr_i}{m}\bar{V}_{000}(\overset{*}{r}=1), \qquad (34\text{-}i)$$

$$\bar{\theta}_{000}(n=\infty) = -\frac{f_i}{mA_{ex}}(\gamma-1)\bar{V}_{000}(\overset{*}{r}=1), \qquad (34\text{-}j)$$

$$\bar{\rho}_{000}(n=\infty) = -\frac{f_i}{mA_{ex}}\bar{V}_{000}(\overset{*}{r}=1), \qquad (34\text{-}k)$$

$$\bar{P}_{000}(n=\infty) = -\frac{1}{m}\bar{V}_{000}(\overset{*}{r}=1), \qquad (34\text{-}l)$$

In the above, the radial component of the equation of motion

$$\frac{d\bar{P}_{000}}{dn} = 0,$$

has been spent, upon combining with (0,0,0) order of core equations, to replace the pressure terms on the right hand with the inviscid tangential velocity on the wall, $\bar{V}_{000}(r\overset{*}{=}1)$. Once $\bar{V}_{000}(r\overset{*}{=}1)$ is specified, the set is complete and can be determined independently of any other orders. Absent from them are the influences of varying steady flow field, curvature, the second coefficient of viscosity or any other higher-order effect to boundary layer theory. In fact, they are nothing but those of a conventional compressible, unsteady boundary layer, rendered into linearized form. Convective terms being eliminated, the equations are described relative to a helically moving frame of reference: a coordinate in screw motion, revolving with the inviscid swirl V_{ex} and, at the same time, advancing with the inviscid axial velocity W_{ex}.

5.3 (1,0,0) Middle Deck -- Streaming Part

By taking the temporal average of (1,0,0) order of the middle deck, we obtain the equations which will turn out to be the leading terms of streaming. We first list the ones corresponding to continuity, tangential and axial momentum and energy, setting aside, for the time being, radial momentum and equations of state:

$$\frac{A_{ex}}{f_i} \frac{\partial \langle u'_{100} \rangle}{\partial n} + \frac{\partial}{\partial n} \langle \rho'_{000} \cdot u'_{000} \rangle = 0, \qquad (35\text{-a})$$

$$\frac{\partial}{\partial n} \langle u'_{000} \cdot v'_{000} \rangle = \pm \left[\frac{\partial^2}{\partial n^2} \langle v'_{100} \rangle + \frac{f_i}{A_{ex}} \frac{\partial}{\partial n} \left(\left\langle \mu'_{000} \frac{\partial v'_{000}}{\partial n} \right\rangle \right) \right], \qquad (35\text{-b})$$

$$\frac{\partial}{\partial n} \langle u'_{000} \cdot w'_{000} \rangle = \pm \left[\frac{\partial^2}{\partial n^2} \langle w'_{100} \rangle + \frac{f_i}{A_{ex}} \frac{\partial}{\partial n} \left(\left\langle \mu'_{000} \frac{\partial w'_{000}}{\partial n} \right\rangle \right) \right], \qquad (35\text{-c})$$

$$\left\langle u'_{000} \frac{\partial \theta'_{000}}{\partial n} \right\rangle + \left\langle v'_{000} \frac{\partial}{\partial \phi} \left(\theta_{000} - (\gamma-1) \frac{f_i}{A_{ex}} P'_{000} \right) \right\rangle$$

$$+ \left\langle w'_{000} \frac{\partial}{\partial z*} \left(\theta'_{000} - (\gamma-1) \frac{f_i}{A_{ex}} P'_{000} \right) \right\rangle$$

$$+ \frac{f_i}{A_{ex}} \left\langle \rho'_{000} \cdot \text{Real} \left[i \overline{\theta}_{000} e^{i(m\phi + kr_i z* - t*)} \right] \right\rangle$$

$$= \pm \frac{1}{P_r} \left[\frac{\partial^2}{\partial n^2} \langle \theta'_{100} \rangle + \frac{f_i}{A_{ex}} \frac{\partial}{\partial n} \left(\left\langle \mu'_{000} \frac{\partial \theta'_{000}}{\partial n} \right\rangle \right) \right]$$

$$\pm (\gamma-1) \frac{f_i}{A_{ex}} \left[\left\langle \left(\frac{\partial w'_{000}}{\partial n} \right)^2 \right\rangle + \left\langle \left(\frac{\partial v'_{000}}{\partial n} \right)^2 \right\rangle \right], \qquad (35\text{-d})$$

where $\langle\ \rangle$ denotes the temporal average and $\pm$ corresponds to either $f_i > 0$ or $f_i < 0$. The boundary conditions are as follows:

$$\langle u'_{100}\rangle = \langle v'_{100}\rangle = \langle w'_{100}\rangle = 0 \quad \text{at } n = 0, \tag{35-e}$$

$$\langle \theta'_{100}\rangle = 0 \quad \text{or} \quad \left\langle \frac{\partial \theta'_{100}}{\partial n}\right\rangle = 0 \quad \text{at } n = 0, \tag{35-f}$$

and for $n \to \infty$,

$$\lim_{n\to\infty} \frac{\partial \langle v'_{100}\rangle}{\partial n} = \lim_{n\to\infty} \frac{\partial \langle w'_{100}\rangle}{\partial n} = \lim_{n\to\infty} \frac{\partial \langle \theta'_{100}\rangle}{\partial n} = 0 \ . \tag{35-g}$$

As for the boundary condition for $n \to \infty$, the original matching condition for v'_{100} reads

$$\langle v'_{100}\rangle_{n\to\infty} = \langle V'_{100}\rangle^{*}_{r=1}$$

and streaming in the core will be in need of this; for now, as usual (Riley, ibid.; Batchelor 1967, p.360.) the weaker condition $\langle v'_{100}\rangle_{n\to\infty}$ = finite or equivalently $\frac{\partial \langle v'_{100}\rangle}{\partial n} \to 0$ as $n \to \infty$ suffices; the similar conditions apply to w'_{100} and θ'_{100}; as for u'_{100}, one does not need any condition at $n \to \infty$.

$\langle u'_{100}\rangle, \langle v'_{100}\rangle$, $\langle w'_{100}\rangle$ and $\langle \theta'_{100}\rangle$ are completely and uniquely determined in the middle deck from the above. These d.c. components of velocity and temperature field are dependent upon only $(0,0,0)$ order in the middle deck and they are independent, among others, of the streaming part for $(1,0,0)$ in the core; on the other hand, the latter will be dependent upon the former. This holds regardless of the magnitude of the streaming Reynolds number, R_s .

The sequential dependence on these is depicted schematically in Figure 3 as a "family tree" of streaming (applicable to d.c. component of temperature as well).

The set of the foregoing equations, (35), is independent of variations in the steady state and of both steady and unsteady displacement effects. They are independent of curvature effect, as can be readily recognized by re-expressing them first in terms of the conventional boundary layer coordinates and identifying them as time-averaged forms of the boundary layer equations, where the second-order terms of the unsteady disturbances are retained: The issue of curvature effect was first raised by Stuart (ibid.) who also justified its neglect, irrespective of the value of R_s, on physical grounds and Riley (ibid.) confirmed this afresh by a matched asymptotic expansion.

Observe in (35-b) and (35-c) the presence of terms in the form of $\mu'_{000} \frac{\partial v_{000}}{\partial n}$, which correspond to the Reynolds stresses, generated by the fluctuation of viscosity responding to the unsteadiness in the temperature μ'_{000} and coupled with the temporal oscillation of the strain $\frac{\partial v_{000}}{\partial n}$; likewise in (35-d) the term $\mu'_{000} \frac{\partial \theta'_{000}}{\partial n}$ represents the heat flux caused by a similar fluctuation of thermal conductivity and temperature gradient.

In contrast with the d.c. component of velocity and temperature, the temporal averages of pressure and density, $\langle p'_{100} \rangle$ and $\langle \rho'_{100} \rangle$, respectively, can not be determined from the following equations and boundary

conditions alone, which have been intentionally held over so far:

$$\frac{\partial}{\partial n} \langle P'_{100} \rangle = 0 \ , \tag{35-h}$$

$$\gamma \frac{f_i}{A_{ex}} \langle P'_{100} \rangle = \langle \rho'_{100} \rangle + \langle \theta'_{100} \rangle + \frac{f_i}{A_{ex}} \langle \rho'_{000} \theta'_{000} \rangle \tag{35-i}$$

with

$$\lim_{n \to \infty} \langle \rho'_{100} \rangle = \langle R'_{100} \rangle^*_{r=1} \ \text{and} \ \lim_{n \to \infty} \langle P'_{100} \rangle = \langle P'_{100} \rangle^*_{r=1}.$$

They need to be matched with the corresponding ones in the core.

5.4 (1,0,0) Core - Streaming Part

In the core, $(1,0,0)$ streaming is driven by
the streaming of the same order in the middle deck--
regardless of the value of R_s, no matter how large or small. As
is now well know, the structure of streaming outside of the un-
steady boundary layer is, however, strongly dependent
upon R_s, as pointed out first by Stuart (1963, p. 384)
and subsequently confirmed explicitly by such experiments
as for a cylinder oscillating in otherwise stationary
fluid (Bertelsen, 1974).

If we take simply the temporal average of
equations of the order of $(1,0,0)$ in the core, they
correspond to the case of $R_s \ll 1$ and are given by:

$$\langle U_{100}' \rangle = 0, \qquad (36\text{-a})$$

$$-\chi_0 \frac{V_{ex}}{f_i} \frac{2}{r*} (1 + \xi_0) \langle V_{100}' \rangle - \frac{V_{ex}^2}{f_i A_{ex}} \frac{1}{r*}(1 + \xi_0)^2 \langle R_{100}' \rangle$$

$$+ \frac{1}{r*} \frac{\partial}{\partial r*}\left[r* \chi_0 \langle U_{000}'^2 \rangle \right]$$

$$- \frac{1}{r*}\chi_0 \langle V_{000}'^2 \rangle - 2 \frac{V_{ex}}{A_{ex}} (1 + \xi_0) \langle R_{000}' \cdot V_{000}' \rangle$$

$$= - \frac{\partial}{\partial r*} \langle P_{100}' \rangle, \qquad (36\text{-b})$$

$$\frac{f_i}{A_{ex}} \gamma \langle P_{100}' \rangle = \tau_0 \langle R_{100}' \rangle + \chi_0 \langle \Theta_{100}' \rangle + \frac{f_i}{A_{ex}} \langle R_{000}' \cdot \Theta_{000}' \rangle ,$$

$$\text{(36-c)}$$

with boundary conditions

$$\langle V_{100}' \rangle_{r*=1} = \lim_{n \to \infty} \langle v_{100}' \rangle \qquad \text{(36-d)}$$

$$\langle W_{100}' \rangle_{r*=1} = \lim_{n \to \infty} \langle w_{100}' \rangle , \qquad \text{(36-e)}$$

$$\langle \Theta_{100}' \rangle_{r*=1} = \lim_{n \to \infty} \langle \theta_{100}' \rangle , \qquad \text{(36-f)}$$

together with the similar boundary conditions to be satisfied on the outer cylinder surface. In deriving these, we have made use of the phase properties of $(0,0,0)$ order of the core flow, already referred to in Section 3.2.

Missing from the above set is the energy equation, which vanishes identically by virtue of equations (7-b), (33-e) and (33-f): the equation of continuity and the momentum equations in ϕ and z directions, they all collapse to yield (36-a).

Viscous terms being also absent in the above momentum equations, they are of inviscid type. The boundary conditions (36-d) and (36-e) correspond, however, to the non-slip ones on the "walls: they are set in spiralling motion by streaming in the middle deck and to the prescribed surface temperature of (36-f). Then, not only some of the equations are lacking, but due to their

depressed order, ostensibly they do not satisfy the
boundary conditions. The latter is, however, not an
indication of some kind of breakdown, but the missing
ones are to be supplied from the terms of higher order
than the present $(1,0,0)$. That this is so can be illu-
strated by referring to the streaming induced by fluc-
tuation in incompressible flow, which is otherwise at
rest. For $V_{ex} = 0$, (36-b) is reduced to

$$\frac{1}{r*} \frac{\partial}{\partial r*} \left[r* \chi_0 \langle U_{000}'^2 \rangle \right] - \frac{1}{r*} \chi_0 \langle V_{000}'^2 \rangle = - \frac{\partial}{\partial r*} \langle P_{100}' \rangle , \quad (37)$$

and we note that $\langle V_{100}' \rangle$ or the tangential velocity is
now completely lost from this or, for that matter, from
everywhere else. It can be recovered only from the con-
sideration of viscous terms of $(1,2,0)$ order, a higher order
term in the expansion series: after some algebra, we
obtain

$$\frac{\partial}{\partial r*} \left\{ \frac{\partial}{\partial r*} \left[r* \frac{\partial \langle V_{100}' \rangle}{\partial r*} \right] - \frac{\langle V_{100}' \rangle}{r*} \right\} = 0 . \quad (38)$$

Introducing a time-averaged stream function
$\langle \Psi_{100}' \rangle$ which satisfies
$$\langle V_{100}' \rangle = \frac{\partial \langle \Psi_{100}' \rangle}{\partial r*} , \quad (39)$$

We may express the above as

$$\langle \nabla^4 \, \Psi_{100}' \rangle = 0, * \tag{40}$$

since any derivatives of $\langle \Psi_{100}' \rangle$ with regard to ϕ are
zero; the biharmonic equation is originally due to
Rayleigh (ibid., 4 lines above his equation (23)) and de-
rived anew by Riley (ibid) by matched asymptotic expan-
sions.

The foregoing illustrates the fact that higher-
order series terms in expansion scheme are needed, in
general, to determine the present (1,0,0) order stream-
ing in the core; this presents the entanglement of the
formidable backward linking between terms in series,
as opposed to more direct forward linking.

The presence of the backward linking is explicitly
brought out here, since several investigators, without
recourse to the apparatus of the matched asymptotic ex-
pansion, seem to have unfortunately erred on this score

---

* To avoid any false misconception, we take heed of the fact that
although the streaming satisfies the biharmonic equation,
it is not the Stokes flow in the sense that the inertia terms
are nil; instead, the inertia terms are comprised of lower
order terms as seen from equation (37).

by matching the exterior streaming, obtained from the inviscid equations expressed only to the second order of disturbances,with the one derived from viscous consideration near the solid boundary.

We turn now to the case or $R_s \gg 1$. The fundamental equation governing the exterior streaming for this was established by Riley (ibid.) for incompressible flow in an otherwise state of rest; it corresponds to the full Navier-Stokes equations for steady flow, where R_s replaces the Reynolds number and plays its role. Thus in order to conquer it, nothing short of wholly numerical computation (Duck and Smith, 1979; Haddon and Riley, 1979) seem to be effective.

In view of these complications, we shall not attempt to obtain streaming in the core, being content instead that the phenomena of our interest can be explained, as seen shortly, by inspecting the behavorial change in streaming at the outer edge of the middle deck, whose lead the streaming in the core follows.

5.5 Others

Although the remainder of the series will not
contribute to the leading term of acoustic streaming, we
record here, for the sake of completeness, their main
features.

For the time-variant part of (1,0,0) order, the
situation is different from the preceeding streaming part;
that is, contrary to the latter, the former in the core
is determined completely by the (0,0,0)term in the core and it is
of inviscid and non-heat conducting type; it is indepen-
dent of its counterpart in the middle deck or the time-variant
part of (1,0,0) order which is, in turn, dependent on the
time-variant part of (1,0,0) order in the core.

(0,1,0) series in the core is affected directly
by (0,0,0) order in the middle deck and independent of
its own counterpart in the middle deck; the boundary
conditions represent an instantaneous displacement effect
for the unsteady boundary layer and this turns out to be
non-zero.

For (0,1,0) order in the middle deck, the
pressure gradient in the direction normal to the boundary
layer is no longer equal to zero, it being balanced in-
stead by a centrifugal force related to the local curva-
ture; the second coefficient of viscosity is still missing
therein and all these features are analogous to the
second-order theory of the steady boundary layer (Van Dyke

1962 a, ibid.). In addition, the influence of radial variation in steady flow field appears for the first time in the unsteady boundary layer equations.

All these, including (0,0,1) series, possess sinusoidal time-dependences;hence, once time-averaged, they all vanish, leaving the streaming part of (1,0,0) order as the leading term.

6. Solutions in the Middle Deck

We now present solutions in the middle deck.
Consider at first the case corresponding to the thermal
boundary condition where the fluctuation of temperature is
maintained to be zero on the wall.

From equation (34), by straightforward calculation
solutions for (0,0,0) order in the middle deck follow
at once:

$$\bar{u}_{000} = im\, \bar{V}_{000}\, (r_*=1) \left\{ \frac{1}{\Delta} \left[1 + \left(\frac{kr_i}{m}\right)^2 \right] \left[1 - \exp(-\Delta n) \right] \right.$$
$$+ \left(\frac{f_i}{A_{ex}{}^m}\right)^2 \frac{\gamma-1}{Pr^{1/2}\Delta} \left[1 - \exp(-Pr^{1/2}\Delta n) \right]$$
$$\left. + n \left[\left(\frac{f_i}{A_{ex}{}^m}\right)^2 - 1 - \left(\frac{kr_i}{m}\right)^2 \right] \right\} , \qquad (41\text{-}a)$$

$$\bar{v}_{000} = \bar{V}_{000}\, (r_*=1) \left[1 - \exp(-\Delta n) \right] , \qquad (41\text{-}b)$$

$$\bar{w}_{000} = \frac{kr_i}{m} \bar{V}_{000}(r_*=1)\left[1 - \exp(-\Delta n) \right] , \qquad (41\text{-}c)$$

$$\bar{\rho}_{000} = -\frac{f_i}{A_{ex}{}^m} \bar{V}_{000}(r_*=1)\left[1 + (\gamma-1)\exp(-Pr^{1/2}\Delta n) \right] , \qquad (41\text{-}d)$$

$$\bar{P}_{000} = -\frac{1}{m} \bar{V}_{000}(r_*=1), \qquad (41\text{-}e)$$

$$\bar{\theta}_{000} = -\frac{f_i}{A_{ex}{}^m} (\gamma-1) \bar{V}_{000}(r_*=1)\left[1 - \exp(-Pr^{1/2}\Delta n) \right] , \qquad (41\text{-}f)$$

$$\bar{\mu}_{000} = -\left[\frac{d\sigma}{d\tau}\right]_{\tau=1} \frac{f_i}{A_{ex}{}^m} (\gamma-1) \bar{V}_{000}(r_*=1)\left[1 - \exp(-Pr^{1/2}\Delta n) \right],$$
$$(41\text{-}g)$$

where $\Delta = \dfrac{1}{\sqrt{2}} (1 \pm i)$ and $\pm$ corresponds to $f_i > 0$ or $f_i < 0$, respectively.

Our principal formula , the streamings at the outer edge of the middle deck near the inner cylinder is immediately obtained from equation (35-b). To render the final expressions explicit, we need, in m_{000} terms, the specific relationship between viscosity and the temperature. For this we choose the Sutherland's formula:

$$\mu = \mu^* \left(\frac{\theta}{\theta^*}\right)^{3/2} \frac{\theta^* + s_1}{\theta + s_1} \, ,$$

where μ^* is the viscosity at the reference temperature θ^*, and s_1, is $114^\circ K$ for air. Then, the tangential streaming at $n \to \infty$ or at the outer edge of the middle deck near the inner cylinder is given, with the original r restored in place of r^*, as

$$\langle v' \rangle_i = \frac{\left[\tilde{u} \, \bar{V}_{000}(r=r_i)\right]^2 m}{2r_i \left[\omega - \frac{m}{r_i} V_{ex}(r=r_i) - kW_{ex}(r=r_i)\right]}$$

$$\times \left\{ \frac{3}{2} \left[1 + \left(\frac{kr_i}{m}\right)^2\right] - G + \frac{(\gamma-1)}{Pr(Pr+1)} G \right.$$

$$\left. - (\gamma-1) \frac{Pr}{Pr+1} G \left[\frac{3}{2} - \frac{\theta_{ex}(r=r_i)}{\theta_{ex}(r=r_i) + s_1}\right] \right\} \, , \qquad (42\text{-a})$$

where $G = \left[\dfrac{r_i(\omega - \frac{m}{r_i} V_{ex}(r=r_i) - kW_{ex}(r=r_i)}{mA_{ex}(r=r_i)}\right]^2 .$ $\qquad (42\text{-b})$

This we regard as one of our central results.

Here, once again, we recall the following meaning of notations appearing in the above: $\tilde{u}\,\bar{V}_{000}(r=r_i)$ is the amplitude, on the wall $r = r_i$, of the tangential component of "inviscid" linearized disturbance, their wave structure being in the form of $e^{i(m\phi + kz - \omega t)}$; V_{ex}, W_{ex}, A_{ex} and θ_{ex} are the steady "inviscid" tangential, axial velocity, sound speed, and temperature respectively, all evaluated on the inner wall; Pr is the Prandl number γ, the ratio of specific heats and $s_1, 114^{\circ}K$.

From equation (35-c), the axial streaming is given likewise by

$$\langle w'\rangle_i = \frac{\left[\tilde{u}\,\bar{V}_{000}(r=r_i)\right]^2 k}{2\left[\omega - m\,\dfrac{V_{ex}(r=r_i)}{r_i} - kW_{ex}(r=r_i)\right]}$$

$$\times \left\{\frac{3}{2}\left[1 + \left(\frac{kr_i}{m}\right)^2\right] - G + (\gamma-1)\,\frac{G}{Pr(Pr+1)}\right.$$

$$\left. - (\gamma-1)\,\frac{Pr}{Pr+1}\,G\left[\frac{3}{2} - \frac{\theta_{ex}(r=r_i)}{\theta_{ex}(r=r_i)+s_1}\right]\right\}.$$

$$(43)$$

The streaming in the tangential and axial direction is observed to be independent of viscosity, as to be expected. To our end, we need not correct for the Stokes drift. We also emphasize that the expression is not restricted to any specific, radial profile of the steady flow field.

The radial streaming is given, from equation (35-a),

$$\langle u'\rangle_i = \left[2N_{ex}(r=r_i)|\omega - \frac{mV_{ex}(r=r_i)}{r_i} - kW_{ex}(r=r_i)|\right]^{1/2} \left[\frac{uV_{000}(r=r_i)}{2A_{ex}(r=r_i)}\right]^2$$

$$\times \left\{ 1 + \left(\frac{kr_i}{m}\right)^2 + (\gamma-1)\frac{1}{Pr^{1/2}}G\right\} , \qquad (44)$$

where $N_{ex}(r=r_i)= \dfrac{M_{ex}(r=r_i)}{R_{ex}(r=r_i)}$.

$N_{ex}(r=r_i)$ being the steady "inviscid" kinematic viscosity on the inner wall; the radial streaming is now dependent upon viscosity.

For the thermally insulated wall, the results can formally be obtained from the above by letting $P_r \to \infty$. That is, for tangential streaming, we have

$$\langle v'\rangle_i = \frac{\left[\tilde{u}\,\bar{V}_{000}(r=r_i)\right]^2 m}{2r_i\left[\omega - \frac{m}{r_i}V_{ex}(r=r_i)-kW_{ex}(r=r_i)\right]}$$

$$\times\left\{ \frac{3}{2}\left[1 + \left(\frac{kr_i}{m}\right)\right]^2 - G - (\gamma-1)G\left[\frac{3}{2} - \frac{\theta_{ex}(r=r_i)}{\theta_{ex}(r=r_i)+s_1}\right]\right\} ,$$

$$(45)$$

and the like.

The foregoing expression (42) or (45) for the tangential streaming embraces the well-known results as its special cases. In the present representation of disturbances, $e^{i(m\phi+kz-\omega t)}$, let k = 0 and in the place of ϕ , introduce

the circumferential distance x measured along the
perimeter of the cylinder. Then the disturbance may
be regarded as a plane wave traveling in the x direction;
that is, $e^{i(\ell x - \omega t)}$ where $\ell = m/r_i$. Moreover, con-
sider the fluid otherwise in a state of rest; then,
$V_{ex} = W_{ex} = 0$ and A_{ex} and Θ_{ex} are uniform. If the fluid
is incompressible, G vanishes by taking $A_{ex} \to \infty$ and
equation (42) or (45) condenses to

$$\langle v' \rangle = \frac{3}{4} (\tilde{u}\, \bar{V}_{000})^2 \frac{\ell}{\omega} \ . \tag{46}$$

This is but a classical result of streaming at the outer
edge of an unsteady shear layer (e.g. Bachelor, ibid.,p.360).
On the other hand, if the fluid is compressible, G is
easily shown to be unity and we obtain, for example,
from equation (45) for the thermally insulated wall

$$\langle v' \rangle = \frac{(\tilde{u}\, \bar{V}_{000})^2}{4A_{ex}} \left\{ 1 - (\gamma-1) \left(3 - \frac{2\Theta_{ex}}{\Theta_{ex} + s_1} \right) \right\} \ , \tag{47-a}$$

where in A_{ex} and Θ_{ex}, the spatial dependence is now suppressed.
The second term in the curly bracket corresponds to the
streaming induced by the Reynolds stresses which are
caused by the variation of viscosity in response to tem-
perature fluctuation, coupled with the unsteady change in
strain. Numerically, this is by no means small; for

instance, at $\Theta_{ex}= 20^{O}C = 293^{O}K$, it is equal to 0.62 , as compared to unity of the first term. This notwithstanding, if we choose to ignore it, the above becomes

$$<v'> = \frac{(\tilde{u}\,\bar{V}_{000})^2}{4A_{ex}} ,$$ (47-b)

which is also a classical result for compressible flow (e.g. Lighthill, 1978 b, p. 347).

Returning to the equation (42) or (45) for the tangential streaming in swirling flow, of utmost importance to our objective is the presence of the Doppler effect in the form of

$$\omega - \frac{m}{r_i}\,V_{ex}(r=r_i) - kW_{ex}(r=r_i)$$

in the denominantor. Surely, then, this reveals that the tangential streaming can reverse its direction around turning points defined by

$$\omega - \frac{m}{r_i}\,V_{ex}(r=r_i) - kW_{ex}(r=r_i) = 0 .$$ (48)

And at the same time, the absolute magnitude of streaming tends to become increased as such a point is approached; the axial streaming also exhibits the same features while the radial streaming does not.

We proceed to discuss this turning point in more detail in the next section.

7. Turning Points, Threshold Swirl
   and Energy Separation

We define the threshold swirl as the steady tangential velocity which corresponds to the turning point; that is, $V_{ex}(r=r_i)$ which satisfies equation (48). This is determined by the competition between frequency, axial velocity and wave numbers of linear disturbances. They are interwoven with each other by the boundary condition for linear waves, equation (10-g). The explicit representations of such relationships demand the complete specification of the radial profile of swirl, their derivation for a given swirl being offered in the Appendix. By making reference to them, first we discuss the threshold swirl where the radial steady profile is of free vortex type confined within an annulus; then we consider Rankine and forced vortices occupying a single tube.

7.1 Free Vortex between Co-annular Cylinders

Here our "inviscid" velocity profile takes the following form:

$$U_0 = 0, \qquad\qquad (49\text{-}a)$$

$$V_0(r) = \frac{\Gamma}{r}, \qquad\qquad (49\text{-}b)$$

$$W_0 = \text{constant}, \qquad\qquad (49\text{-}c)$$

for $r_i < r < r_o$. The last condition satisfies the radial uniformity of stagnation enthalpy, as discussed in Section 3.1.

The relationship between the frequency and the above inviscid velocity profile, an aforementioned prequisite for the determination of the threshold swirl, is obtainable numerically in the manner described in (a) of the Appendix. Let

$$M_\phi = \frac{\Gamma}{A_{ex}(r = r_o) r_i}, \qquad\qquad (50)$$

$$\chi_n = \frac{(\omega - k W_{ex}) r_i}{A_{ex}(r = r_o)}, \qquad\qquad (51)$$

$$\kappa = k r_i . \qquad\qquad (52)$$

The first is the swirl Mach number referred to the "inviscid" acoustic speed at the outer cylinder radius, $A_{ex}(r = r_o)$; the second, a dimensionless frequency parameter where the

suffix n stands for the order of the radial mode. Then,

illustrated in Figure 4 (a) - (d) as the solid lines, are the thus

computed curves of χ_0 corresponding to the lowest eigen-

value or the first radial mode, drawn as functions of M_ϕ

for the various radius ratios λ; the tangential modes corres-

pond to the first (m=1) and the second (m=2) and $\kappa = 0,1$;the ones

lying in the range of positive M_ϕ correspond to the dis-

turbances spinning in the same direction as the steady

swirl; those for negative M_ϕ correspond to the distur-

bances spinning in the opposite direction.* Observe that

over a wide range the frequency is nearly proportional to

the swirl Mach number, a feature pointed out in Section

1.1 in connection with the annular cascade data. The

virtual linearity suggests immediately an analytical so-

lution by resorting to the expansion in terms of the swirl

Mach number; such an approximate formula is given by

equation (A-8) of the Appendix, shown as chain lines in

Figure 4, and, on the whole, the results stand in reasonable

agreement with the wholly numerical results. The agreement

is closer for a narrow annulus; this will afford us to use

and exploit the analytical results for such a case, as to

be seen shortly.

With the aid of these relationships, equation

(42) or (45) furnish the result for tangential streaming.

Figure 5 (a) -(d) typify the one for several radius ratios; in all

of them, the dimensionless tangential streaming near the inner cylinder

---

*One can also represent this backward traveling wave by the
one with negative m in the positive range of M_ϕ .

is plotted as a function of the steady swirl Mach number, M_ϕ ; the mode in the radial direction is the fundamental, $m = 1$, and $\kappa = 0$, and the frequency relationship used therein is that obtained by the numerical procedure; the solid lines correspond to the thermal condition where the fluctuation of the temperature is maintained to be zero on the wall of the inner cylinder, the broken lines to thermally insulated walls. There, the positive value of streaming means that its direction is the same as that of steady swirl, negative being obviously the other way. Thus, the figures indeed display the reversal of the streaming direction at the threshold swirl Mach number. And the absolute magnitude of streaming tends to become sizable in its neighborhood with the threshold swirls serving as asymptotes. To obtain the total magnitude of "d.c." swirl, we only add or subtract the streaming to the steady swirl imposed, of course; therefore, beyond the threshold, the entire swirl becomes reduced near the inner cylinder. Notice also that the threshold swirl Mach number decreases as the ratio of the outer to inner radius of the cylinder λ is progressively increased.

The point appears more directly in Figure 6 (a)-(b) where the threshold swirl Mach numer of the foregoing first radial mode is drawn against the radius ratio for the first and second tangential modes, $m = 1$ and

m = 2; as an example, for the radius ratio of 5, the threshold swirl for m = 1 and κ = 0 is only 0.37, a low value for tangential velocity indeed.

The threshold swirl is independent of the thermal condition at the wall; it corresponds to the disturbances spinning in the same direction as the steady swirl; no threshold is found for the ones in the opposite direction. In addition, we can show that for any values of κ, whether negative or positive, the lowest threshold swirl Mach number occurs at κ = 0.

Figure 6 also reveals that as the radius ratio λ approaches unity, the threshold swirl becomes exceedingly high. In fact we can prove that for such a narrow annulus, in its limit, the threshold swirl approaches infinity; that is, whatever the amount of swirl, no retrogression of the tangential streaming occurs. This comes from the fact that as exhibited by the aforementioned analytical solution (A - 19) of the Appendix, the frequency-swirl relation for the lowest eigenvalue and κ= 0 becomes such that it corresponds, in effect, to the plane wave -- traveling with the phase speed equal to the sum and difference of swirl and $A_{ex}(r = r_o)$. To the extent no reversal of the streaming direction takes place for the plane wave, no retrogression of tangential swirl occurs in the present limit. As a matter of fact, we can expressly prove that for such a case, the expression

of equation (42) or (45) is reduced to such as equation
(47); the denominator now becomes A_{ex}, a constant, and
therefore no reversal takes effect.

For the foregoing reason, the reversal in the
streaming direction is intimately connected to the pre-
sent three-dimensional geometry, which compels the
lowest mode of disturbances to deviate from the plane
waves; also, no less indispensable is the presence of
steady swirl.

For the outer cylinder, Figure 7 shows that
the tangential streaming at the outer edge of its middle
deck. Although, contrary to Figure 5, no reversal is
experienced therein, this is still indirectly affected
by the significant change of streaming near the inner
cylinder: the reduction in tangential streaming of the latter
induces, in the annular core, a complex radial redistri-
bution of the angular momentum, whose precise details are
outside the scope of the present work; however, due to the
fact that the torque acting upon the annular core remains vir-
tually zero, we can say that this decrease has to be com-
pensated by the corresponding increase of tangential velocity
elsewhere, including the region near the outer cylinder.

When synthesized, the transformation of the total
d.c. swirl above the threshold appears as shown schematically
in Figure 8; thus, post-conversion behavior would plainly
separate the total temperature in the radial direction,
even if the static temperature remained uniform (we shall

discuss this latter aspect in the next subsection 7.2.

The almost linear dependence of frequency upon swirl, the existence of threshold swirl, the reduction of total d.c. component of swirl near the inner cylinder beyond the threshold and the radial gradient of total temperature or the Ranque-Hilsch effect--- all appear to agree, at least qualitatively, with the key features mentioned on the annular cascade in Section 1.1. (For now, further quantitative comparison is beyond us for want of more data surrounding the threshold swirl.)

In reference to Figure 5, as the threshold swirl is approached with increasing amounts of streaming, the assumption of small parameter of α and β breaks down; moreover, the change induced in the base flow pattern starts to modify the frequency-swirl relationship. Neverthe-less, we assert that the phenomenon is, at the very least, an indication of what is to be expected of the actual one at or near such a condition, the only substantive modification in reality being more gradual reversal of the streaming direction rather than the abrupt one across the asymptotes depicted in the figure.

Still referring to Figure 5, just below the threshold swirl, we observe that the streaming enlarges its magnitude; this would increase the total d.c. component of swirl near the inner cylinder. We venture to state, however, that in reality such development is unlikely to

occur due to the ensuing unbalance of radial pressure
gradient and centrifugal force. This expels outward the
lumps of fluid, which is, at the same time, swept down-
stream. It is replaced afresh by another fluid
element replenished from the mainstream. This new lump,
while migrating inward through the virtually inviscid
region, increases its tangential velocity in accord with
Kelvin's theorem until it attains, upon arrival at the
inner radius, the originally imposed steady tangential
velocity; thereabout the steady swirl remains, in effect,
unchanged.

On the other hand, above the threshold swirl,
the reduction in total d.c. component of the swirl
can occur indeed. The unbalance of radial pressure
gradient and centrifugal force tends, in this instance,
to submerge the lump of fluid toward the wall of the
inner cylinder. But, it is prevented from doing so by the
radial outflow resulting from the steady radial velocity
ejected from the steady boundary layer, in addition to the
radial component of acoustic streaming directed also and
always outward, as seen from equation (44); hence, the
fluid element is forced to remain adhered to the inner
cylinder with its magnitude of tangential velocity now
reduced.

7.2 Rankine Vortex

We consider the Rankine vortex within a single tube represented by

$$V_0(r) = \Omega r , \quad \text{for} \quad 0 < r < r_i , \quad (53\text{-}a)$$

$$V_0(r) = \frac{\Gamma}{r} , \quad \text{for} \quad r_i < r < r_o , \quad (53\text{-}b)$$

where $\Gamma = \Omega r_i^2$ and r_i now denotes the radius at the interface of a forced and free vortex. In addition, $U_0 = 0$ and $W_0(r)$ is an arbitrary function of r.

Furthermore, we are interested in the unsteady disturbance with $k = 0$ or $\kappa = 0$ and the first radial mode.

As shown in equation (A-24 b) of the Appendix, the frequency-swirl relationship for such a case can adequately be represented by

$$\omega = \pm(|m| - 1 + \lambda^{-2|m|})\Omega \quad (54)$$

$\pm$ sign corresponding to $m > 0$ or $m < 0$ respectively, provided the swirl Mach number at the interface remains well in the subsonic range. This formula asserts that the frequency is proportional to the swirl, a distinguishing characteristic of vortex whistle first discovered by Vonnegut (1954); see also Chanaud (1963, 1965). Its

linearity is to such an extent and with such accuracy
that, by creating swirl and measuring its frequency,
it can be exploited for use either as a sensor of
aircraft speed (Nichlas, 1957) or a flow meter, provided
in the latter the ratio of swirl to axial velocity is
made to remain constant (Rodely, Chanaud and White,
1965). (Equation (54) is applicable even to incompres-
sible flow, as may be inferred to be so by noting the
absence of acoustic speed and density thereof; this can
also be directly verified by examining the incompressible
solution of Kelvin (ibid.). The proportionality of surge
frequency to rotational speed of water turbines, as
observed earlier by Rheingaus (1940) in draft tubes of
hydroelectric plants is yet another practical manifestation
of the vortex whistle in incompressible flow.)

Although both for a Rankine and free
vortex, the relationship between the frequency and swirl
is found to be linear, the difference between full
proportionality (i.e. $\omega \to 0$ as $\Omega \to 0$) for the present
Rankine vortex and mere linearity ($\omega \neq 0$ as $\Gamma \to 0$)
for the free vortex of the preceeding section is enough
to compel a notable change in the turning point, as will
be seen below.

Making use of (54), the tangential streaming
can at once be obtained from either equation (42) or (45)

by replacing the subscript i with o. Figure 9
exemplifies such calculated results; the tangential streaming
at the tube periphery is rendered into dimensionless form and drawn
as a continuous function of circumferential wave number
m, though, in reality, m of course takes only integer
values; the swirl Mach number at the interface
$\Gamma/r_i A_{ex}(r=r_o)$, is taken to be 0.2, λ being 2. Observe
that the direction of the tangential streaming is
always positive or in the same direction as the steady
swirl; this is so, not only for positive values of m
corresponding to the disturbances spinning in the same
direction as steady swirl, but also for negative
m corresponding to the ones in the opposite direction.
Observe also that the magnitude of streaming increases
as the circumferential wave number is decreased. In
fact, at $m = \pm 1$ or the first tangential mode, it can be
readily shown from equations (42) or (45) combined with
(54) that the magnitude of steady streaming becomes in-
finitely large, regardless of the value for steady swirl,
or of λ or of the thermal condition on the wall; this implies
that the turning point, contrary to the free vortex, does
not exist for the present case. (Of course, in reality,
the magnitude does not become that much, but again we
take it as an indication of what actually happens.)

For the reason stated in the foregoing sub-
section 7.1 , the unbalance between the radial pressure

gradient and the centrifugal force work in such a
way as to bring the increase of streaming at the tube
perimeter into being.

Schematically drawn in Figure 10 is the
conversion of the original Rankine vortex to a forced
one by streaming. Acoustic streaming, if induced,
being present regardless of the axial position in the
tube, the transformation can immediately take effect
right at its entrance. This metamorphosis toward
a forced vortex and this alone, to say nothing about
the static temperature gradient, again tends to separate
the total temperature into a colder stream near the center and
the hotter stream near the perphery of the cylinder.

If and when the geometry of the tube arrangement
favors the excitation of such particular unsteady dis-
turbance as the one with the lowest eigenvalues in the
radial direction, $m = 1$, and $\kappa = 0$, a forced vortex
filling out the entire tube is always formed and the
total temperature becomes separated, even near the inlet;
otherwise, the Rankine vortex and the total temperature
remain unchanged. This appears to explain the dichotomy
of the radial profile mentioned in the Introduction: a
forced vortex for a Ranque-Hilsch tube with separated
total temperature and Rankine vortex for others without
any such separation.

By appealing to the streaming as the predominant
mechanism, we can also readily explain the other character-
istics of the Ranque-Hilsch effect: the radial difference
of total temperature is known to increase as the pressure of
the incoming air is raised. As the pressure is stepped up, the
amplitude of disturbances as well as the amount of steady
swirl increases (Cassidy and Falvey, 1970); from equation
(42-a), this, in turn, is observed to induce more streaming
and hence more energy separations.

So far, we have not touched upon the role of
static temperature. The steady state or time-averaged component
of static temperature induced by the unsteady disturbances at the outer
edge of the middle deck is always of insignificant magni-
tude; hence it would not sensibly affect the basic radial
"inviscid" pattern of static temperature, determined uniquely
by swirl, for any pattern of which the following holds:
higher temperature at the outer radius and a colder one
near the center. In fact, the data of Eckert and Hartnett
and Lay (ibid.) all show such radial distribution of static
temperature for Ranque-Hilsch tubes; the actual preservation of this in
the presence of unsteadiness existing in the flow may
indeed involve the Knoernschild effect (ibid.), which
is applicable whether the disturbance is of organized origin
or of stochastic nature. In any event, this difference in
static temperature, when added, aids to separate furthermore
the temperature.

Once the formation of a forced vortex is thus predicted, then, based on this, together with assumed distribution of static temperature such as an adiabatic one, and from these two alone, it is a simple matter to construct the so-called performance curve resembling the one given by Hilsch; in other words, upon only the above two the performance curve rests; hence, once they are somehow gotten in any theory whatsoever, the performance curve follows at once and, contrary to what might be believed, the mere reproduction od the curve does not substantiate the postulated mechanism.

7.3. Forced Vortex

Consider a forced vortex given by

$$V_0(r) = \Omega r , \qquad 0 < r < r_o , \qquad (55)$$

and $U_0 = W_0 = 0$. With the aid of the relationship between ω and Ω obtained numerically by Sozou (1969), we can show that no turning point exists for such swirl.

In the foregoing, we have considered situations where, in addition to the steady swirl and axial flow, both the tangential and axial wave numbers are specified and the frequency is to be determined; on the other hand, if the frequency of the disturbances is enforced upon the swirling flow, held fixed and the axial wave number is to be determined, such a case may be treated in a similar manner, the streaming still being given by equations (42) to (45).

8. Summary

In this last section, we summarize the foregoing results on streaming, interpreting them now in physical terms from the outset.

We begin by recalling that for a wave traveling uni-directionally through a gas in an otherwise state of rest, the effect of viscosity manifests itself in the form of the tilted trajectory of a fluid particle near the solid wall; it is this skewness that gives rise to the streaming. By skewness is meant that the axes of the particle path tracing a closed loop are slanted as referred, for example, to the normal to the wall surface. We draw the control surface, parallel to the wall and intersecting the loop, and reckon the momentum transported by the lump of fluid circling along the loop, in and out of the surface. Then, the very asymmetry of slanting trajectory results in the unbalance of the momentum budget, once averaged temporally; the Reynolds stresses, thus generated and of orderly origin, act upon the fluid layer to set forth the streaming.

If the wave is propagating in the x direction with waveform given as $\tilde{u}e^{i(\ell x - \omega t)}$ at the outer edge of the unsteady boundary layer, the streaming in the x direction at the edge takes the form of

$$\frac{\tilde{u}^2 \ell}{\omega} (\ldots) ,$$

when by positive value we mean that its direction is the same as that for the wave propagation.

If the wave is spinning in the circumferential direction with waveform given by $\tilde{u}e^{i(m\phi - \omega t)}$ at the outer edge of the unsteady boundary layer formed over a cylindrical surface of radius r_i, the streaming in the tangential direction follows immediately from the above as

$$\frac{\tilde{u}^2 m}{\omega r_i} \ (\ldots) \ .$$

If, in addition, the gas itself swirls, with its magnitude at the outer edge given as V_{ex}, the Doppler shift changes the above

$$\frac{\tilde{u}^2 m}{\left(\omega - m \dfrac{V_{ex}}{r_i}\right) r_i} \qquad (\ldots)$$

so that to an observer situated on the frame of reference rotating with peripheral speed V_{ex}, this would apparently become the same as the one for the gas which is otherwise at rest. The above can readily be generalized to the three-dimensional situation where the waveform is now represented by $e^{i(m\phi + kz - \omega t)}$; besides swirl, the steady velocity now possesses an additional axial component W_{ex}. Then, in place of the foregoing Doppler shift term $\omega - m \dfrac{V_{ex}}{r_i}$, we only have to replace with $\omega - m \dfrac{V_{ex}}{r_i} - kW_{ex}$, the frame of reference being now in screw motion, advancing

axially with W_{ex}, while rotating with V_{ex}. The elaborate apparatus of the matched asymtotic expansion applied to the full Navier-Stokes equation, has led us, in fact, to this form as the leading term of streaming in the tangential direction, the entire formula of which is given as equation (42) or (45).

The very form of the above Doppler shift implies that the tangential streaming can change its rotational direction. For $\omega - m \dfrac{V_{ex}}{r_i} - kW_{ex} > 0$, it rotates in the same direction as the steady swirl; for $\omega - m \dfrac{V_{ex}}{r_i} - kW_{ex} < 0$, the streaming is now rotating in the opposite direction --- retrogression occurs. As such a turning point is approached, the absolute magnitude of streaming increases sizably.

The turning point is determined by the relative values of competing factors such as frequency ω, steady flow field, V_{ex} and W_{ex}, and the wave numbers, m and k; in turn, they are dependent upon the specific radial profile of swirl and the geometry of cylindrical configurations.

For a free vortex distribution contained between two concentric cylinders of radii, r_i and r_o, the threshold swirl corresponding to the turning point decreases as the radius ratio $\lambda = \dfrac{r_o}{r_i}$ is increased, in a fashion depicted in Figure 6. Above the threshold, the streaming, when added to the steady swirl, tends to reduce the total d.c. amount of swirl near the inner cylinder.

For a Rankine vortex, within a single cylinder and subject to the particular wave corresponding to the lowest eigenvalue, $m = 1$, and $\kappa = 0$, there is no threshold swirl; instead, any amount of swirl introduces, along the cylinder periphery, a streaming rotating in the same direction as the steady swirl and of considerable strength, converting it into a forced vortex. For waves other than this, the effect of streaming remains insignificant.

Be it a free vortex or a Rankine vortex, if the original steady swirl metamorphoses into a forced vortex, then this and this alone, suffices to give rise to the Ranque-Hilsch effect (though the presence of depressed static temperature distribution near the center also furthers this).

The foregoing appears to account for the phenomena described in connection with the annular cascade and the issues raised for the Ranque-Hilsch tube alike, as detailed in the Introduction.

Finally, we close this paper with the remark that to the extent the temperature separation arises due to the unsteadiness in flow, the present subject is the converse to the phenomena of Rijke tube and thermally driven acoustic oscillation of liquid helium (e.g. Clement and Gaffney, 1960) where the very difference in temperature gives rise to unsteady disturbance; and in broader

contexts, to the extent that we seek the present
mechanism as of organized origin distinct from the
stochastic process, this falls under the same mor-
phological class as the study of large-scale structure
in the mixing layer (Brown and Roshko, 1974).

REFERENCES

Batchelor, G. K., 1967 An Introduction to Fluid Mechanics ,
Cambridge Univ. Press.

Batson, J. L. and Sforzini, R. H., 1970 J. Spacecraft
and Rocket, 7,2,159-163.

Bertelsen, A. F., 1974 J. Fluid Mech., 64, 3, 589-597.

Brown, G. L. and Roshko, A., 1974 J. Fluid Mech. 64, 4,
775-816.

Bruun, H. H., 1969 J. Mech. Eng. Sci. 11, 6, 567-582.

Cassidy, J. J. and Falvey, H. J., 1970 J. Fluid Mech. 41,4,
727-736.

Chanaud, R. C., 1963 J. of Acous.Soc. of Amer., 35, 7,
953-960.

Chanaud, R. C., 1965 J. Fluid Mech. 21, 1, 111-127.

Clement, J. R. and Gaffney, J., 1960 "Thermal Oscillations
in Low Temperature Apparatus", Advances in
Cryogenic Engineering, Vol.1, Plenum Press, New
York, 302-306.

Cooke, J. C., 1952 J. Aero. Sci. 19, 7, 486-490.

Danforth, C. E., 1977 a private communication.

Deissler, R. G. and Perlmutter, M., 1960 Int. J. Heat
Mass Transfer 1, 173-191.

Duck, P. W. and Smith, F. T., 1979 J. Fluid Mech., 91, 1,
93-110.

Dunn, D. W. and Lin, C. C., 1955 J. Aero. Sci. 22,7,
455-477.

Eckert, E. R. G. and Hartnett, J. P., 1955 Proc. of the
Fourth Midwestern Conf. on Fluid Mech., 69-92.

Faraday, M., 1831 Roy. Soc. of London, Phil. Trans. 121,
299-340.

Flandro, G. A., 1964 AIAA J. 2. 7., 1303-1306.

Flandro, G. A., 1967 Rotating Flows in Acoustically
Unstable Rocket Motors, Ph. D. Thesis, Calif.
Inst. of Tech.

Gyarmathy, G., 1969 AIAA J.,7, 10, 1838-1845.

Haddon, E. W. and Riley, N., 1979 J. Mech. Appl. Math,
17, 3, 265-282.

Hall, M. G., 1972 "Vortex Breakdown", Annual Review of
Fluid Mech. Vol 4, Ed. by M. Van Dyke and W. G.
Vincenti, Annual Review Inc. Palo Alto, 195-
217.

Hartmann, J., 1931 Phil. Mag. 11, 926-948.

Hartnett, J. P., and Eckert, E. R. G., 1957 Trans. ASME,
79, 751-758.

Hilsch, R., 1947 Review of Sci. Instrum. 18, 2, 108-
113.

Kelvin, Lord, 1880 Phil. Mag. 5, 155-168.

Kendall, J. M., 1962 Experimental Study of a Compressible
Viscous Vortex, Tech. Rep. No. 32-290, JPL,
Calif. Inst. of Tech.

Kerrebrock, J. L., 1977 AIAA J. 15, 6, 794-803.

Keyes, J. J., 1961 Amer. Rocket Soc. J. 31,9,
1204-1210.

Knoernschild, E., 1948 "Friction Laws and Energy Transfer
in Circular Flow, Part II - Energy Transfer in
Circular Flow and Possible Applications (Explana-
tion of the Hilsch or Ranque Effect)", Tech. Rep.
No. F-TR-2198-ND, GS - USAF. Wright Patterson Air
Force Base No. 78.

Lay, J. E., 1959 J. Heat Transfer. ASME, 81, 3, 202-
212.

Lighthill, M. J., 1978 a) J. Sound and Vib. 61, 3, 391-
418.

Lighthill, M. J., 1978 b) Waves in Fluids , Cambridge Univ.
Press. p. 347.

Linderstrøm-Lang, C. U., 1971 J. Fluid Mech. 45, 1, 161-
187.

Mack, L. M., 1960 J. Fluid Mech. 8, 284-292.

Marble, F. E., 1964 "Three-Dimensional Flow in Turbomachines",
Chapter C, Aerodynamics of Turbines and Compressors,
Vol. 5, High Speed Aerodynamics and Jet Propulsion,
Princeton Univ. Press.

McGee, R.,Jr., 1950 Refri. Eng. 58, 974-975.

Nicklas, J. P., 1957 Cornell Aero Lab. Rep No.
        1 H 942-P-2.

Ragsdale, R. G., 1961 NASA TN. D-1051.

Rakowski, W. J., Ellis, D. H., and Bankhead, H. R., 1978
        AIAA Paper No. 78-1089.

Rakowski, W. J. and Ellis, D. H., 1978 "Experimental
        Analysis of Blade Instability Vol 1", R78 AEG 275,
        General Electric Company Report for F 33615-76-
        C-2035, to Air Force Aero Propulsion Laboratory,
        WPAFB. 67-71.

Ranque, G. J., 1933 J. de Phys. et rad. 7,4, p. 112.

Rayleigh, Lord, 1884 Phil. Trans. 175, 1-21.

Reynolds, A. J., 1961 Z. für angew. Math. und Phy.,
        7, 343-357.

Rheingans, W. J., 1940 Trans. ASME, 62, 171-184.

Riley, N., 1967 J. Inst. Maths. Applc. 3, 419-434.

Rodely, A. E., Chanaud, R. C. and White, D. F., 1965
        ASME Paper No. 65-WA/FM-6.

Savino, J. M. and Ragsdale, R. G., 1961 J. of Heat
        Transfer, Tran. ASME, 83, 1, 33-38.

Scheller, W. A. and Brown, G. M., 1957   Indust. and Eng.
        Chemistry, 49, 6, 1013-1016.

Schepper, G. W., Jr., 1951 Refrig. Eng. 59, 985-989.

Secomb, T. W., 1978 J. Fluid Mech., 88, 2, 273-288.

Sibulkin, M., 1962 J. Fluid Mech. 12, 2, 269-293.

Sozou, C., 1969 J. Fluid Mech. 36, 3, 605-612.

Sozou, C. and Swithenbank, J., 1969 J. Fluid Mech. 38, 4,
        657-671.

Sprenger, H., 1951 Z. für angew. Math. und Phy. 2,
        293-300.

Sprenger, H., 1954 "Über thermische Effekte in Resonanzrohren", Mitt. Int. Aerodyn. ETH, Zurich, Nr. 21, p. 18.

Stuart, J. T., 1963 "Unsteady Boundary Layers", Chapter 7, in Laminar Boundary Layers, ed. by L. Rosenhead, Oxford Univ. Press, p. 384.

Stuart, J. T., 1966 J. Fluid Mech. 24, 4, 673-687.

Swithenbank, J., and Sotter, G., 1964 AIAA J., 2, 7, 1297-1302.

Syred, N. and Beer, J. M., 1972 Proc. of the Second Int. J. S. M. E. Symp. on Fluid Mech. 111-120.

Takahama, H., 1965 Bulletin of JSME, 8, 31, 433-440.

Takahama, H. and Soga, N., 1966 Bulletin of JSME, 9, 33, 121-130.

Taylor, G. I., 1950 Quart. J. Mech. and Applied Mech. 3, 2, 129-139.

Ter Linden, A. J., 1949 Proc. of Inst. Mech, Eng., 160, 233-240.

Tsai, D. H., 1964 AIAA J. 2, 9, 1504-1505.

Tyler, J. M. and Sofrin, T. G., 1962 SAE Trans. 70, 309-332.

Van Deemter, 1952 Appl. Sci. Res. A, 3,174-196.

Van Dyke, M., 1962 a) "Second-order Compressible Boundary Layer Theory with Application to Blunt Bodies in Hypersonic Flow: in Hypersonic Flow Research ed. by F. R. Riddle, Academic Press, New York, 37-75.

Van Dyke, M., 1962 b) J. Fluid Mech. 14, 161-177.

Van Dyke, M., 1969 "Higher-order Boundary Layer Theory", in Annual Review of Fluid Mechanics, Vol 1., ed. by W. R. Sears, Annual Reviews, Inc. , Palo Alto, 265-292.

Vonnegut, B., 1950 Review of Scientific Instruments, 21, 2, 136-141.

Vonnegut, B., 1954 J. of Acos. Soc. of Amer. 26, 1, 18-20.

Watson, G. N. 1966 A Treatise on the Theory of Bessel Functions , Cambridge Univ. Press.

Appendix

This appendix concerns the relationship between the frequency and the steady swirl corresponding to section 7.1 and 7.2; it will be obtained from the unsteady, inviscid linearized approximation, equation (10) or equivalently equation (33).

a) Free Vortex Between Co-Annular Cylinders

For this, equation (49) specifies the steady profile. Choosing $r*\bar{v}$ or the moment of angular momentum as our primary dependent variable, we can extract, from equation (10) and with the aid of equation (8), the following, single, second-order differential equation:

$$\frac{d^2}{dr*^2}(\overset{*}{r}\bar{v}) + \frac{1}{r*}\left\{1 + \frac{M_\phi^2}{r*^2\left[1 - \frac{\gamma-1}{2}M_\phi^2\left(\frac{1}{\overset{*}{r}2} - \frac{1}{\lambda^2}\right)\right]}\right\}\frac{d}{dr*}(r*\bar{v})$$

$$+ \left[\frac{\left(-\chi_n + \frac{mM_\phi}{\overset{*}{r}2}\right)^2}{1 - \frac{\gamma-1}{2}M_\phi^2\left(\frac{1}{\overset{*}{r}2} - \frac{1}{\lambda^2}\right)} - \kappa^2 - \frac{m^2}{\overset{*}{r}2}\right](\overset{*}{r}\bar{v}) = 0,$$

$$(A-1)$$

with the boundary condition given by

$$\frac{d(\overset{*}{r}\bar{v})}{dr*} = 0 \quad \text{at } r* = 1 \text{ and } r* = \lambda. \quad (A-2)$$

The definitions of M_ϕ, χ_n and κ are given in equation (50) to (52). The eigenvalues χ_n are to be determined once the values of M_ϕ, κ, m and λ are given;

Figure 4 in the text has been obtained by the standard eigenvalue search procedure using the fourth order Runge-Kutta method.

In addition to this wholly numerical procedure, we can also obtain an approximate analytical representation of eigenvalues and this we discuss next.

Consider at first the case of no swirl. Then $r*\bar{v}^{(o)}$ be expressed as a linear combination of Bessel functions such as

$$r*\bar{v}^{(o)} = A\left[J_m(z_n r*) - Y_m(z_n r*)\ \frac{J_m{'}(z_n)}{Y_m(z_n)}\right] \tag{A-3}$$

where A is a constant, z_n is given by

$$J_m{'}(z_n*)\ Y_n{'}(z_n) - Y_m{'}(z_n*)\ J_m{'}(z_n) = 0, \tag{A-4}$$

where z_n* is related to z_n by

$$z_n* = z_n\lambda\ . \tag{A-5}$$

In (A-4), the primes denote the derivatives with respect to the argument of the Bessel function. z_n is related to χ_n by

$$\chi_n = \sqrt{\kappa^2 + z_n^2} \tag{A-6}$$

Based upon this, when the swirl is present, we expand $r^*\bar{v}$ and χ_n in terms of the swirl Mach number, M_ϕ and retain only the linear term:

$$r^*\bar{v} = r^*\bar{v}^{(0)} + M_\phi \ r^*\bar{v}^{(1)} + \text{---} \qquad (A-7)$$

$$\chi_n = \sqrt{\kappa^2 + (z_n)^2} + mS_{nm}M_\phi + \text{---} \qquad (A-8)$$

where $r^*\bar{v}^{(1)}$ and S_{nm} are to be determined. Substituting into (A-1), retaining only terms up to 0 (M_ϕ) and satisfying (A-2) and making use of the integral formulae involving products of the Bessel function (e.g. Watson 1966, pp.134-137), we obtain, for $m > 0$

$$S_{nm} = \frac{\Delta_1}{\Delta_2} z_n^2 \qquad (A-9)$$

where

$$\Delta_1 = 2J_m{'}(z_n)Y_m{'}(z_n{}^*) \ I_{11}(JY) - Y_m{'}(z_n) \ Y_m{'}(z_n{}^*) \ I_{12} \ (J^2)$$

$$- J_m{'}(z_n) \ J_m{'}(z_n{}^*) \ I_{13} \ (Y^2), \qquad (A-10)$$

$$\Delta_2 = 2J_m{'}(z_n) \ Y_m{'}(z_n{}^*) \ I_{21}(JY) - Y_m{'}(z_n) \ Y_m{'}(z_n{}^*) \ I_{22} \ (J^2)$$

$$- J_m{'}(z_n) \ J_m{'}(z_n{}^*) \ I_{23} \ (Y^2) \ ,. \qquad (A-11)$$

I_{11}, I_{12}, etc. are given by

$$I_{11}(JY) = -\frac{1}{2m} \left[J_0(z)Y_0(z) + 2 \sum_{\ell=1}^{m-1} J_\ell(z) Y_\ell(z) \right. $$
$$\left. + J_m(z) Y_m(z) \right] \begin{array}{c} z = z_n^* \\ z = z_n \end{array} \qquad (A-12)$$

$$I_{12}(J^2) = -\frac{1}{2m} \left[J_0(z)^2 + 2 \sum_{\ell=1}^{m-1} J_\ell(z)^2 + J_m(z)^2 \right] \begin{array}{c} z = z_n^* \\ z = z_n \end{array} ,$$

$$(A-13)$$

$$I_{13}(Y^2) = -\frac{1}{2m} \left[Y_0(z)^2 + 2 \sum_{\ell=1}^{m-1} Y_\ell(z)^2 + Y_m(z)^2 \right] \begin{array}{c} z = z_n^* \\ z = z_n \end{array} ,$$

$$(A-14)$$

$$I_{21}(JY) = \left\{ \frac{1}{4} z^2 \left[2J_m(z) Y_m(z) - J_{m-1}(z)Y_{m+1}(z) - J_{m+1}(z)Y_{m-1}(z) \right] \right\} \begin{array}{c} z=z_n^* \\ z=z_n \end{array}$$

$$(A-15)$$

$$J_{22}(J^2) = \left\{ \frac{1}{2} z^2 \left[J_m(z)^2 - J_{m-1}(z) J_{m+1}(z) \right] \right\} \begin{array}{c} z = z_n^* \\ z = z_n \end{array} ,$$

$$(A-16)$$

$$J_{23}(Y^2) = \left\{ \frac{1}{2} z^2 \left[Y_m(z)^2 - Y_{m-1}(z) Y_{m+1}(z) \right] \right\} \begin{array}{c} z = z_n^* \\ z = z_n \end{array} .$$

$$(A-17)$$

From (A-12) to (A-17), $\left[f(z) \right]_{z=z_n}^{z=z_n^*}$ denotes the following:

$$\left[f(z)\right] \begin{matrix} z = z_n{}^* \\ z = z_n \end{matrix} = f\,(z_n{}^*) - f(z_n) \ . \qquad\qquad \text{(A-18)}$$

(If $m < 0$, S_{nm} remains the same for $m > 0$.)

The values of the lowest eigenvalue z_0 and corresponding S_{nm}, computed from equation (A-4) and (A-9), are listed in Table 1.

	z_0			
λ	m=1	m=2	S_{01}	S_{02}
1.01	0.99503	1.99006	0.99009	0.99016
1.05	0.97571	1.95141	0.95202	0.95202
1.1	0.95274	1.90550	0.90772	0.90770
1.5	0.80509	1.60810	0.64760	0.64420
2.0	0.67734	1.34060	0.45551	0.43714
3.0	0.51362	0.97749	0.25366	0.21202
5.0	0.34102	0.60694	0.10241	0.07354
7.0	0.25240	0.43556	0.05240	0.03686
10.0	0.18035	0.30529	0.02516	0.01793

TABLE 1.

The comparison of the foregoing analytical representation with the numerical procedure over a wide range of swirl is given in Figure 4.

As a special case of the above, we focus expressly our attention to the narrow annulus; let $\lambda \to 1$.

Then, we can show explicitly that

$$z_0 \to |m| \; ,$$

and

$$S_{0m} \to \frac{1}{\lambda} \; .$$

For $k = 0$, this leads immediately to

$$\omega = A_{ex}(r = r_0) \frac{|m|}{r_i} + \frac{m\Gamma}{r_0 r_i} \; ,$$

from equations (A-8) and (51). Then the disturbance represented by $e^{i(m\phi - \omega t)}$ becomes, for the narrow annulus

$$\exp \left\{ im \left[\pm \frac{A_{ex}(r = r_0)}{r_i} + \frac{\Gamma}{r_0 r_i} \right] \left[\frac{r_i \phi}{\pm A_{ex}(r = r_0) + \frac{\Gamma}{r_0}} - t \right] \right\}.$$

$$(A-19)$$

The term within the second $\left[\; \right]$ shows that this corresponds to a plane wave propagating at the acoustic speed while being convected at the swirl velocity, as to be expected.

If we change our viewpoint slightly and regard ω as given and κ to be sought, then by insisting that κ is real in (A-8) and (51), the so-called cut-off condition for the propagation of disturbances through ducts can be obtained; this generalizes the Tyler-Sofrin formula (1962) by including the presence of both the swirl and the axial flow.

b) Rankine Vortex

For the radial profile given by equation (53), the boundary conditions for the unsteady disturbances are:

$$\bar{u} \ (r = r_o) = 0, \tag{A-20a}$$

$$\bar{\rho} \text{ and } \bar{u} \text{ are continuous at } r = r_i. \tag{A-20b}$$

Sozou and Swithenbank (1969) calculated the corresponding frequency relationship by wholly numerical computation. (Their treatment is limited to the two-dimensional flow. Although, as stated in Section 7.2, the axial velocity is, at present, allowed to exist, as long as κ is set equal to zero, its presence will affect only the axial disturbance, leaving the rest same as two-dimensional flow.) Here we offer an approximate analytical representation, choosing $\bar{\rho}$ as a primary dependent variable. In the innermost core of a forced vortex region defined by $0 < r < r_i$, the governing equation is given, upon combining equation (10) together, by

$$\frac{d^2 \bar{\rho}}{dr^2} + \left[\frac{1}{r} + \frac{(2\gamma - 3) \ \Omega^2 \ r}{A_0^2(r)} \right] \frac{d\bar{\rho}}{dr}$$

$$+ \left[\frac{2m \ \Omega^3}{\lambda_1 \ A_0^2(r)} + \frac{2(\gamma - 2) \ \Omega^2}{A_0^2(r)} - \frac{m^2}{r^2} + \frac{D}{A_0^2(r)} \right] \bar{\rho} = 0.$$

$$\tag{A-21a}$$

where $A_0(r)$, λ_1, and D are given by the following:

$$A_0^{\;2}(r) = A_{ex}^{\;2}(r=r_o) + \tfrac{1}{2}(\gamma - 1)\,\Omega^2\,(r^2 - r_o^{\;2}), \qquad (A\text{-}21b)$$

$$\lambda_1 = \Omega m - \omega, \qquad (A\text{-}21c)$$

$$D = (\Omega m - \omega)^2 - 4\Omega^2 . \qquad (A\text{-}21d)$$

$\bar{u}$ is related to $\bar{\rho}$ by

$$\bar{u} = \frac{i}{R_0(r)D}\left\{ \lambda_1 A_0^{\;2}(r)\frac{d\bar{\rho}}{dr} + \bar{\rho}\left[\frac{2mA_0^{\;2}(r)\Omega}{r}\right.\right.$$
$$\left.\left. - (2-\gamma)\,\lambda_1\, r\,\Omega^2 \right]\right\} \qquad (A\text{-}21e)$$

On the other hand, in the free vortex region defined by $r_i < r < r_o$, the governing equation is given by

$$\frac{d^2\bar{\rho}}{dr^2} + \left[\frac{1}{r} + \frac{(2\gamma - 3)\,\Gamma^2}{A_0^{\;2}(r)r^3} + \frac{4m\Gamma}{\lambda_2(r)r^3}\right]\frac{d\bar{\rho}}{dr}$$
$$+ \left[\frac{\lambda_2^{\;2}(r)}{A_0^{\;2}(r)} - \frac{m^2}{r^2} + \frac{2m(2\gamma - 3)\,\Gamma^3}{\lambda_2(r)r^6 A_0^{\;2}(r)} + \frac{8(m\Gamma)^2}{\lambda_2^{\;2}(r)r^6}\right.$$
$$\left. - \frac{4m\Gamma}{\lambda_2(r)r^4} + \frac{2(2-\gamma)\,\Gamma^2}{A_0^{\;2}(r)r^4}\right]\bar{\rho} = 0 , \qquad (A\text{-}22a)$$

where $A_0^{\;2}(r) = A_{ex}^{\;2}(r=r_o) + \tfrac{1}{2}(\gamma-1)\left[\Omega^2(r_i^{\;2}-r_o^{\;2}) - r^2\left(\frac{1}{r^2} - \frac{1}{r_i^{\;2}}\right)\right] ,$

$$(A\text{-}22b)$$

$$\lambda_2(r) = \frac{m\Gamma}{r^2} - \omega , \qquad (A\text{-}22c)$$

and u is related to $\bar{\rho}$ by

$$\bar{u} = \frac{i}{R_0(r)}\left\{\frac{A_0^{\;2}(r)}{\lambda_2(r)}\frac{d\bar{\rho}}{dr} + \bar{\rho}\left[\frac{2mA_0^{\;2}(r)\Gamma}{\lambda_2^{\;2}r^3} - \frac{(2-\gamma)\Gamma^2}{\lambda_2 r^3}\right]\right\}.$$

$$(A\text{-}22d)$$

Expand $\bar{\rho}$, $\bar{u}$ and ω in the power series of

$$\bar{\rho} = \rho^{(0)} + \Omega\rho^{(1)} + \text{---} \tag{A-23a}$$

$$\bar{u} = u^{(0)} + \Omega u^{(1)} + \text{---} \tag{A-23b}$$

$$\omega = \omega^{(0)} + \Omega\omega^{(1)} + \text{---} . \tag{A-23c}$$

We confine our attention to the limit of $\omega^{(0)} \to 0$, which corresponds to the lowest engenvalue for the case without swirl, or, in the terminology of Sozou and Swithenbank, to a slow wave. We substitute (A-23) into (A-21) to (A-22) and retain the terms up to $0(\Omega)$. This yields the following expression for $\omega^{(1)}$:

$$\omega^{(1)} = \pm \zeta|m| - 1 + \lambda^{-2|m|}\zeta, \tag{A-24a}$$

and, ω becomes from (A-23c)

$$\omega = \pm (|m| - 1 + \lambda^{-2|m|})\Omega \tag{A-24b}$$

where + sign corresponds to $m > 0$, - sign to $m < 0$.

For the special case of $m = 1$, this is reduced to

$$\frac{\omega}{\Omega} = \frac{1}{\lambda^2} ,$$

which is identical to equation (9) of Sozou and Swithenbank, which appears to have been obtained by the inspection of their numerically computed values (see their Figure 8(a)). In their table 3, they also list the results of computed ω; in the

following Table 2, we compare their results with our analytical formula (A-24b) side by side, the latter being shown in parentheses. The column left blank is unavailable from Sozon and Swithenbank. On the whole, our expression appears to be satisfactorily close to the numerical results, as long as the swirl Mach number, defined as $\Omega r_i/A_0(0)$ by them, remains less than 0.5 or so. Though not to be included here, if λ is not too close to unity, the amplitude of $\bar{u}$, (A-23b) is also in good agreement with their Figure 6.

$\dfrac{\Omega r_i}{A_0(0)}$	λ	m=1 $\dfrac{\omega r_i}{A_0(0)m}$	m=2 $\dfrac{\omega r_i}{A_0(0)m}$	λ	m=1 $\dfrac{\omega r_i}{A_0(0)m}$	m=2 $\dfrac{\omega r_i}{A_0(0)m}$
0.10	1.09	0.0841 (0.0841)	0.0854 (0.0854)	1.03	0.0942 (0.0942)	0.0944 (0.0944)
0.10	1.5	0.0444 (0.0444)	0.0598 (0.0598)	1.2	0.0694 (0.0694)	0.0741 (0.0741)
0.10	5	0.0040 (0.0040)	0.0050 (0.0050)	2	0.0250 (0.0250)	0.0531 (0.0531)
0.25	1.09	0.2099 (0.2104)	0.2132 (0.2135)	1.03	0.2353 (0.2356)	0.2359 (0.2361)
0.25	1.5	0.1105 (0.1111)	0.1490 (0.1497)	1.2	0.1729 (0.1736)	0.1848 (0.1852)
0.25	5	0.0100 (0.0100)	0.1246 (0.1252)	2	0.0622 (0.0622)	0.1321 (0.1328)
0.50	5	0.0199 (0.0200)		2	0.1222 (0.1250)	0.2603 (0.2656)
0.75	5	0.0296 (0.0300)		2	0.1807 (0.1875)	0.3814 (0.3984)
1.0	5	0.0392 (0.0400)		2	0.2367 (0.2500)	0.4941 (0.5312)

TABLE 2.
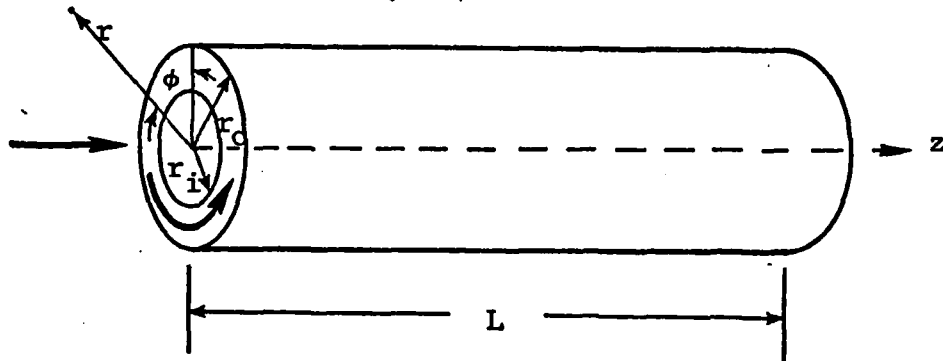
Figure 1. Definition sketch.
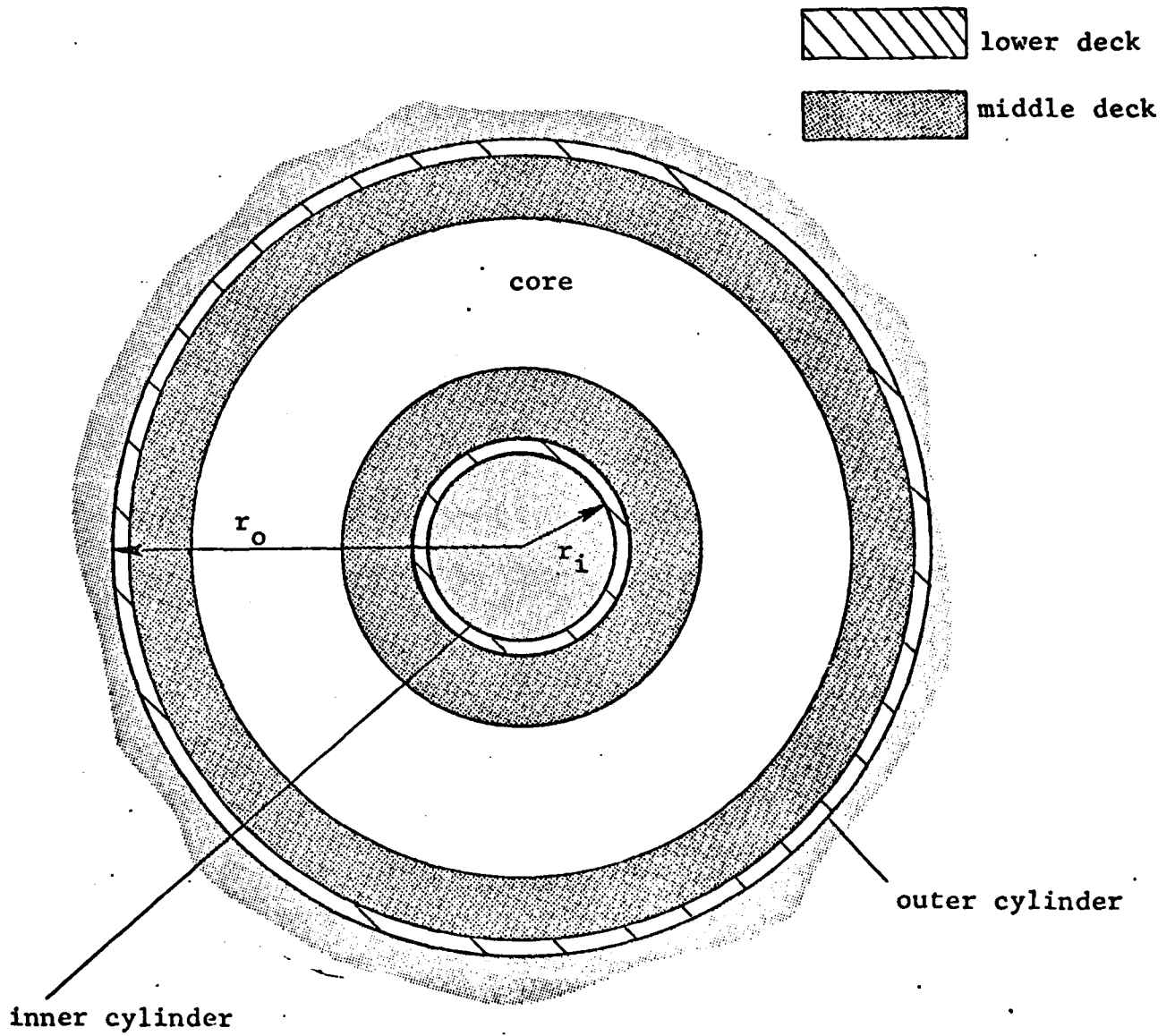
Figure 2. Lower deck, middle deck and core.

```
┌─────────────────────────────────┐
│ (0,0,0)  core                   │
└─────────────────────────────────┘
                 │
                 ▼
┌─────────────────────────────────┐
│ (0,0,0)  middle deck            │
└─────────────────────────────────┘
                 │
                 ▼
┌─────────────────────────────────┐
│ (1,0,0)  middle deck streaming  │
└─────────────────────────────────┘
                 │
                 ▼
┌─────────────────────────────────┐
│ (1,0,0)  core streaming         │
└─────────────────────────────────┘
```
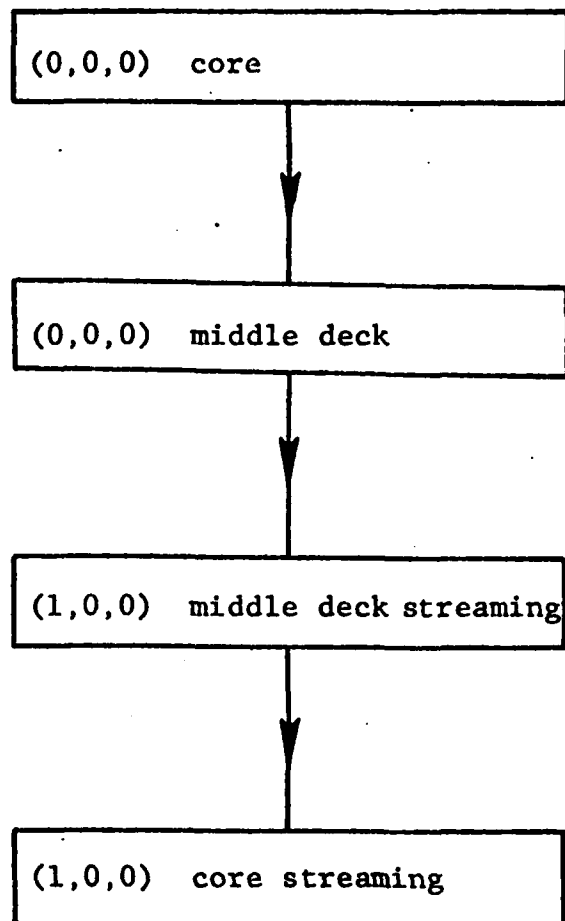
Figure 3. "Family tree" of streaming.
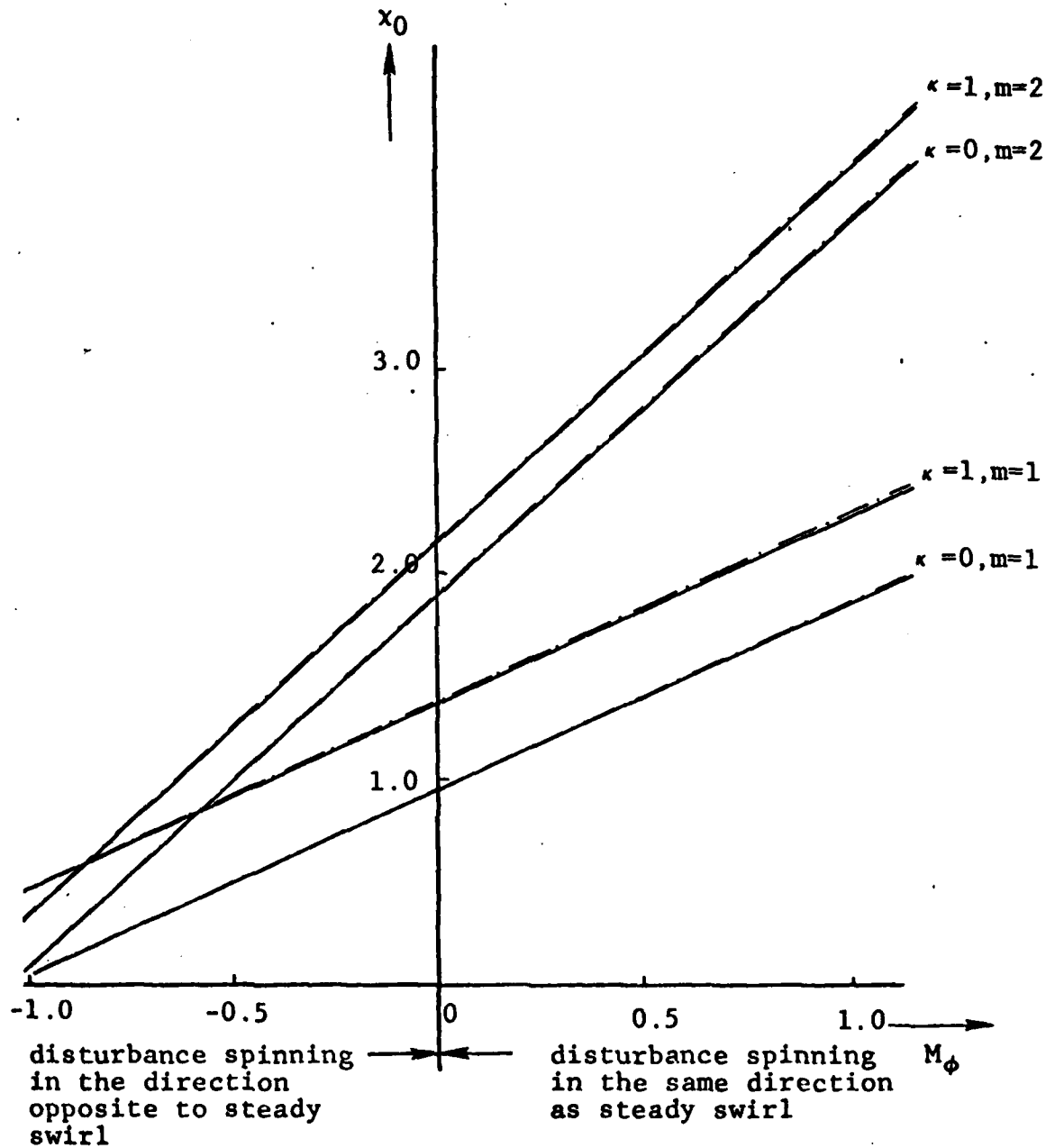
Figure 4(a)   Frequency vs. swirl Mach number
$\lambda = 1.1$

solid lines: numerically computed values
chain lines: analytical results from
equation (A-8)
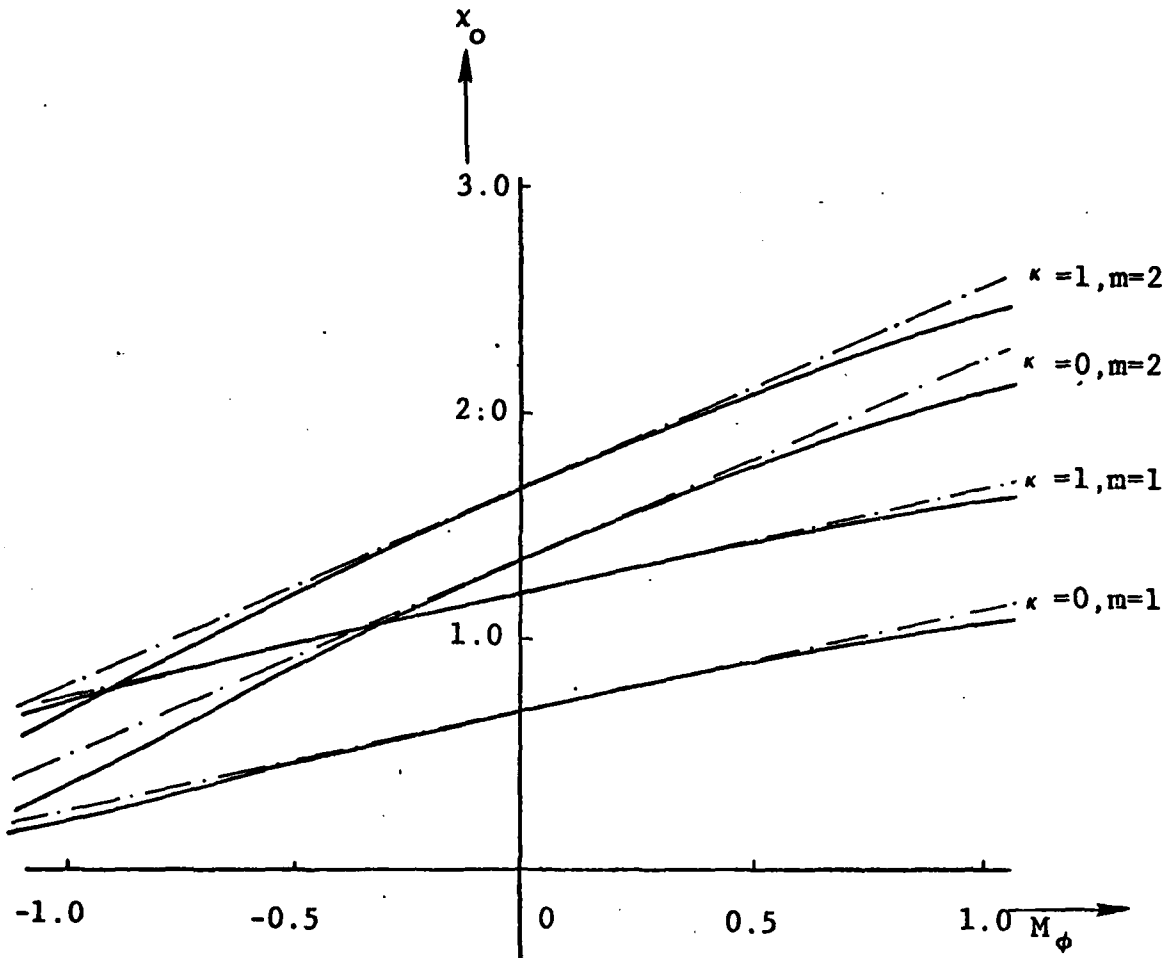
Figure 4(b) $\lambda = 2.0$.
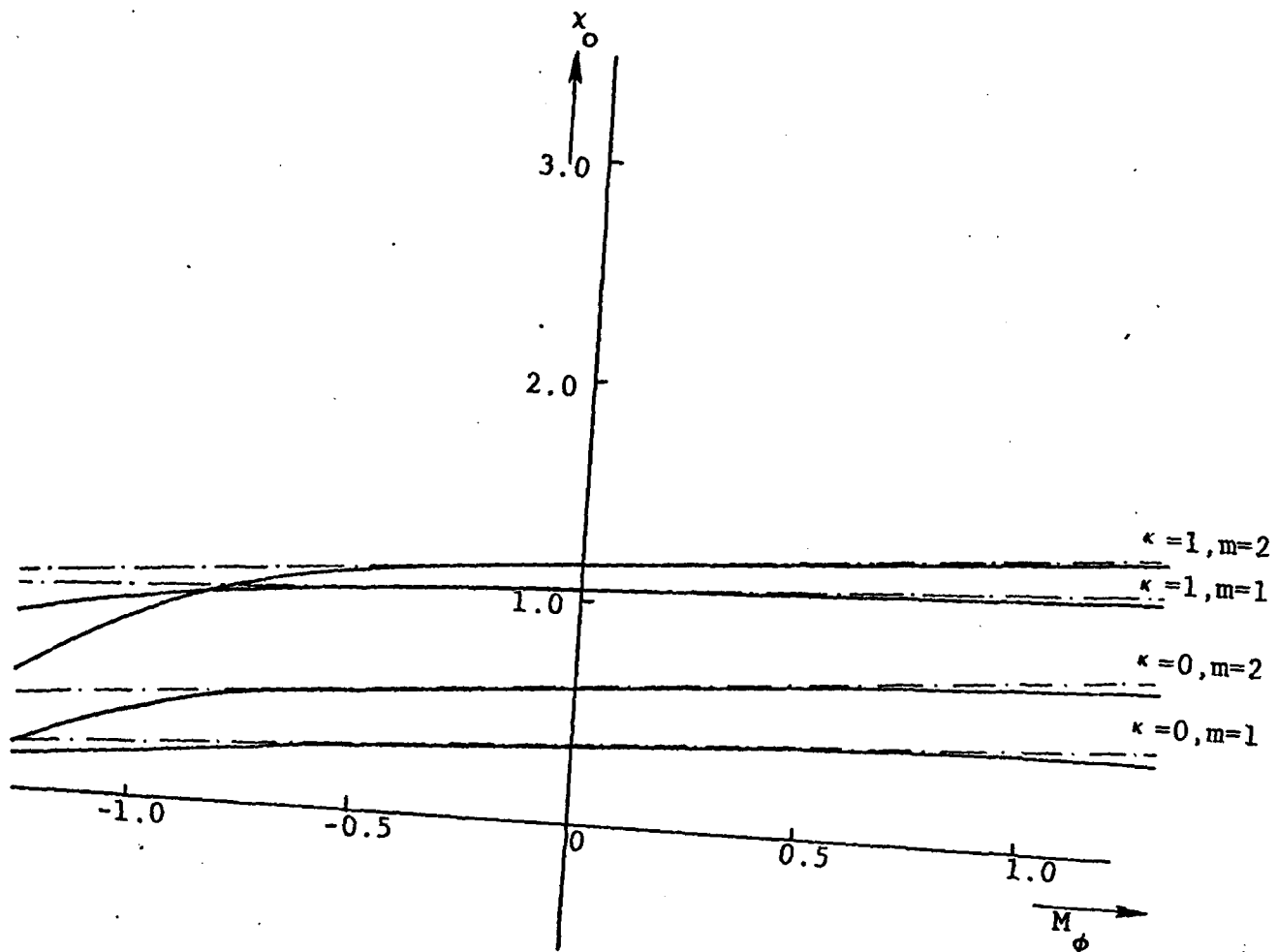
Figure 4(c) $\lambda = 5.0$.
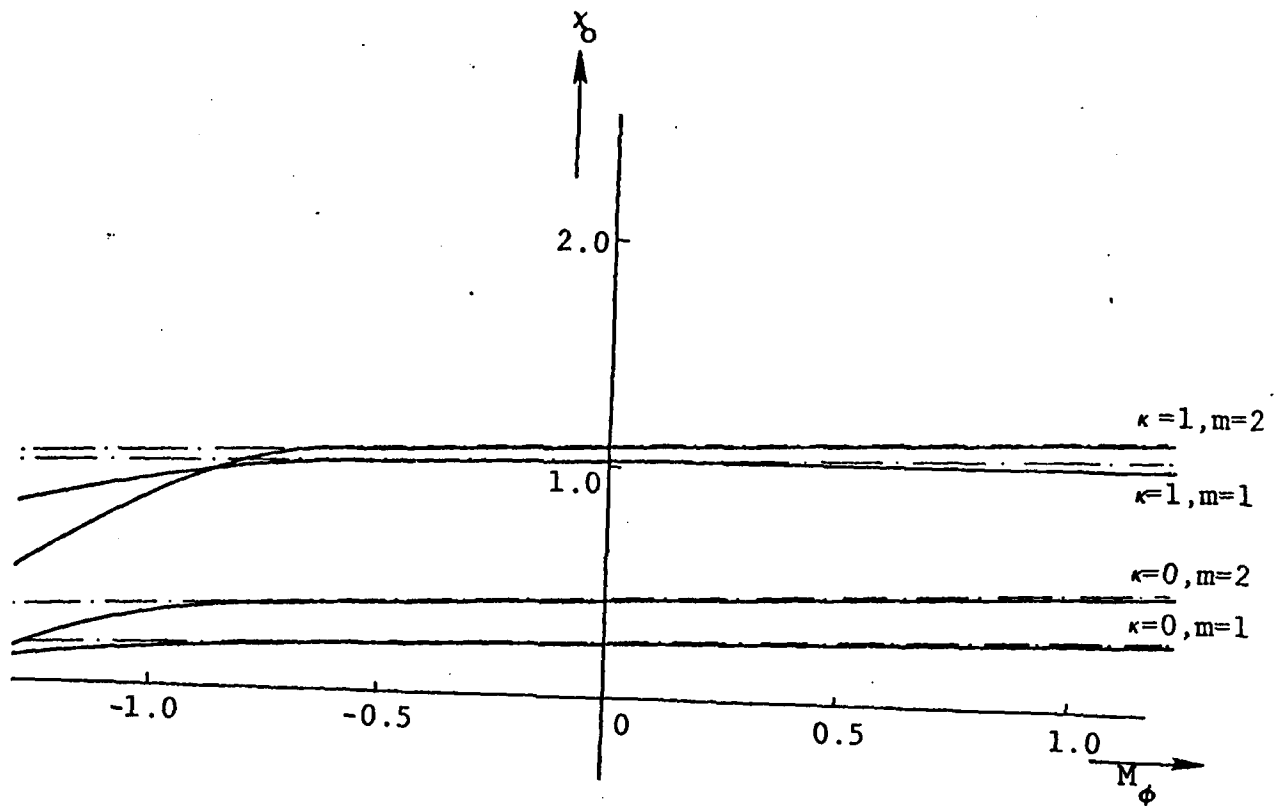
Figure 4(d) $\lambda = 7.0$.

$$\frac{\langle \cdot v' \rangle_i \ A_{ex}(r=r_o)}{\left[\tilde{u} \ \bar{v}_{000}(r=r_i) \right]^2}$$
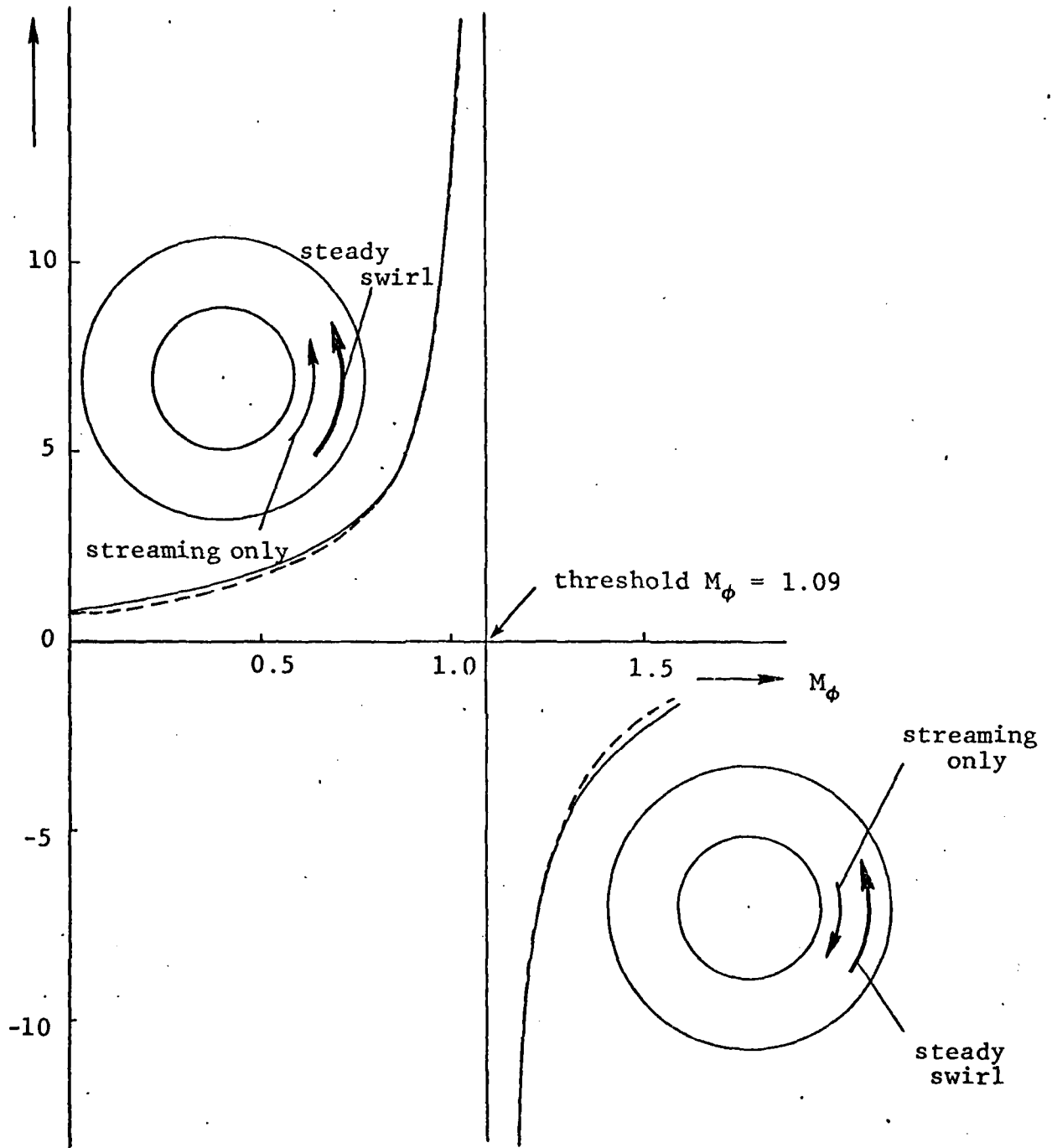
steady swirl

streaming only

threshold $M_\phi = 1.09$

10

5

0

0.5   1.0   1.5 M_ϕ

-5

-10

streaming only

steady swirl

Figure 5(a) Tangential streaming near the inner cylinder, showing the reversal of streaming at threshold swirl for the first radial mode. $\lambda = 2.0$

$\kappa = 0$, m=1; temperature at outer cylinder wall, 20°C, $P_r = 0.71$; $\gamma = 1.4$.

solid lines; inner wall temperature maintained at its steady value.
broken lines; thermally insulated inner wall.

$$\frac{\langle v' \rangle_i \, A_{ex}(r=r_o)}{\left[\tilde{u} \, \bar{V}_{000}(r=r_i)\right]^2}$$

threshold $M_\phi = 0.653$
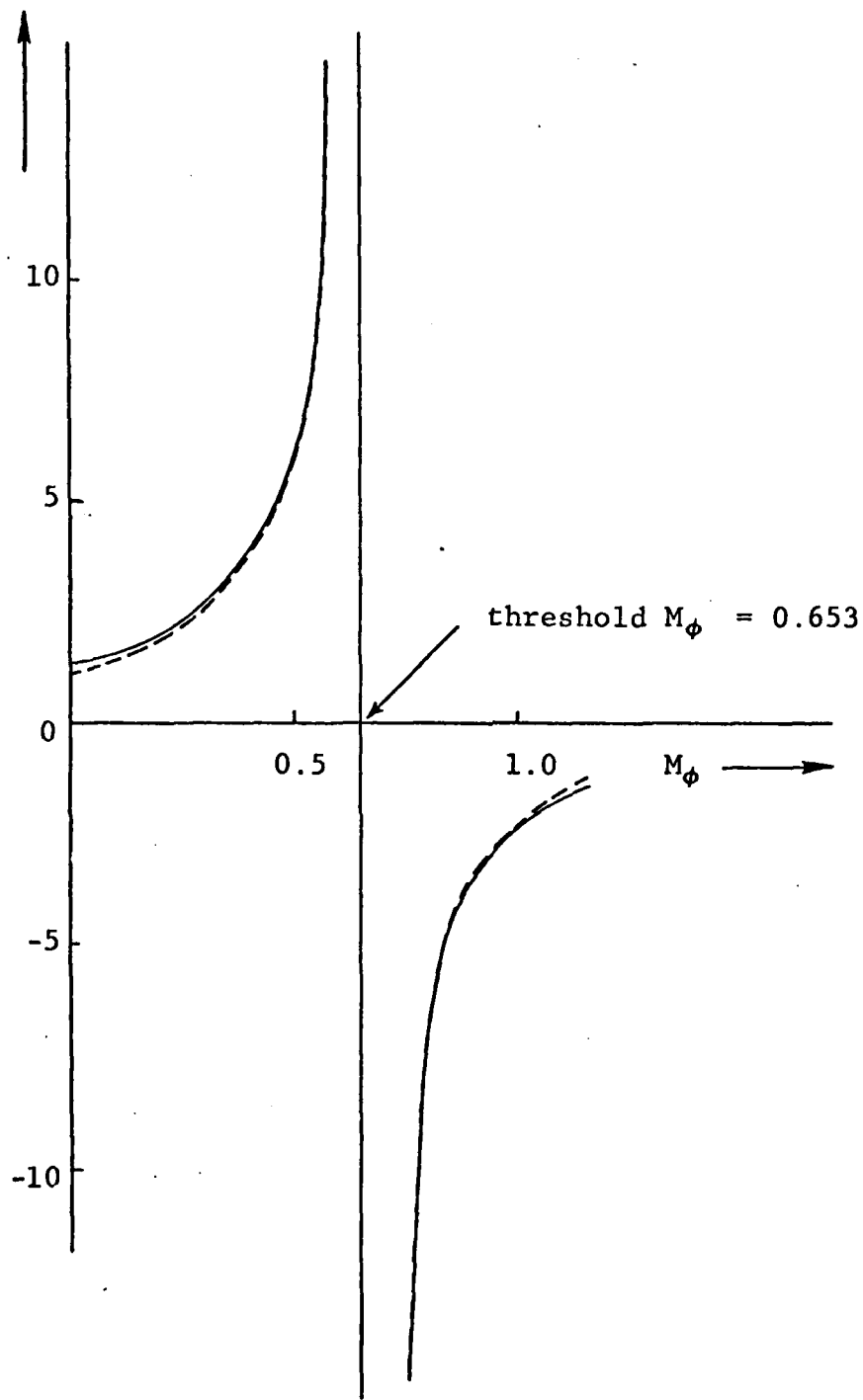
Figure 5(b) $\lambda = 3.0$.

$$\frac{\langle v' \rangle_i \; A_{ex}(r=r_o)}{\left[\tilde{u} \; \bar{V}_{000}(r=r_i) \right]^2}$$

threshold $M_\phi = 0.374$
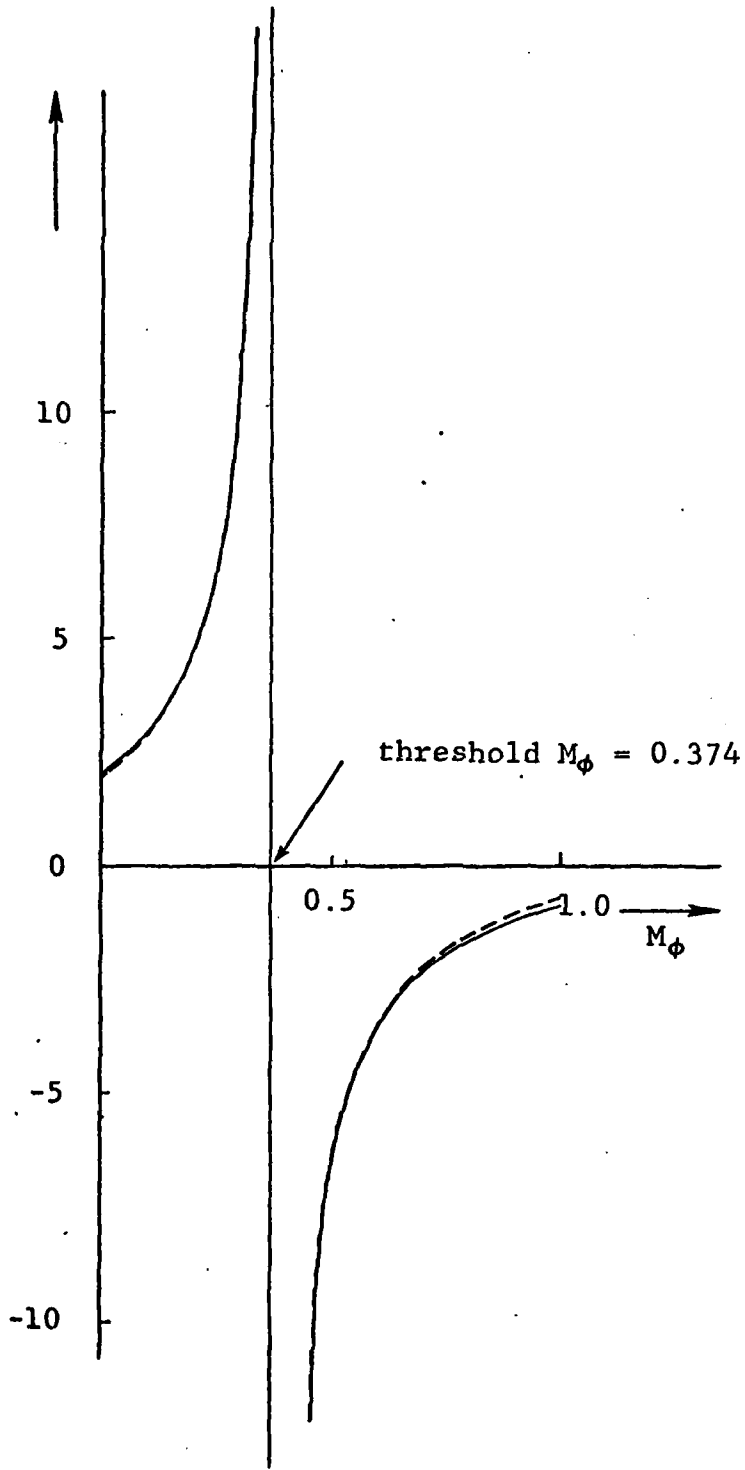
Figure 5(c) $\lambda = 5.0$.

$$\frac{\langle v \rangle_i \; A_{ex}(r=r_o)}{\left[\tilde{u} \; \bar{V}_{000}(r=r_i)\right]^2}$$
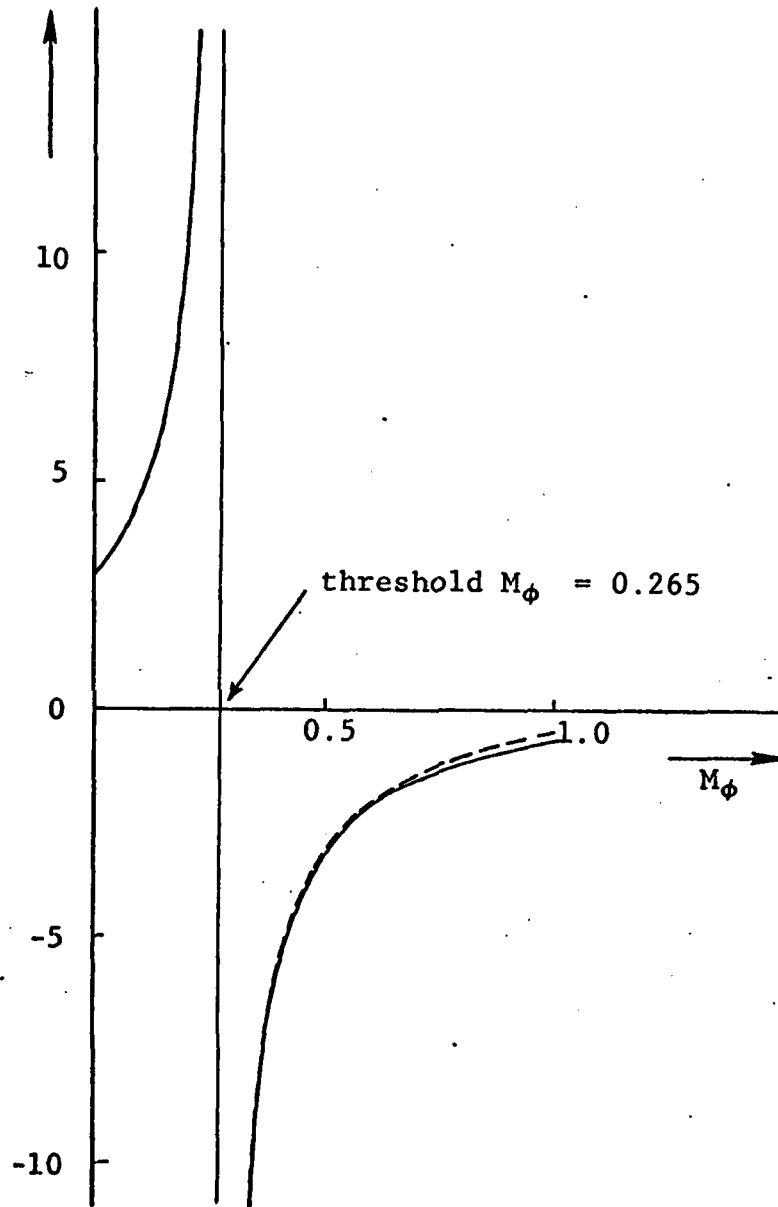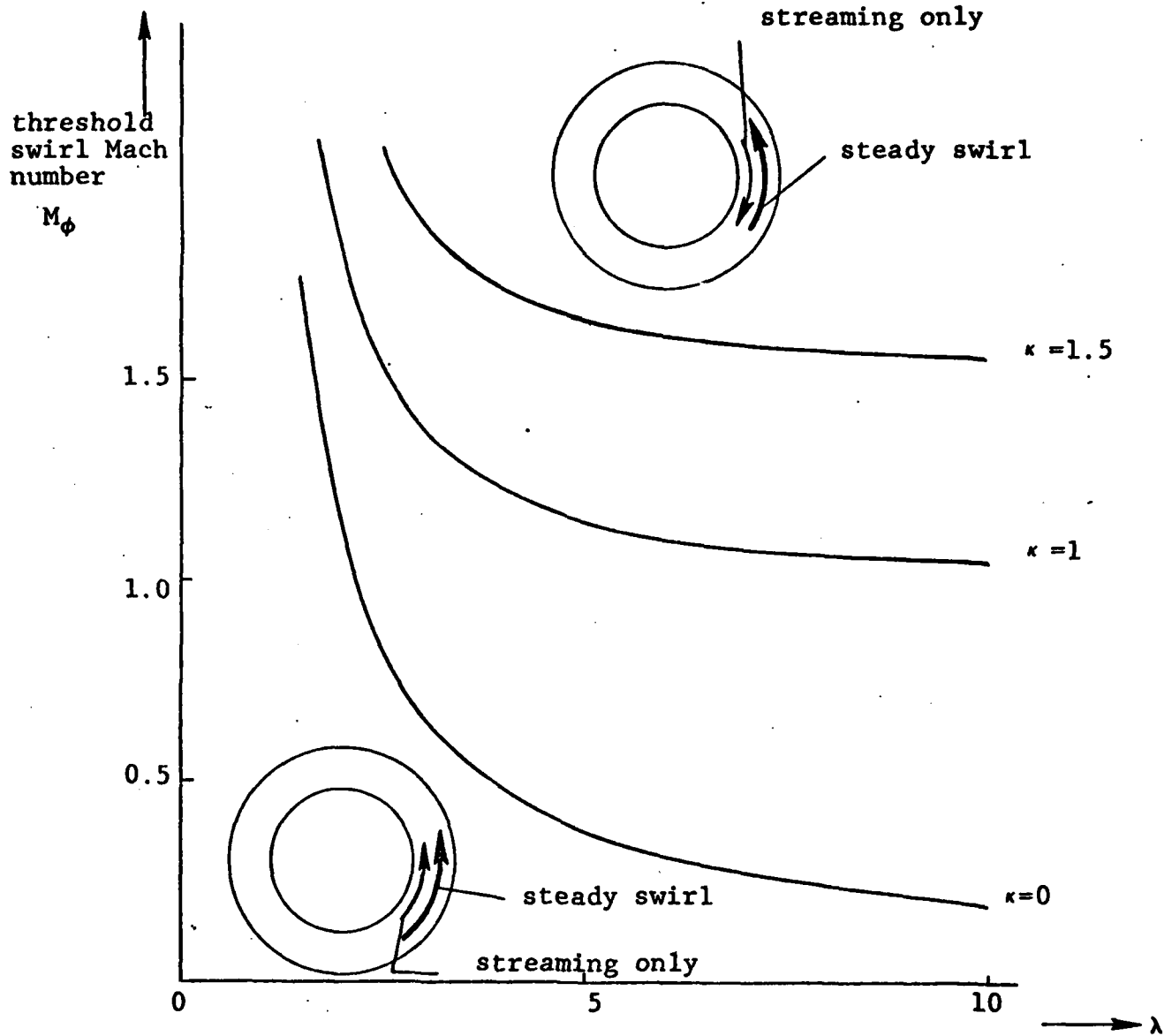
threshold $M_\phi = 0.265$

Figure 5(d) $\lambda = 7.0$.

Figure 6(a)   Threshold swirl Mach number for the first
              radial mode vs. radius ratio.   m = 1.
              Above the threshold, the direction of the
              tangential streaming is opposite to that
              of steady swirl; below it, the direction
              is the same.

Figure 6(b)   m = 2.

$$\frac{\langle v \rangle_o A_{ex}(r=r_o)}{\left[\widetilde{u}\ \overline{V}_{000}(r=r_o)\right]^2}$$
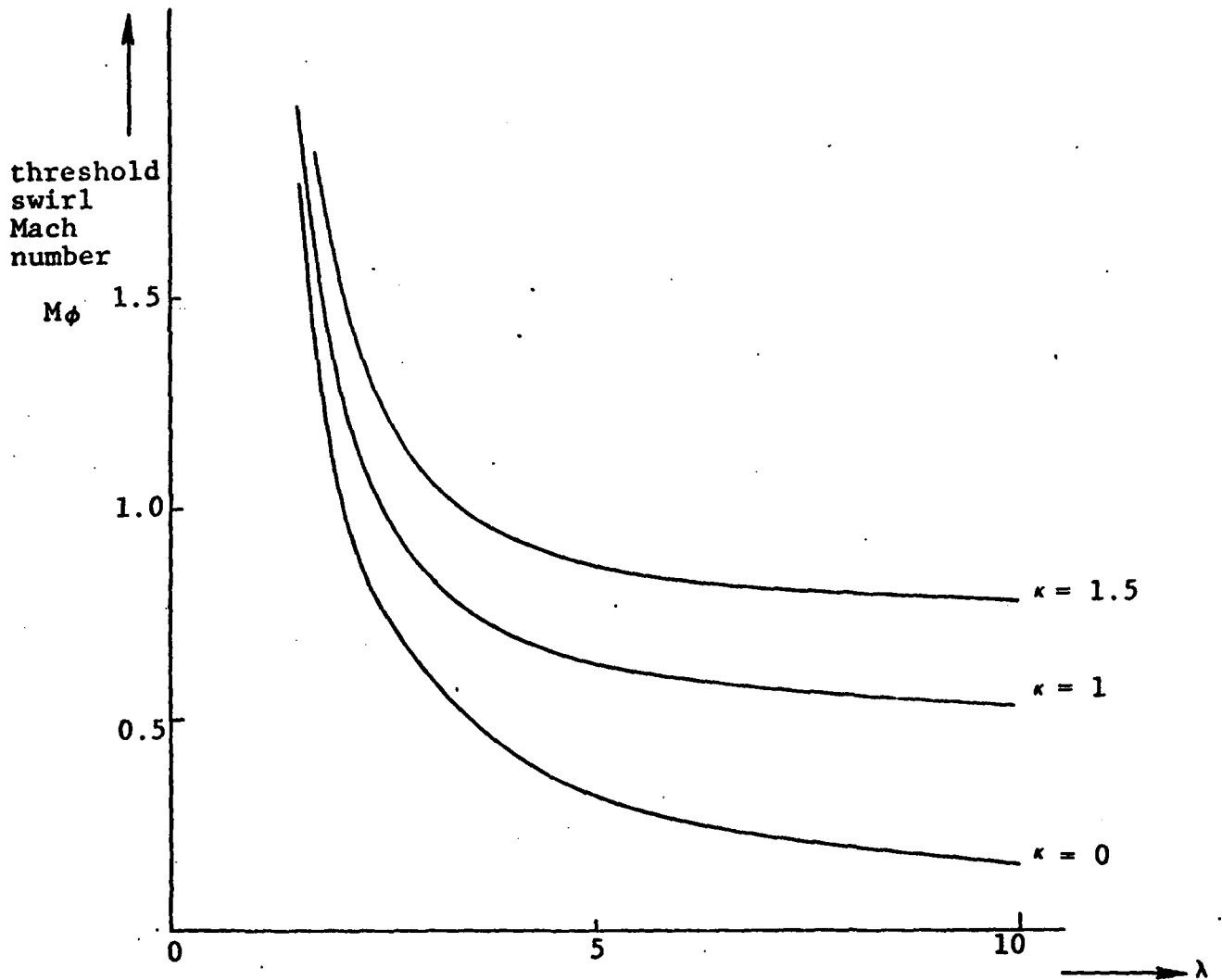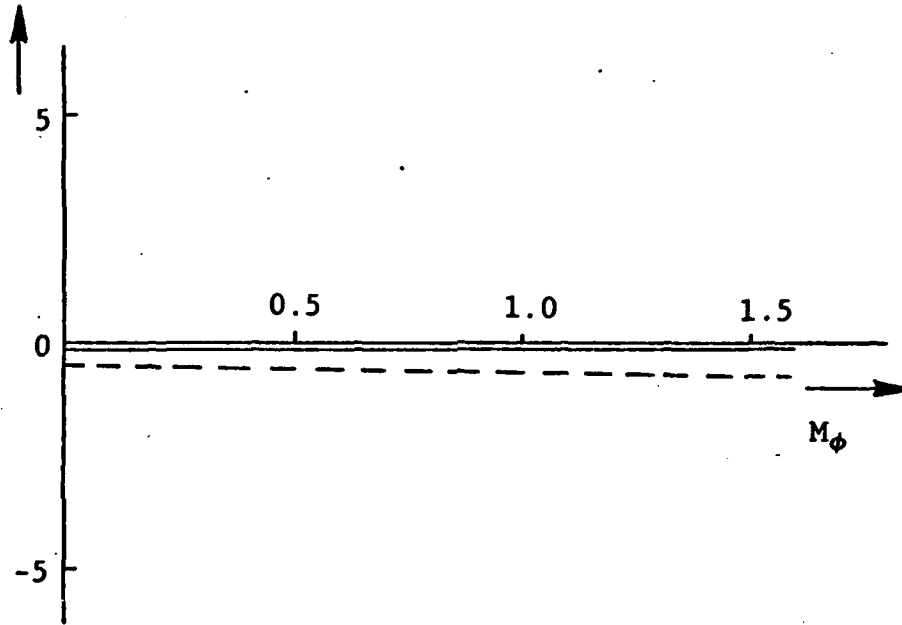
Figure 7(a)   Tangential streaming near the outer cylinder. $\lambda = 2.0$.

$\kappa = 0$, $m = 1$; legends and conditions are the same as those in Figure 5.

$$\frac{\langle v \rangle_o A_{ex}(r=r_o)}{\left[\tilde{u} \, V_{000}(r=r_o) \right]^2}$$
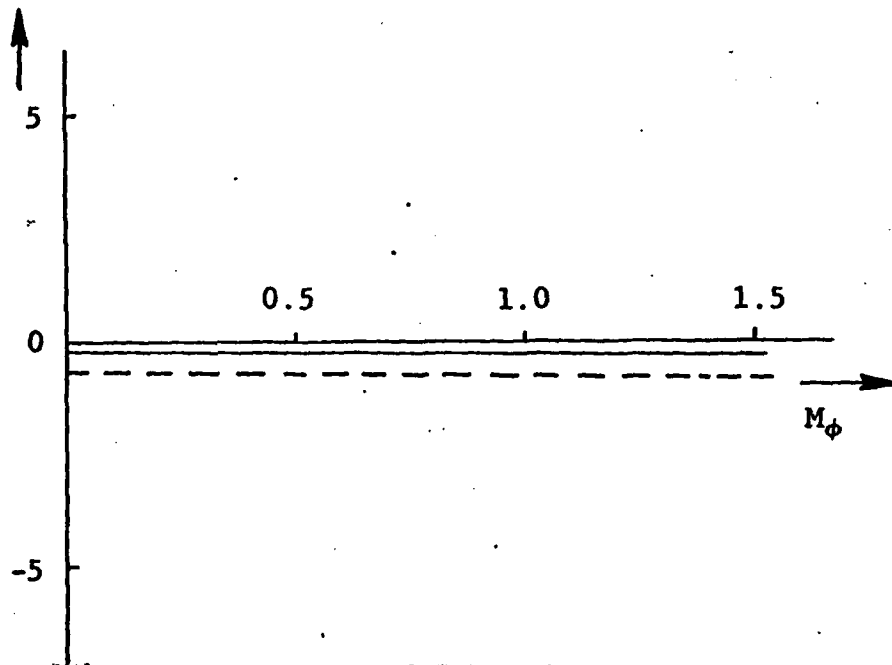
Figure 7(b) $\lambda = 5.0$.

$$\frac{\langle v'\rangle_o A_{ex}(r=r_o)}{\left[\tilde{u}\ \bar{V}_{000}(r=r_o)\right]^2}$$
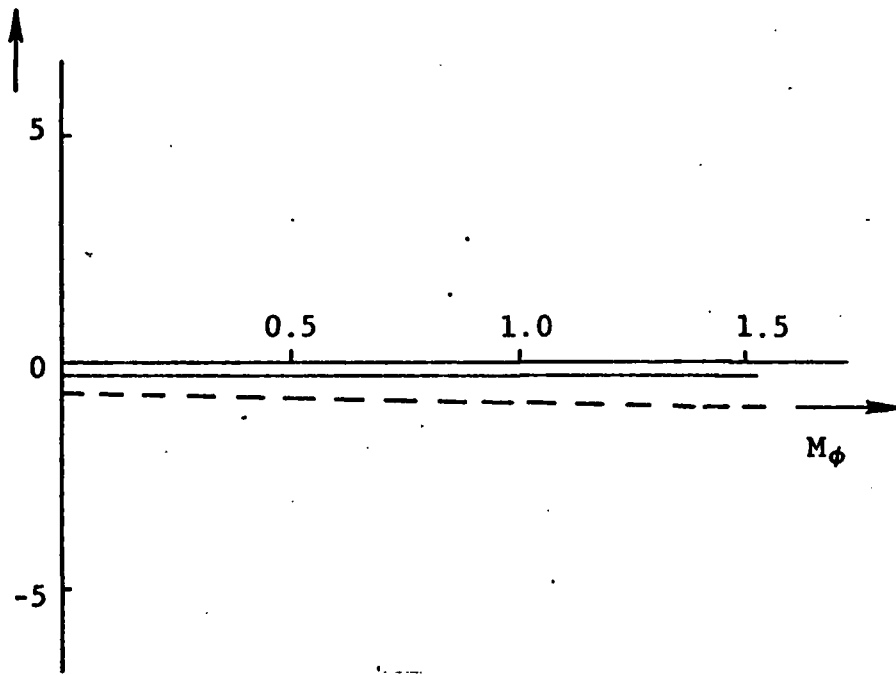
Figure 7(c) $\lambda = 7.0$.
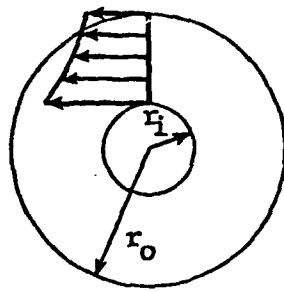
below threshold swirl   above threshold swirl
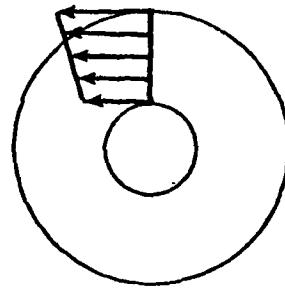
Figure 8.   Metamorphosis of total d.c. swirl for
            a free vortex.
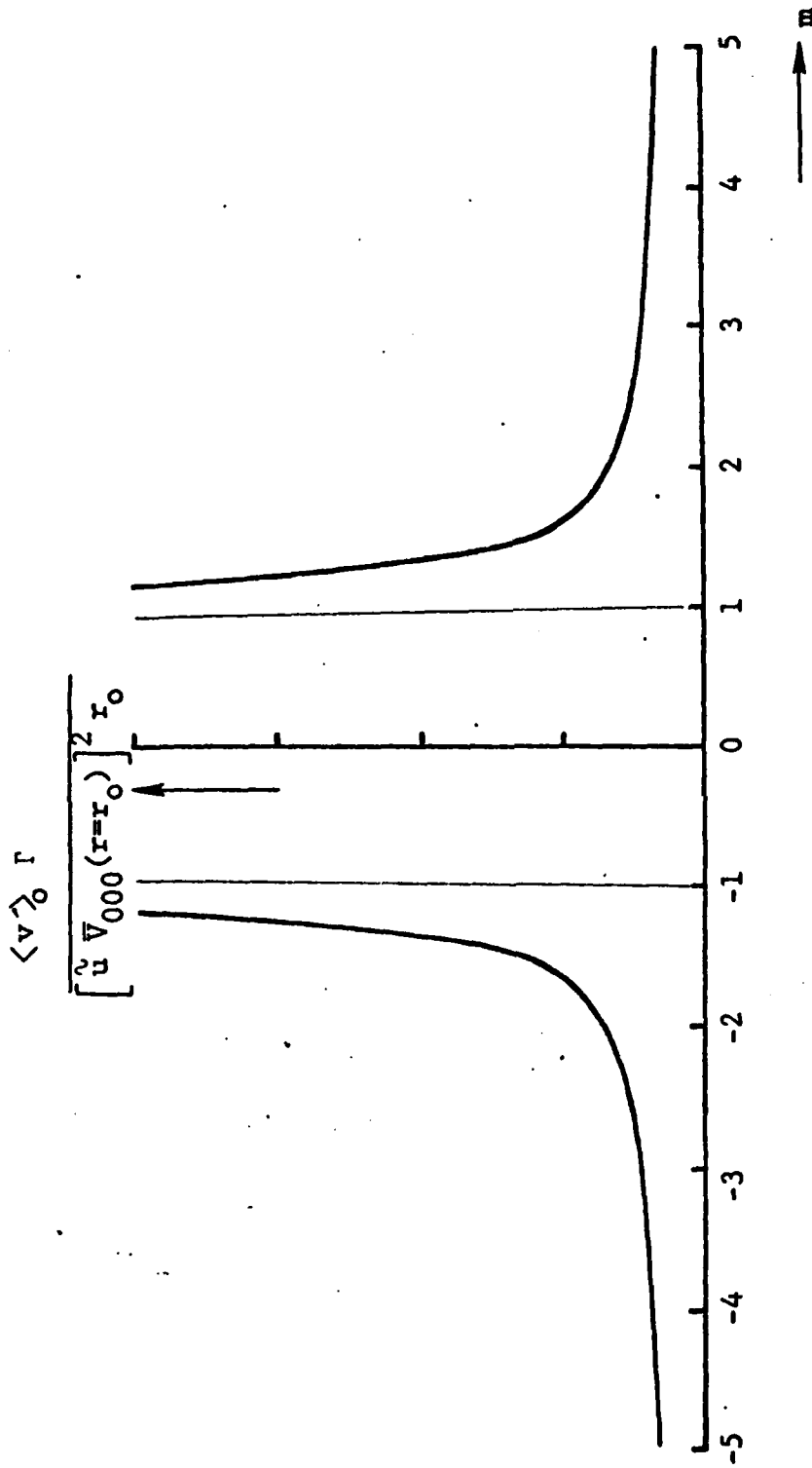
Figure 9. Tangential streaming near the tube periphery, showing that its direction is always the same as that of steady swirl. $\Gamma/(r_1 A_{ex}(r=r_1)) = 0.2$; $\lambda = 2$; $\kappa = 0$; first radial mode; $P_r = 0.71$; $\gamma = 1.4$; wall temperature is always maintained at its steady value, $20^\circ C$.
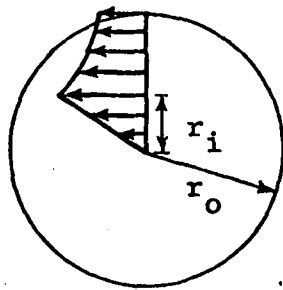
without unsteady disturbance   with acoustic streaming
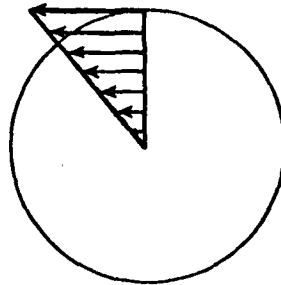
Figure 10. Metamorphosis of total d.c. swirl for a
Rankine vortex.

FIGURE CAPTIONS

Figure 1.   Definition sketch.

Figure 2.   Lower deck, middle deck and core.

Figure 3.   "Family tree" of streaming.

Figure 4.   (a)   Frequency vs. swirl Mach number. $\lambda = 1.1$.

Figure 4.   (b) $\lambda = 2.0$.

Figure 4.   (c) $\lambda = 5.0$.

Figure 4.   (d) $\lambda = 7.0$.

Figure 5.   (a)   Tangential streaming near the inner cylinder, showing the reversal of streaming at threshold swirl for the first radial mode. $\lambda = 2.0$.

Figure 5.   (b) $\lambda = 3.0$.

Figure 5.   (c) $\lambda = 5.0$.

Figure 5.   (d) $\lambda = 7.0$.

Figure 6.   (a)   Threshold swirl Mach number for the first radial mode vs. radius ratio. $m = 1$. Above the threshold, the direction of the tangential streaming is opposite to that of steady swirl; below it, the direction is the same.

Figure 6.   (b) $m = 2$.

Figure 7.   (a)   Tangential streaming near the outer cylinder. $\lambda = 2.0$.

Figure 7.   (b) $\lambda = 5.0$.

Figure 7.   (c) $\lambda = 7.0$.

Figure 8.   Metamorphosis of total d.c. swirl for a free vortex.

Figure 9.   Tangential streaming near the tube periphery, showing that its direction is always the same as the steady swirl. $\Gamma / (r_i A_{ex}(r=r_o)) = 0.2$; $\lambda = 2$; $\kappa = 0$; first radial mode; $P_r = 0.71$; $\gamma = 1.4$; wall temperature is always maintained at its steady value, $20^o C$.

Figure Captions

Page 2

Figure 10.   Metamorphosis of total d.c. swirl for a
             Rankine vortex.